A Sponsored Supplement to *Science*

HUMBLE BEGINNINGS, BRIGHT FUTURE

Institute of Physics (CAS) at 90

1928-2018






Sponsored by

中国科学院物理研究所 Institute of Physics CAS 1928

1928–2018
中国科学院物理研究所九十周年
90th ANNIVERSARY OF INSTITUTE OF PHYSICS CAS

Produced by the
Science/AAAS Custom
Publishing Office

Science
AAAS

ScienceCareers
FROM THE JOURNAL SCIENCE AAAS

Step up your job search with *Science* Careers

- Access thousands of job postings
- Sign up for job alerts
- Explore career development tools and resources

Search jobs on **ScienceCareers.org** today

Humble Beginnings, Bright Future Institute of Physics (CAS) at 90

Introductions

Articles

TABLE OF CONTENTS CONTINUED >

Humble Beginnings, Bright Future
Institute of Physics (CAS) at 90

Cover: Black/white photos on the first line. Left: The Institute of Physics, Academia Sinica (1928); Right: The Institute of Physics, National Academy of Peiping (1930).

Color photos on the second line: Building A (built in 1958, remodeled in 2013), Building D (2002), Building M (2012).

This supplement was produced by the *Science*/AAAS Custom Publishing Office and sponsored by the Institute of Physics, CAS.

Editors: Jackie Oberst, Ph.D.; Sean Sanders, Ph.D.;
Proofreader/Copyeditor: Bob French
Designer: Amy Hardcastle

Materials that appear in this supplement have not been peer-reviewed nor have they been assessed by *Science*. Articles can be cited using the following format: [AUTHOR NAME(S)] [CHAPTER TITLE] in Humble beginnings, bright future: Institute of Physics (CAS) at 90. (*Science*/AAAS, Washington, DC, 2018), p. [xx-xx].

Xiaoying Chu
Director, Global Collaboration
and Business Development, Asia
xchu@aaas.org
+86-131-6136-3212

Danny Zhao
Regional Sales Manager, Asia
dzhao@aaas.org
+86-131-4114-0012

© 2018 by The American Association for the Advancement of Science. All rights reserved.
11 May 2018

Articles continued

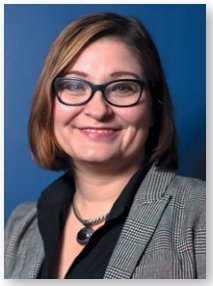

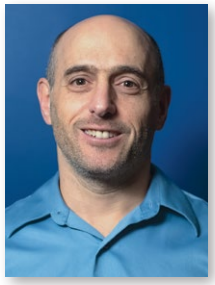

Extreme Science: Celebrating 90 years of cutting-edge research at IOP CAS

Physics is a field of extremes. It studies the microworld, including subatomic particles, and the macroworld, including magnetic fields and plasma found in space. It explores the lowest and highest limits of temperature, pressure, and speed. These seemingly disparate subfields are all housed at the Institute of Physics, Chinese Academy of Sciences (IOP CAS), which is commemorating its 90th year.

At the nexus of all these extremes is superconductivity, or the ability of an element, intermetallic alloy, or compound to conduct electricity without resistance or energy loss below a certain temperature. Magnets and very cold temperatures—on the order of 39 K (–234°C, –389°F)—are used to control the flow of electricity. Remarkably, an electrical current will flow forever in a closed loop of superconducting material, which makes it the closest thing to perpetual motion—a sort of Rube Goldberg machine for electricity.

These near-magical materials are employed in devices that have revolutionized theoretical physics; for example, particle accelerators probe the inner workings of atoms, while tokamaks contain hot plasma that could one day be used in thermonuclear fusion. Superconductors are also an important factor in other technological breakthroughs, including magnetic resonance imaging machines that reduce the need for exploratory surgery, digital and quantum computers that store and transmit ever-increasing amounts of data, and Maglev trains that carry people over long distances in a much shorter time than conventional trains.

Inside this supplement is a sampling of the variety of cutting-edge research that is taking place at IOP. This prestigious institute is extensively pursuing superconductivity as well as the physics of condensed and soft matter, optics, subatomic particles, plasma, magnets, and computers. Join us in celebrating IOP's long history and its incredible contributions not just to science, but to humankind.

Jackie Oberst, Ph.D.
Sean Sanders, Ph.D.
Science/AAAS Custom Publishing Office

PHOTOS: ALEX LEE

From the Director

Throughout its history, IOP has filled many gaps in China's modern physics research.

Ninety years ago, the Institute of Physics (IOP) of the Chinese Academy of Sciences (CAS) was founded as the first national institute dedicated to physics research in China. Today we are celebrating our role in the international research community by honoring the past and reimagining the future.

IOP has made essential contributions to the founding of modern physics research in China. The growth trajectory of IOP is almost in sync with the development of modern China. It started with a very limited number of researchers working on a small range of activities, and expanded into a large-scale research institution with an extensive, multidisciplinary scope, covering fields including condensed matter physics, optical physics, atomic and molecular physics, plasma physics, and theoretical and computational physics. Now, IOP is designated as the National Research Center for Condensed Matter Physics by the Ministry of Science and Technology of China.

Throughout its history, IOP has filled many gaps in China's modern physics research. It developed the country's first hydrogen and helium liquefiers, synthesized its first artificial diamond, and built its first ruby laser. IOP has also made significant breakthroughs with global impact, such as the discovery of copper- and iron-based high-temperature superconductors, topological insulators, the quantum anomalous Hall effect, and Weyl semimetals. IOP is very proud of its high-tech products as well—its high-quality neodymium permanent magnets, lithium-ion batteries, single-crystal silicon carbide substrates, and high-temperature superconductivity filters have all successfully entered either the domestic or global markets.

In recent years, IOP has implemented a series of reforms to optimize its organizational structure and administration. Multilevel talent programs have been introduced to attract experts with various backgrounds; and multiple collaborative platforms have been established to break down silos and to maximize research performance. IOP nurtures and encourages original research with an open organizational culture, and has a long-established tradition of pursuing excellence without fear of failures.

As a national research center, IOP has secured sufficient funding for its sustainable development. It is now devoting unprecedented effort to attracting international scientists to its well-regarded programs. Meanwhile, several large-scale research facilities are under construction, such as the Synergetic Extreme Condition User Facility (SECUF)—facilities that will significantly expand IOP capacity as well as China's national capacity for research in materials science. With these investments, IOP is confident that it can build an internationally recognized, first-class frontier physics research center.

This special supplement provides an overview of IOP as well as reviews and perspectives on the important research being performed there. We welcome readers to join us for the celebration of our 90th anniversary.

Thank you,

Zhong Fang

Zhong Fang, Ph.D.
Director, Institute of Physics, CAS

THE INSTITUTE OF PHYSICS: 90 years and beyond

Jiangping Hu, Ph.D., Deputy Director, Institute of Physics, Chinese Academy of Sciences

Institute of Physics Building D

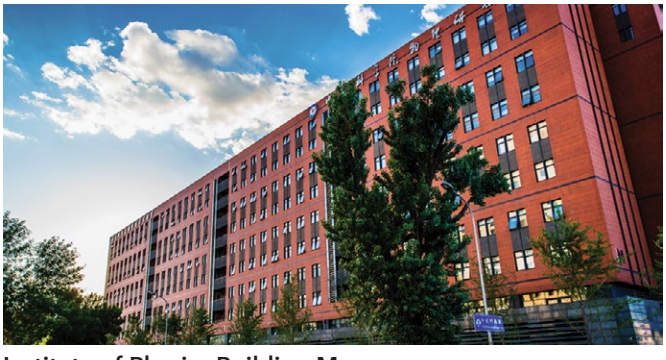

Institute of Physics Building M

Introduction

The Institute of Physics (IOP), Chinese Academy of Sciences (CAS), with its origins reaching back to 1928, was the first national physics research institute in China. The two predecessors of the current IOP were the Institute of Physics, Academia Sinica (founded in 1928) and the Institute of Physics, National Academy of Peiping (founded in 1929), which merged to form the Institute of Applied Physics (IOAP) in 1950. IOAP took its current name, IOP, in 1958, to reflect its expansion to a broader range of research fields.

IOP has made many important research contributions to a variety of fields in physics. It is now a comprehensive, multidisciplinary institution that covers fundamental and applied research in condensed matter physics, optical physics, atomic and molecular physics, plasma physics, soft matter physics, and computational physics. The institute is designated as both a national laboratory and national research center by the Ministry of Science and Technology of the People's Republic of China, i.e., the Beijing National Laboratory for Condensed Matter Physics (BNLCP) and the National Research Center for Condensed Matter Physics (NRCCMP). Presently, within the framework of BNLCP and NRCCMP, IOP hosts three state key laboratories (the Surface Physics Laboratory, the Superconductivity Laboratory, and the Magnetics and Magnetic Materials Laboratory) and seven CAS key laboratories (the Laboratory of Optical Physics, the Laboratory for Advanced Materials and Electron Microscopy, the Nanoscale Physics and Devices Laboratory, the Laboratory for Renewable Energy, the Laboratory of Extreme Conditions Physics, the Laboratory of Soft Matter Physics, and the Laboratory of Condensed Matter Theory and Computation), and two IOP key laboratories (the Solid State Quantum Information and Computation Laboratory, and the Laboratory of Microfabrication). Groups at IOP are also organized to form seven virtual research centers to target essential research fields and strategic needs, including the Spallation Neutron Source, the International Center for Quantum Structures, the Quantum Computation Center, the Functional Crystal Center, the Quantum Simulation Science Research Center, the Center for Renewable Energy Research, and the Center for Superconductivity Technology Application. These centers serve as collaboration platforms for cross-disciplinary research.

Basic research highlights

IOP, as the flagship physics research institute in China, can boast of many noteworthy achievements in its 90-year history—but the turning point of that history was around 1980, when China started its reform and began opening up to the world.

IOP has made many important research contributions to a variety of fields in physics.

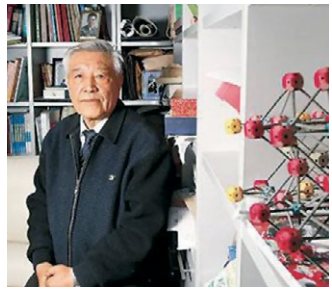

Z. X. Zhao, father of Chinese superconductivity research

Prior to 1980, IOP researchers were mainly trying to catch up with the scientific developments and trends of advanced countries, and the remarkable breakthroughs made during this period were the results of a series of pioneering efforts by Chinese scientists; for example, the development of the first hydrogen and helium liquefiers, the first dilution refrigerator with a cooling temperature down to 0.01 kelvin (K) above absolute zero, and the development of the first tokamak fusion research facility in China; the first-time growth of single-crystal silicon and high-quality rock crystals, and the first synthesis of the artificial diamond in China; and the measurement of the crystal structure of 1.8-Å porcine insulin in collaboration with the Institute of Biophysics at CAS and Peking University.

After 1980, as China's economy started accelerating, IOP entered a rapid growth period. This is evidenced not only by the steady increase in the number of publications and citations in scientific journals during the past three decades, but also by IOP's ability to attract top international scientists, the improvement of China's scientific research infrastructure, and the institute's increasing development of state-of-the-art research equipment in recent years. IOP is now a world-renowned research institute and is at the frontier of many research fields, including those described below.

Low-temperature physics and superconductivity

Low-temperature physics and superconductivity research began at IOP back in the late 1950s and has been one of its strongest research areas since then. Because of a breakthrough in high-temperature superconductors in 1987, the Chinese government established the National Laboratory for Superconductivity in 1991. The laboratory has become a national center for superconductivity research, a talent incubator, and a base for academic exchange between domestic and foreign scholars.

PHOTO: (RIGHT) LI-WANG JIN

Recently, IOP groups have played a leading role in researching iron-based superconductors—including the discovery of the CeFeAsOF superconductor, the first iron-based superconductor with a critical temperature (Tc) over 40 K under ambient pressure, and SmFeAsO, with a record Tc of 55 K—and also in uncovering many fundamental electronic properties of these materials. Most recently, IOP scientists have also discovered the first manganese (Mn)-based superconductor, manganese monophosphide (MnP), after observing pressure-induced superconductivity in chromium alloys (CrAs). IOP's achievement in iron (Fe)-based superconductors was included in one of the "Top 10 Scientific Breakthroughs of 2008" by *Science* magazine and one of the "Top Ten Physics News Stories of 2008" by the American Physical Society.

Topological matters and topological effects in physics

The concept of topology has spread into every facet of condensed matter physics research in the past decade. IOP scientists have pioneered research in topological physics. The first theoretical prediction of three-dimensional (3D) topological insulators was made by IOP groups. Scientists from IOP and Tsinghua University collaborated and realized the quantum anomalous Hall (QAH) effect in the thin films of chromium (Cr)-doped $(Bi,Sb)_2Te_3$. Recently, topological semimetals were predicted and measured due to a close collaboration between theoretical and experimental groups at IOP. Significant progress in topological photonics and topological magnetism has also been made at IOP. The discovery of topological Weyl semimetals was selected as one of 2015's "Highlights of the Year" by *Physics* magazine (American Physical Society), and one of the "Top 10 Breakthroughs of 2015" by *Physics World* magazine (the Institute of Physics in the United Kingdom).

IOP has enjoyed a long and glorious journey through its first 90 years, with many remarkable achievements to its credit.

IOP logo made from metallic plastic

Advanced materials

IOP is known for its achievements in advanced materials. IOP has many groups that focus on different functional materials, including quantum materials for condensed matter physics, soft/biological matter, amorphous materials, energy materials, and magnetic materials. The Laboratory of Extreme Conditions Physics and the Laboratory of Advanced Materials and Electron Microscopy have been created to understand the structural and electronic properties of these materials. Many articles in this supplement address specific achievements related to specific materials. A few recent achievements in bulk materials research include: a novel cerium (Ce)-based bulk amorphous alloy called "metallic plastic," which displays properties of both metal and plastic; the superplastic bulk metallic glass ZrCuNiAl; and a novel type of diluted magnetic semiconductor, Li (Zn, Mn) As, exhibiting a high critical Néel temperature (the temperature above which an antiferromagnetic material becomes paramagnetic).

Dimensionality is one of the major degrees of freedom to affect material properties. Nanomaterials and two-dimensional (2D) materials occupy a large portion of IOP's current research. The institute has been equipped with cutting-edge scientific facilities and equipment to study these materials. Recent efforts have been focused on designing and creating new nanostructures and 2D materials with unexpected properties, and on tailoring and characterizing them for elaborate band structure modulations and functional device applications. The Key Laboratory for Surface Physics is also focusing on growing 2D materials with a variety of methods and is committed to developing new probes to study them. For example, the laboratory has developed novel high-resolution electron energy loss spectroscopy (HREELS), which can measure the energy and momentum of scattered electrons in 2D mapping by using a specially designed lens system in the electron source combined with a hemispherical electron energy analyzer.

Quantum technologies and quantum computing

IOP has many years of experience in the fabrication of superconducting devices and measurement at ultralow temperatures. These experiences have enabled IOP to be the first institute in China to fabricate 10 superconducting qubit devices. Moreover, IOP has made significant progress in searching for Majorana modes and is now ready to use these modes to develop topological quantum qubits, the fundamental units for quantum computers. Apart from superconductor-based qubits, groups at IOP have also made important progress in developing qubits based on nitrogen-vacancy centers in diamonds and on quantum dots in silicon-based semiconductors.

Intense laser–matter interactions

IOP has been involved in researching ultrafast lasers and intense laser–matter interactions since 1997. A series of custom-built titanium (Ti): sapphire lasers have been developed at IOP's eXtreme Light (XL) facilities. These facilities can generate laser pulses with the duration of a few laser cycles (several femtoseconds), with power above 1 petawatt (10^{15} watts) and an intensity of 10^{20} W/cm^2. These laser systems have enabled research into laser-driven particle acceleration and novel X-ray and terahertz radiation sources, laboratory astrophysics, fundamental physical processes relevant to advanced nuclear fusion concepts, long-distance propagation of femtosecond laser pulses in air, and ultra-relativistic laser–matter interactions.

Technology transfer and industrialization

Basic research at IOP has created fertile ground to systematically grow new technologies for the benefit of society as well as for national strategy needs. IOP files over 60 patents each year, and new technologies from IOP have helped to launch six high-tech companies. China's rapid economic growth and its need for economic restructuring present IOP with not only an opportunity but also an obligation to contribute more to technology transfer and industrialization. Below are a few examples of the technologies developed at IOP.

Nd-Fe-B permanent magnets

IOP began research on rare-earth magnetic materials in the 1970s, and successfully developed neodymium (Nd-Fe-B) permanent-magnet materials in collaboration with the Institute of Electronics in 1983. In 1985, San Huan New Materials R&D Company was founded with technology investment from IOP, and China started manufacturing Nd-Fe-B permanent magnets, becoming the third country to do so after the United States and Japan, which had been the only two countries manufacturing

The range of electric vehicles powered by Li-ion batteries manufactured by Phylion Battery Co., Ltd.

Vacuum ultraviolet laser-based angle-resolved photoemission spectroscopy (ARPES) facility

Nd-Fe-B permanent magnet materials. In 2000, Beijing Zhong Ke San Huan High-Tech Co. Ltd. (developed and renamed from the San Huan Company) was successfully listed on the Shenzhen Stock Exchange. It is now the world's second-largest supplier of rare-earth permanent magnet materials for R&D and production.

Lithium-ion batteries

IOP started research on rechargeable lithium (Li)-ion batteries in the 1980s. Beijing Phylion Battery Co., Ltd., and Suzhou Phylion Battery Co., Ltd., were founded in 1998 and 2003, respectively, with seed investments from IOP. Suzhou Phylion Battery Co. is ranked number 1 in the Chinese market segment manufacturing batteries for electric bicycles, and is one of the three largest e-bike battery suppliers for the European market. It is also the first Li-ion battery supplier for rail vehicles and the largest Li-ion battery supplier for light electric vehicles (EVs) in China. It has successfully entered the European market for pure EVs as well, and has become the first provider of hundred-kW–class lithium batteries for automobiles.

Silicon carbide wafers

IOP began its research into the growth of silicon carbide (SiC) single crystals in 1999. TankeBlue Semiconductor Co., Ltd. was founded in 2006, based on technology developed by IOP. It was the first company in China targeting mass production of SiC single crystals. In 2011, the largest SiC wafer production line was developed, where 2 in.–4 in. conductive and semi-insulating SiC wafers were mass produced. In 2014, 6-in. SiC single-crystal substrates were successfully developed, with crystal quality matching that of the world's top suppliers. Since then, China has no longer relied on imports for the key materials used for domestic manufacturing of high-performance SiC-based optoelectronic devices.

Research infrastructure and facilities

Over the past three decades, IOP has benefited greatly from China's rapid economic growth. The institute has doubled its overall research lab space twice in the past 20 years and is currently in the midst of construction to triple it. Scientific equipment and facilities have been continuously improved as well. IOP is now fully equipped with cutting-edge equipment for research and is a powerhouse for the development of new techniques and assays. A few of these technologies are listed below.

Angle-resolved photoemission spectroscopy

In 2006, IOP announced the development of vacuum ultraviolet laser-based angle-resolved photoemission spectroscopy (ARPES)—a world first. The primary innovation was the use of a laser (with its unprecedented precision) as the light source rather than the traditional ARPES light source based on synchrotron radiation. Now, ARPES has entered its second generation and is able to complete scans that cover an entire 2D reciprocal space.

eXtreme Light facilities

IOP started R&D on its ultraintense femtosecond laser facilities in 1997, and has developed a series of XL (eXtreme Light) facilities. The 1.16-PW XL-III ultraintense femtosecond titanium (Ti): sapphire laser facility was completed in 2011, with the contrast ratio of the main laser pulse at around 10^{10}, and the duration of the compressed pulse reaching 27.9 femtoseconds. The peak power of 1.16 PW was the highest on record at that time. This facility is available to researchers from both China and abroad, and has been used in studies of large-size cluster electron acceleration and femtosecond laser-driven proton acceleration.

The 1.16-PW XL-III femtosecond ultraintense titanium (Ti): sapphire laser facility

Low-temperature scanning probe microscope molecular beam epitaxy system at IOP

Molecular beam epitaxy

IOP collaborated with the Institute of Semiconductors at CAS and developed a series of molecular beam epitaxy (MBE) apparatuses between the 1980s and 1990s. The technique has proved to be very successful in growing complex oxide thin films including superlattices and all-oxide epitaxial hetero junctions. Currently IOP owns a range of advanced MBE equipment used to grow different types of materials, and also used as a standard tool to design functional materials with novel properties.

IOP's new campus in Huairou Science City

Large-scale facilities

IOP has led or participated in the construction of several large-scale facilities. Currently the institute is also playing a major role in the construction of Huairou Science City in Beijing (see below). The completed projects include the "Green Bamboo" thermal neutron triple-axis spectrometer (Beijing, 2014), the "Dream Line" beamline station of the Shanghai Synchrotron Radiation Facility (Shanghai, 2015), and the Engineering Center for Target Station and Neutron Instruments for the China Spallation Neutron Source (CSNS) (Guangdong). CSNS generated its first neutron beam in September 2017.

Development of Huairou Science City

Huairou, a suburb of Beijing, has been designed as a future science city. It will host the National Science and Innovation Center, with large infrastructure and facilities for scientific research, including the National Northern Synchrotron Station. IOP is presently leading or coleading the construction of many multidisciplinary platforms as part of the national and CAS R&D infrastructure. The ongoing projects include:

Synergetic Extreme Condition User Facility (SECUF)

SECUF is a major project of the national infrastructure for scientific research, with IOP being its legal entity. Construction began in September 2017, and it is expected to take about five years to complete the world's first synergetic user facility integrating various extreme conditions such as ultralow temperature, ultrahigh pressure, ultrahigh magnetic fields, and ultrafast optical fields. The facility will significantly expand the capacity for matter science research to pioneer the discovery of new states, new phenomena, and new rules of matter. The planned construction area is 48,000 square meters, with a total investment of RMB 1.6 billion (USD 250 million).

Center for Clean Energy (CCE)

CCE is a collaborative project between CAS and Huairou Science City. With construction started in May 2017, it is designed to be a platform for the measurement, diagnosis, and analysis of clean energy materials. It includes several subplatforms for advanced testing and analysis of chemical energy storage, physical energy storage, solar cells, and LEDs as well as a synchrotron radiation beamline end station for clean energy research. This project will significantly improve the testing of the safety and effectiveness of clean energy materials and devices. It will be the world's first platform to perform testing and analysis of these materials from the atomic to the macro scale, and is an example of IOP's innovative R&D. The final facility will cover 30,000 square meters and cost approximately 440 million RMB (USD 70 million).

Center for Materials Genome Initiative (CMGI)

CMGI also came about through the collaboration between CAS and Huairou Science City. It will bring together three main research processes: computation, synthesis, and characterization. CMGI will be China's largest platform for research into the materials genome, with the most sophisticated technology available. It is expected to greatly accelerate the discovery of new materials and significantly shorten the transition time between discovery and application. The planned construction area for CMGI is 40,000 square meters, with an investment of RMB 540 million (USD 86 million). Construction started in May 2017, and the center is expected to begin pilot runs by the end of 2020.

Looking forward

IOP has enjoyed a long and glorious journey through its first 90 years, with many remarkable achievements to its credit. Now, with unprecedented investment in attracting talents and expanding its research facilities, and with renewed vigor and confidence, IOP heads toward its grand centenary with great expectations.

Frontier research on superconductivity at the Institute of Physics

Xingjiang Zhou* and Jiangping Hu

A humble beginning

Superconductivity was discovered in 1911 by the Dutch physicist Heike Kamerlingh Onnes. However, superconductivity research in China started rather late. It began in the early 1960s after the Low Temperature Physics Lab was established at the Institute of Physics (IOP) in the late 1950s, which made liquid helium available. In the late 1970s, researchers at IOP introduced the idea of exploring superconductors with a high critical temperature. After reviewing the status of superconductivity research up to that time, Zhongxian Zhao proposed his ideas on how to search for high-temperature superconductors (*1*). National workshops on the exploration of high-critical-temperature superconductors were held every two years, from 1976 to 1986. These endeavors gathered a group of talents for superconductivity research in China and laid a solid foundation for the ensuing breakthroughs in this field.

High-temperature cuprate superconductors

In 1986, Bednorz and Mueller reported possible high-temperature superconductivity in the La (lanthanum)-Ba (barium)-Cu (copper)-O (oxygen) (La-Ba-Cu-O) system (*2*). Zhongxian Zhao was one of the earliest to realize the significance of the Bednorz–Mueller result in 1986. He immediately organized a team at IOP to work on the subject. They successfully prepared Sr(Ba)-La-Cu-O superconductors with a critical temperature (T_c) of over 40 K (*3*). Soon after, they independently discovered a Y (yttrium)-Ba (barium)-Cu (copper)-O (oxygen) (Y-Ba-Cu-O) superconductor with a high critical temperature, (T_c)≈92.8 K, which is above the boiling point of liquid nitrogen (77 K) (*4*). Because of the breakthrough in high-temperature superconductor research, the National Lab for Superconductivity was conceived by the Chinese government in 1988, and was fully established in 1991 at IOP. The lab, now equipped with advanced experimental techniques such as laser-based angle-resolved photoemission spectroscopy, neutron scattering, scanning tunneling microscopy, and nuclear magnetic resonance in extreme conditions of high pressure–low temperature and high magnetic fields, has become a national center for superconductivity research, a talent incubator, and a base for academic exchange among domestic and foreign scholars.

After more than 30 years of intensive research, the mechanism of high-temperature superconductivity in cuprate superconductors remains unclear. Taking advantage of the high resolution of the vacuum ultraviolet laser-based angle-resolved photoemission spectroscopy (ARPES) systems developed at IOP (*5*), Xingjiang Zhou's group has provided new information on the Fermi surface topology, energy gap, and many-body effects in cuprate superconductors (*6–11*). The pairing interaction functions, which provide important information for understanding the pairing mechanism in the high-temperature cuprate superconductors, are quantitatively determined (*11*).

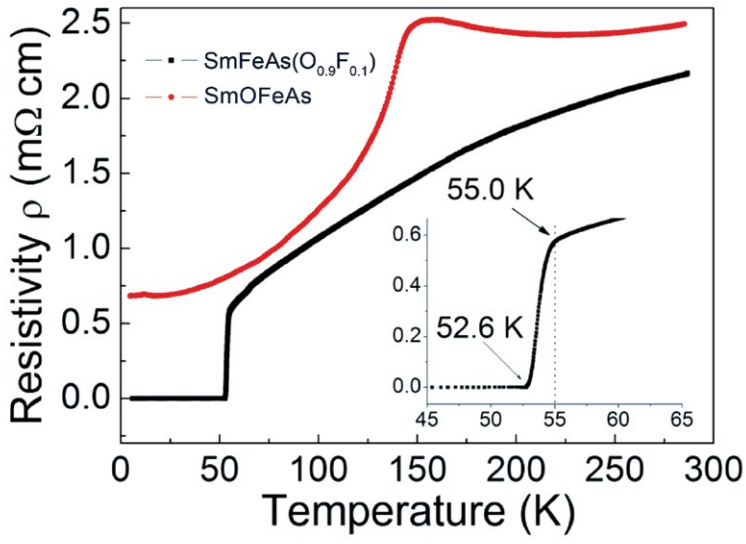

FIGURE 1. Discovery of superconductivity at 55 K in samarium (oxygen, fluoride) iron arsenide [$SmFeAs(O_{0.9}F_{0.1})$] (*18*).

Iron-based superconductors

In 2008, right after Hosono *et al.* reported their pioneering work on the observation of superconductivity with T_c≈26 K in an iron pnictide $LaFeAs[O_{1-x}F_x]$ (*12*), scientists in China, particularly those at IOP, quickly seized the opportunity and made significant contributions to the discovery of new iron-based superconductors and the study of their related physics and superconductivity mechanisms (*13–23*). A series of REFeAs(O,F) and $REFeAsO_{1-x}$ (RE=rare earth) superconductors were discovered with a T_c above 50 K (*17*), and a record high T_c of 55 K was discovered in the $SmFeAs(O_{0.9}F_{0.1})$ superconductor (Figure 1) by Zhongxian Zhao's group at IOP (*18*). Another class of iron-based superconductors, lithium iron arsenide (LiFeAs), was discovered by Changqing Jin's group at IOP, with a T_c of 18 K (*19*). Meanwhile, spin-density-wave instability was proposed in the parent compound lanthanum iron arsenic oxide (LaFeAsO) by Nanlin Wang's and Zhong Fang's

Institute of Physics, Chinese Academy of Sciences, Beijing, China
*Corresponding author: xjzhou@iphy.ac.cn

groups (*20*), and was later directly confirmed by neutron measurements (*21*). The first evidence of the Fermi surface sheet-dependent, nearly isotropic superconducting gap of the barium, potassium iron arsenide [$(Ba,K)Fe_2As_2$] superconductor (Figure 2) was revealed by the ARPES measurements at IOP (*22, 23*).

In 2010, by intercalating potassium (K) into the iron selenide (FeSe) superconductor, a new type of the iron-based superconductor potassium iron selenide $K_xFe_{2-y}Se_2$ was discovered by Xiaolong Chen's group at IOP, with $T_c \approx 32$ K (*24*), which is much higher than that of bulk FeSe ($T_c \approx 8$ K) (*25*). The $A_xFe_{2-y}Se_2$ [A= thallium (Tl), K, rubidium (Rb), cesium (Cs), etc.] superconductors show a distinct electronic structure in which only electron-like Fermi surface sheets are present (*26–28*). This presents a challenge to the Fermi-surface nesting picture, where the electron scattering between the hole-like Fermi surface sheets around the Brillouin zone center and the electron-like sheets around the zone corner is considered to play a dominant role in dictating the superconductivity of the iron-based superconductors. Two superconductivity domes were observed, and superconductivity with $T_c \approx 48$ K was achieved in the $A_xFe_{2-y}Se_2$ system under high pressure (*29*).

A remarkable discovery of superconductivity with an expected $T_c \approx 80$ K was reported in single-layer FeSe films grown on a $SrTiO_3$ substrate by Qikun Xue's group at Tsinghua University and IOP (*30*). Subsequent ARPES measurements on the superconducting single-layer FeSe/$SrTiO_3$ films by Xingjiang Zhou's group at IOP revealed the simplest electronic structure among the iron-based superconductors: There was no Fermi surface around the zone center and only electron pocket(s) around the zone corner (Figure 3) (*31*). A nearly isotropic superconducting gap was also observed (*31*). Optimization of carrier concentration resulted in the observation of the signature of superconductivity at $T_c \approx 65$ K (*32*), which was later confirmed by other groups (*33–35*). The single-layer FeSe/$SrTiO_3$ films with high T_c and a simple distinct electronic structure provide an ideal platform for studying interface superconductivity and superconductivity mechanisms in iron-based superconductors.

Inspired by the discovery of high-temperature superconductivity in single-layer FeSe/$SrTiO_3$ films, a new type of iron-based superconductor, lithium, iron hydroxide iron selenide [(Li,Fe)OHFeSe], with $T_c \approx 42$ K, was discovered by Xianhui Chen's group at the University of Science and Technology of China (*36*). Single crystals of this superconductor

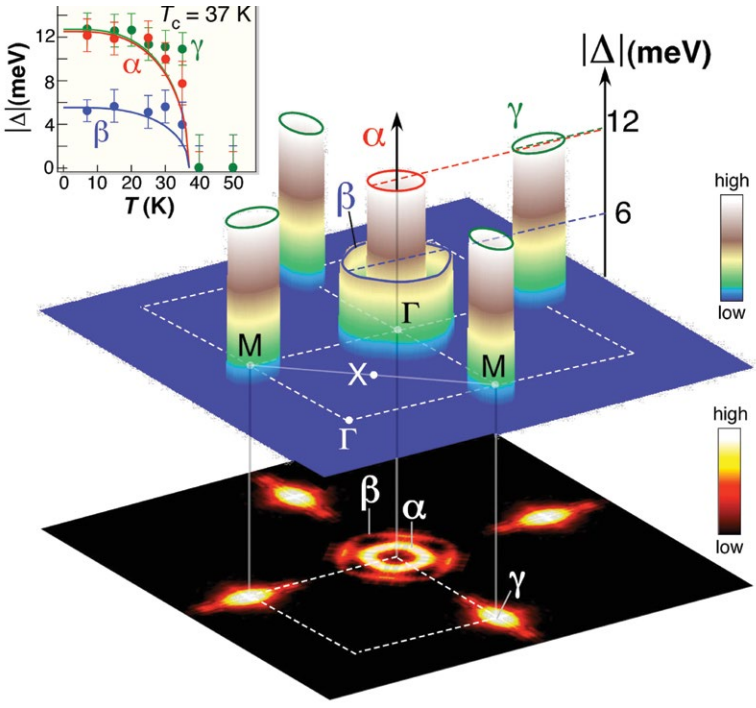

FIGURE 2. Superconducting gap in the barium, potassium iron arsenide [$(Ba,K)Fe_2As_2$] superconductor (*22, 23*).

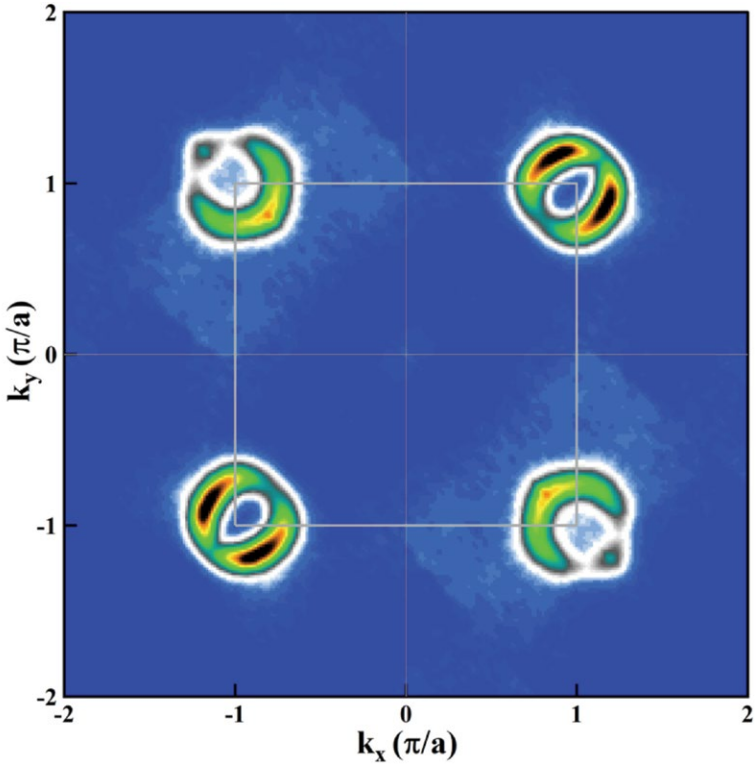

FIGURE 3. Distinct Fermi surface of the superconducting single-layer iron selenide/strontium titanium oxide (FeSe/$SrTiO_3$) films (*31*).

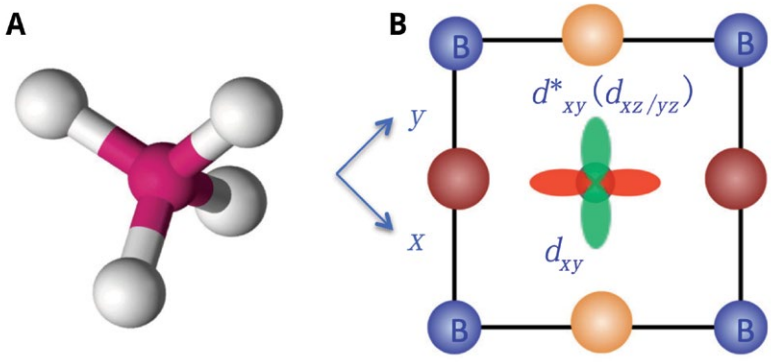

FIGURE 4. Local electronic environment of a tetrahedral complex (A) and selected orbitals (B) in iron-based superconductors (*43*).

were successfully grown at IOP, and the electronic phase diagram was established by Zhongxian Zhao's group (*37*). This single-phase bulk superconductor was found to exhibit an electronic structure very similar to that of the superconducting single-layer FeSe/$SrTiO_3$ films (*38*), providing new insights into the superconductivity mechanism in iron-based superconductors.

Chromium (Cr-) and manganese (Mn)-based superconductors

No superconductors were discovered in the chromium (Cr)- and manganese (Mn)-based 3*d* transition-metal compounds for a long time. The breakthrough came when IOP scientists in Jianlin Luo's and Jinguang Cheng's groups discovered superconductivity in chromium arsenide (CrAs) (*39*) and manganese phosphide (MnP) (*40*) under high pressure. This led to the subsequent discovery of superconductivity in $A_2Cr_3As_2$ [A=potassium (K), rubidium (Rb), and cesium (Cs)] at ambient pressure (*41*). These superconductors provide new platforms for finding new superconductors and for the investigation of unconventional superconductivity mechanisms in strongly correlated electron systems.

Theory of superconductivity

IOP has a group of theorists who are dedicated to superconductivity research. The research is characterized by strong collaborations between theoretical and experimental research groups at the institute. Lu Yu published his famous Yu-Shiba state paper in the 1960s (*42*), and has been actively researching high-temperature superconductors for several decades. A group led by Tao Xiang developed state-of-the-art numerical techniques to tackle the problems related to strongly correlated electron systems. Many theorists at IOP have made important contributions toward understanding iron-based superconductors. Jiangping Hu's group is particularly active in the study of iron-based superconductors. By analyzing the characteristics of high-temperature cuprate superconductors and iron-based superconductors, he recently suggested that there is a material gene to regulate the electronic structure of unconventional high-temperature superconductivity, and has made explicit predictions to realize high-T_c superconductivity in cobalt/nickel (Co/Ni)-based materials (Figure 4) (*43*).

References

1. Z. X. Zhao, *Physics* **4**, 211–216 (1977).
2. J. B. Bednorz, A. Mueller, *Z. Phys. B* **64**, 189–193 (1986).
3. Z. X. Zhao *et al.*, *Chin. Sci. Bull.* **3**, 177–179 (1987) (in Chinese).
4. Z. X. Zhao *et al.*, *Chin. Sci. Bull.* **6**, 412–414 (1987).
5. G. D. Liu *et al.*, *Rev. Sci. Instrum.* **79**, 023105 (2008).
6. W. T. Zhang *et al.*, *Phys. Rev. Lett.* **100**, 107002 (2008).
7. W. T. Zhang *et al.*, *Phys. Rev. Lett.* **101**, 017002 (2008).
8. J. Q. Meng *et al.*, *Nature* **462**, 335 (2009).
9. Y. Y. Peng *et al.*, *Nat. Commun.* **4**, 2459 (2013).
10. J. F. He *et al.*, *Phys. Rev. Lett.* **111**, 107005 (2013).
11. J. M. Bok *et al.*, *Sci. Adv.* **2**, e1501329 (2016).
12. Y. Kamihara *et al.*, *J. Am. Chem. Soc.* **130**, 3296 (2008).
13. G. F. Chen *et al.*, *Phys. Rev. Lett.* **101**, 057007 (2008).
14. H. H. Wen *et al.*, *Europhys. Lett.* **82**, 17009 (2008).
15. X. H. Chen *et al.*, *Nature* **453**, 761–762 (2008).
16. G. F. Chen *et al.*, *Phys. Rev. Lett.* **100**, 247002 (2008).
17. Z. A. Ren *et al.*, *Mater. Res. Innov.* **12**, 105–106 (2008).
18. Z. A. Ren *et al.*, *Chin. Phys. Lett.* **25**, 2215–2216 (2008).
19. X. C. Wang *et al.*, *Solid State Comm.* **148**, 538 (2008).
20. J. Dong *et al.*, *Europhys. Lett.* **83**, 27006 (2008).
21. C. de la Cruz *et al.*, *Nature* **453**, 899–902 (2008).
22. L. Zhao *et al.*, *Chin. Phys. Lett.* **25**, 4402 (2008).
23 H. Ding *et al.*, *Europhys. Lett.* **83**, 47001 (2008).
24. J. Guo *et al.*, *Phys. Rev. B* **82**, 180520(R) (2010).
25. F.-C. Hsu *et al.*, *Proc. Nat. Acad. Sci. U.S.A.* **105**, 14262–14264 (2008).
26. Y. Zhang *et al.*, *Nat. Mater.* **10**, 273–277 (2011).
27. T. Qian *et al.*, *Phys. Rev. Lett.* **106**, 187001 (2011).
28. D. X. Mou *et al.*, *Phys. Rev. Lett.* **106**, 107001 (2011).
29. L. L. Sun *et al.*, *Nature* **483**, 67–69 (2012).
30. Q. Y. Wang *et al.*, *Chin. Phys. Lett.* **29**, 03740 (2012).
31. D. F. Liu *et al.*, *Nat. Commun.* **3**, 931 (2012).
32. S. L. He *et al.*, *Nat. Mater.* **12**, 605 (2013).
33. S. Y. Tan *et al.*, *Nat. Mater.* **12**, 634 (2013).
34. J. J. Lee *et al.*, *Nature* **515**, 245 (2014).
35. Z. C. Zhang *et al.*, *Sci. Bull.* **60**, 1301 (2015).
36. X. F. Lu *et al.*, *Nat. Mater.* **14**, 325–329 (2015).
37. X. L. Dong *et al.*, *J. Am. Chem. Soc.* **137**, 66 (2015).
38. L. Zhao *et al.*, *Nat. Commun.* **7**, 10608 (2016).
39. W. Wu *et al.*, *Nat. Commun.* **5**, 5508 (2014).
40. J. G. Cheng *et al.*, *Phys. Rev. Lett.* **114**, 117001 (2015).
41. J. K. Bao *et al.*, *Phys. Rev. X* **5**, 011013 (2015).
42. L. Yu, *Acta Phys. Sin.* **21**, 75–91 (1965).
43. J. P. Hu, *Sci. Bull.* **61**, 561–569 (2016).

Topological quantum matter

Hongming Weng[1,2], Chen Fang[1], Tian Qian[1,2], Youguo Shi[1,2], and Zhong Fang[1,2]*

In 2016, the Nobel Prize for physics was awarded to three scientists who made theoretical discoveries of topological phase transitions and topological phases of matter. Topology is a branch of mathematics that studies the invariant properties of an object undergoing continuous deformation. Since the 1970s, physicists have realized that some states of matter can be identified by topological invariants, and topological phase transitions can happen without breaking any symmetry, which contrasts with the Landau–Ginzburg paradigm of phase transitions. A topological material has topological invariants different from the vacuum or the isolated atoms comprising it. This topological state is robust against external perturbations such as defect, disorder, and boundary configuration. One of the most distinct properties of a topological material is the existence of characteristic boundary states, or states having quantum anomalies, which are uniquely determined and protected by the topology in bulk. In the last 12 years, the field of topological quantum matter has developed rapidly after the breakthrough discovery of time-reversal symmetry (TRS) protected Z_2 topological insulators (TIs) (*1*). The concept of symmetry-protected topological states has since then been extended from states protected by TRS to those protected by crystalline symmetries, and from insulators to metals (*2*). Here, we would like to outline several activities performed at our institute in this noteworthy area of condensed matter physics.

The first activity at our institute can be traced back to 2003, when Zhong Fang *et al.* (*3*) found that the intrinsic contribution to anomalous Hall conductivity in ferromagnetic metals originates from the anomalous transversal velocity of electrons in the longitudinal current. Such anomalous velocity is caused by the Berry curvature, which is a Berry flux field with source and drain at the magnetic monopoles in the momentum space. In current terminology, these magnetic monopoles in the momentum space are called Weyl points (*4*).

Soon after Z_2 TIs based on graphene were proposed in 2005, it was found that the bandgap due to spin–orbit coupling at the Dirac points in graphene is negligibly small at approximately 10^{-6} eV. To increase the bandgap, Liu *et al.* (*5*) proposed silicene and other group IV elements with similar structures as two-dimensional (2D) TIs with considerably enhanced bandgaps. Chen *et al.* (*6*) synthesized silicene samples through molecular beam epitaxy. The electronic structure of silicene was further studied with scanning tunneling microscopy (STM) and angle-resolved photoemission spectroscopy (ARPES)

[1]Beijing National Laboratory for Condensed Matter Physics and Institute of Physics, Chinese Academy of Sciences, Beijing, China
[2]Collaborative Innovation Center of Quantum Matter, Beijing, China
*Corresponding author: zfang@iphy.ac.cn

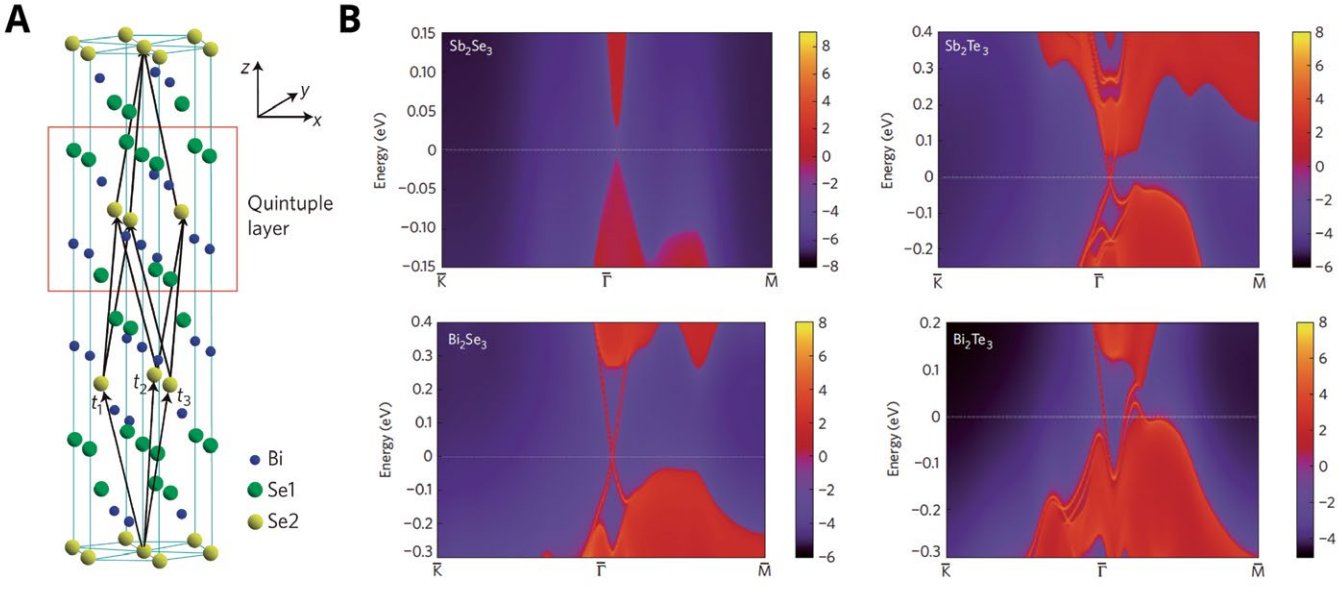

FIGURE 1. 3D Topological insulators of bismuth selenide (Bi_2Se_3) family compounds. (**A**) Crystal structure of Bi_2Se_3 and (**B**) the topological Dirac cone on the (111) surface for each of them. [Adapted from (*13*).]

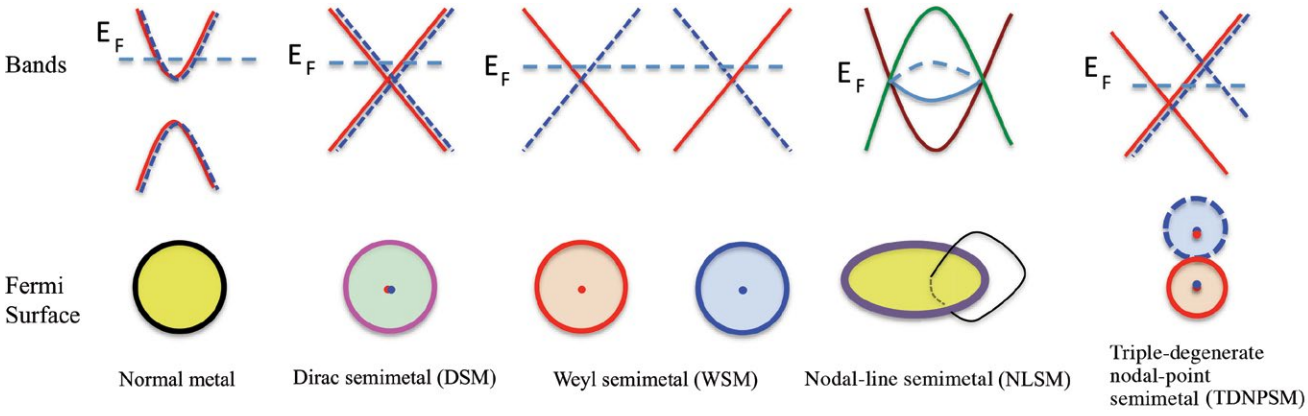

FIGURE 2. The family of topological semimetals. The upper panel is the band structure for each family member, and the corresponding Fermi surface is shown in the lower panel. In the triple-degenerate nodal-point semimetal (TDNPSM), the electron and hole pockets are represented as solid and dashed circles, respectively. The magnetic monopoles of opposite charges are denoted by red and blue dots. [Adapted from (*16*).]

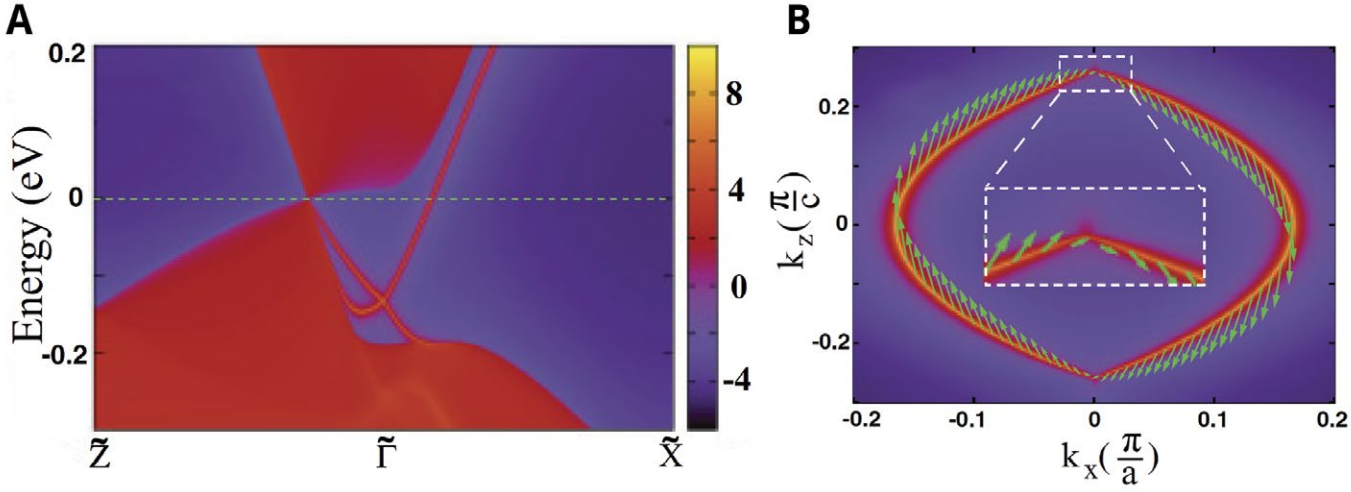

FIGURE 3. The (010)-surface state of Dirac semimetal sodium bismuthide (Na_3Bi). (**A**) Surface band structure with projection of bulk Dirac point and surface Dirac cone. (**B**) Surface Fermi arcs and the in-plane spin vectors on them. [Adapted from (*17*).]

instruments (*7*). Thereafter, silicene has been extensively researched as a promising 2D material compatible with current silicon-based electronic devices. However, the relatively small bandgaps of silicene (1.55 meV) and other 2D TIs like mercury telluride/cadmium telluride (HgTe/CdTe) and gallium antimonide/indium arsenide (GaSb/InAs) quantum wells make the identification and application of their topological helical edge states challenging. In 2014, Weng *et al.* (*8*) proposed 2D TIs, namely the single layers of zirconium pentatelluride ($ZrTe_5$) and hafnium pentatelluride ($HfTe_5$), with bandgaps as large as 0.1 eV. It was further proposed that their 3D crystals, which are stacks of weakly coupled layers, are very close to the topological phase transition point between a strong and a weak TI. This generated controversies on the nature of their topological states. High-quality samples of $ZrTe_5$ and $HfTe_5$ were synthesized at our institute. STM (*9*), ARPES (*10*), transport (*11*), and optical (*12*) measurements were performed on them. These efforts revealed that while the 3D $ZrTe_5$ would be a weak TI, $HfTe_5$ might display all three phases, namely strong TI, Dirac semimetal (DSM), and weak TI, with changes in temperature.

Compared with their 2D counterparts, more 3D TIs were discovered in the early days of the field. Bismuth selenide (Bi_2Se_3) family compounds shown in Figure 1 are probably the most well known and have been extensively studied. Nearly all the topological features of 3D TIs have been closely inspected in them. This family was theoretically predicted by Zhang *et al.* (*13*) in 2009. In 2010, Yu *et al.* (*14*) proposed that chromium (Cr)- or iron (Fe)-doped thin films of Bi_2Se_3 family compounds can realize the long-sought quantum anomalous Hall (QAH) effect. They

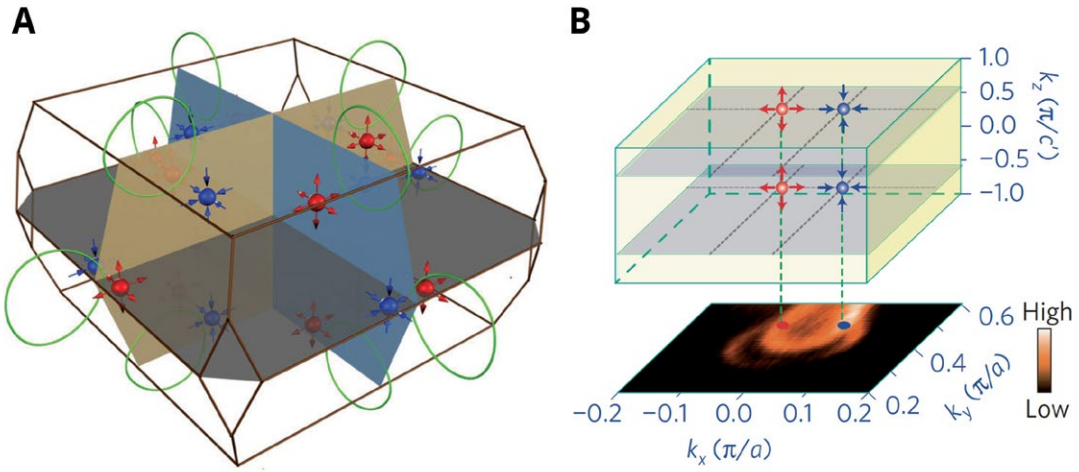

FIGURE 4. Weyl semimetal of tantalum arsenide (TaAs) family compounds. (**A**) The Weyl nodes of opposite chirality (red and blue spheres) distributed in the momentum space. (**B**) The experimentally observed Fermi arc (lower panel) connecting the projection of bulk Weyl nodes on the (001) surface. [Adapted from (*22*) and (*25*).]

revealed that the considerably enhanced susceptibility of Van Vleck paramagnetism due to band inversion creates ferromagnetic insulators, which are different from the carrier-mediated magnetic coupling seen in other systems. This finding was later followed by Chang *et al.* (*15*), who succeeded in demonstrating the first QAH effect.

Meanwhile, topological semimetals (TSMs) were developed in parallel, and now comprise DSM, Weyl semimetals (WSMs), nodal-line semimetals (NLSMs), and multidegenerate nodal-point semimetals, as shown in Figure 2 (*16*). Soon after the proposal of Z_2 TIs, WSMs and DSMs were proposed as possible during the topological phase transition between a normal insulator and TI in 3D, but it is not easy to realize transition by fine-tuning real materials. Inspired by the band inversion mechanism in TIs, Zhong Fang's team at IOP proposed that crystal symmetry can protect band-crossing points if the two inverted bands belong to different irreducible representations. This led to the successful prediction of two DSM materials, sodium bismuthide (Na_3Bi) (*17*) and cadmium arsenide (Cd_3As_2) (*18*), with unique surface states including Fermi arcs, as the former material is shown in Figure 3. In 2014, Chen's team at Oxford University collaborated with Fang's team to experimentally confirm the predictions (*19, 20*). Na_3Bi and Cd_3As_2 are the first two members of the TSM family.

The discovery of DSMs has stimulated the realization of WSMs, as breaking either the TRS or inversion symmetry would cause the separation of Dirac points into Weyl points. In 2011, magnetic WSMs were proposed in magnetic pyrochlore iridates and spinel mercury chromium selenide ($HgCr_2Se_4$) (*21*), but neither prediction has been experimentally confirmed. In 2015, Weng *et al.* (*22*) predicted that tantalum arsenide (TaAs) family compounds including TaAs, tantalum phosphide (TaP), niobium arsenide (NbAs), and niobium phosphide (NbP), are WSMs. Thereafter, TaAs samples were synthesized and chiral anomaly effects were observed by Huang *et al.* (*23*). Lv *et al.* (*24*) performed ARPES measurements on these samples and observed the surface Fermi arcs, which are a hallmark of WSM, as shown in Figure 4. Further studies observed the Weyl nodes in bulk (*25*) and the spin texture (*26*) of Fermi arcs for TaAs. This series of studies announced the discovery of WSM in the TaAs family, which is the first observation of the behavior of Weyl fermions in solids since its original proposal in 1929 by Hermann Weyl, and has been selected as one of *Physics World* magazine's "Top 10 Breakthroughs of 2015" and one of 2015's "Highlights of the Year" by *Physics*. In 2018, both the theoretical prediction and experimental verification papers on TaAs were selected by the American Physical Society to celebrate the 125th anniversary of the *Physical Review* journals.

Dirac and Weyl fermions in solids were first studied in the context of high-energy physics as elementary particles. However, further exploration of the "materials universe" resulted in proposals for the existence of "new fermions" in solids that have no counterpart in field theories. This included the NLSMs (*27*) and the multidegenerate nodal-point semimetals, both of which are incompatible with Lorentz invariance but protected by lattice symmetries. It was proposed that the lattices with nonsymmorphic space group symmetry could stabilize 3-, 6- and 8-fold degenerate nodal points at certain momenta on the boundary of the Brillouin zone. However, Weng *et al.* (*28*) proposed an alternative route for realizing the triply degenerate nodal points (TDNPs): They are the results of band inversion between two doubly degenerate bands and one nondegenerate band, and can be protected by certain point group symmetries instead of nonsymmorphic ones. They predicted that tantalum nitride (TaN) and zirconium telluride (ZrTe) with tungsten carbide (WC)-type crystal structure have TDNPs around the Fermi level, and that these nodal points can move freely along rotation invariant lines in the momentum space instead of being fixed at specific momenta. Shi's team synthesized the single crystals of WC-type molybdenum phosphide

(MoP), and Lv *et al.* (*29*) reported their experimental observation of TDNPs. This is the first experimental verification of three-component fermions in solids. Chen's team synthesized the single crystal of WC and reported on its anisotropic longitudinal magnetoresistivity (*30*), which contrasts with the isotropic resistivity in WSMs and DSMs, but is consistent with the expected response of the TDNPs. The distinct quantum phenomena related to the unconventional three-component fermions are very interesting, and the studies in this direction are at the nascent stage.

As can be seen from the above summary, the researchers at our institute work in close collaboration and have formed an efficient working circle comprising materials prediction, sample synthesis, and experimental measurements. The frequent and timely discussions among these three different groups have stimulated several worthy ideas and greatly advanced scientific progress.

References

1. H. Weng, X. Dai, Z. Fang, *MRS Bulletin* **39**, 849–858 (2014).
2. H. Weng, X. Dai, Z. Fang, *J. Phys. Cond. Matter* **28**, 303001 (2016).
3. Z. Fang *et al.*, *Science* **302**, 92–95 (2003).
4. H. Weng, R. Yu, X. Hu, X. Dai, Z. Fang, *Adv. Phys.* **64**, 227–282 (2015).
5. C. Liu, W. Feng, Y. Yao, *Phys. Rev. Lett.* **107**, 076802 (2011).
6. L. Chen *et al.*, *Phys. Rev. Lett.* **109**, 056804 (2012).
7. Y. Feng *et al.*, *Proc. Nat. Acad. Sci. U.S.A.* **113**, 14656–14661 (2016).
8. H. Weng, X. Dai, Z. Fang, *Phys. Rev. X* **4**, 011002 (2014).
9. R. Wu *et al.*, *Phys. Rev. X* **6**, 021017 (2016).
10. Y. Zhang *et al.*, *Nat. Commun.* **8**, 15512 (2017).
11. L. Zhao *et al.*, *Chin. Phys. Lett.* **34**, 037102 (2017).
12. Z. Chen *et al.*, *Proc. Nat. Acad. Sci. U.S.A.* **114**, 816–821 (2017).
13. H. Zhang *et al.*, *Nat. Phys.* **5**, 438 (2009).
14. R. Yu *et al.*, *Science* **329**, 61–64 (2010).
15. C.-Z. Chang *et al.*, *Science* **340**, 167–170 (2013).
16. H. Weng, C. Fang, Z. Fang, X. Dai, *Nat. Sci. Rev.* **4**, 798–799 (2017).
17. Z. Wang *et al.*, *Phys. Rev. B* **85**, 195320 (2012).
18. Z. Wang *et al.*, *Phys. Rev. B* **88**, 125427 (2013).
19. Z. Liu *et al.*, *Science* **343**, 864–867 (2014).
20. Z. Liu *et al.*, *Nat. Mater.* **13**, 677–681 (2014).
21. G. Xu, H. Weng, Z. Wang, X. Dai, Z. Fang, *Phys. Rev. Lett.* **107**, 186806 (2011).
22. H. Weng, C. Fang, Z. Fang, B. A. Bernevig, X. Dai, *Phys. Rev. X* **5**, 011029 (2015).
23. X. Huang *et al.*, *Phys. Rev. X* **5**, 031023 (2015).
24. B. Lv *et al.*, *Phys. Rev. X* **5**, 031013 (2015).
25. B. Lv *et al.*, *Nat. Phys.* **11**, 724–727 (2015).
26. B. Lv *et al.*, *Phys. Rev. Lett.* **115**, 217601 (2015).
27. C. Fang, H. Weng, X. Dai, Z. Fang, *Chin. Phys. B* **25**, 117106 (2016).
28. H. Weng, C. Fang, Z. Fang, X. Dai, *Phys. Rev. B* **93**, 241202(R) (2016).
29. B. Lv *et al.*, *Nature* **546**, 627–631 (2017).
30. J. B. He *et al.*, *Phys. Rev. B* **95**, 195165 (2017).

Two-dimensional materials research

Guangyu Zhang*, Shixuan Du, Kehui Wu, and Hong-Jun Gao

The National Research Center for Condensed Matter Physics and the Institute of Physics (IOP) of the Chinese Academy of Sciences have devoted much effort to many emerging frontiers in the field of condensed matter physics. In 2001, the Nanoscale Physics and Devices Laboratory was established at IOP, with a focus on nanoscale science and technology research. In recent years, the discovery of graphene, an atomically thin material possessing exotic physical properties and having wide-ranging potential applications, has boosted a new research field—the study of two-dimensional (2D) materials. This field has introduced many new concepts into conventional materials science, condensed matter physics, and electronic engineering.

Several research groups at IOP focus on 2D materials research, in order to design and create new materials with unexpected properties and tailoring, and to characterize the structures of 2D materials for elaborate band-structure modulation and functional device applications. The main research activities are described below.

Tailoring graphene by substrates and nanostructures

Graphene growth is usually assisted by a catalytic process. Fabrication of large-scale, high-quality graphene (G) is one of the main challenges in the field of graphene research. Hong-Jun Gao's group has successfully grown defect-free, single-crystalline graphene at the centimeter scale on ruthenium [Ru(0001)] with a highly ordered moiré pattern (*1, 2*). The pattern provides an ideal template for selective absorption of molecules, monodispersed metal atoms, or clusters (*3–10*). The periodic bumps behave like quantum dots with tunable thermoelectric properties. For practical application in nanoelectronic devices, Gao's group developed a technique to intercalate silicon and other elements at the G/Ru interface (Figure 1) (*11–13*) in order to decouple the interaction between graphene and metal crystals.

Since most of graphene-based electronic devices are fabricated on insulating substrates, scaled-up growth of high-quality graphene on insulating surfaces is of technological importance. To this end, Guangyu Zhang's group developed a catalyst-free, plasma-enhanced chemical vapor deposition (PECVD) technique to grow graphene on various insulating substrates at relatively

Institute of Physics, Chinese Academy of Sciences, Beijing, China
*Corresponding author: gyzhang@iphy.ac.cn

low growth temperatures (*14*). They also realized the epitaxial growth of nontwisted graphene on hexagonal boron nitride (G/h-BN) (*15, 16*). The large moiré superlattice originating from the nontwisting overlapping of graphene and h-BN had strong modulation effects on the band structure (Figure 2). Transport measurements on such superlattice samples revealed that superlattice Dirac points and Landau levels originated from the 2D superlattice. Owing to the clean interface, they could observe the fractal gaps of Hofstadter's butterfly, optical transitions between different Landau levels, and optical transitions between superlattice minibands (*17, 18*). Recently, Chen *et al.* characterized polaritons in G/h-BN and found that hyperbolic phonon polaritons in h-BN possess a high quality factor (Q ~ 33), ultraslow group velocity [~2×10^{-4} *c* (where *c* is the speed of light in a vacuum)], and a controll-able dispersion relation. They also identified a new hybridized polariton mode in G/h-BN with a long lifetime of ~1.6 ps (*19, 20*).

Zhang's group developed an anisotropic etching-based "top-down" fabrication technique for graphene nanostructures (Figure 2B) (*21, 22*). The as-fabricated graphene nanostructures have zigzag edge terminations and well-defined line widths (with sub-10 nm resolution capability), benefiting from the anisotropic etching effect in graphene's basal plane. Such zigzag graphene nanostructures are ideal experimental objects for investigating the quantum confinement effect, edge-state related transport, and valleytronics in graphene.

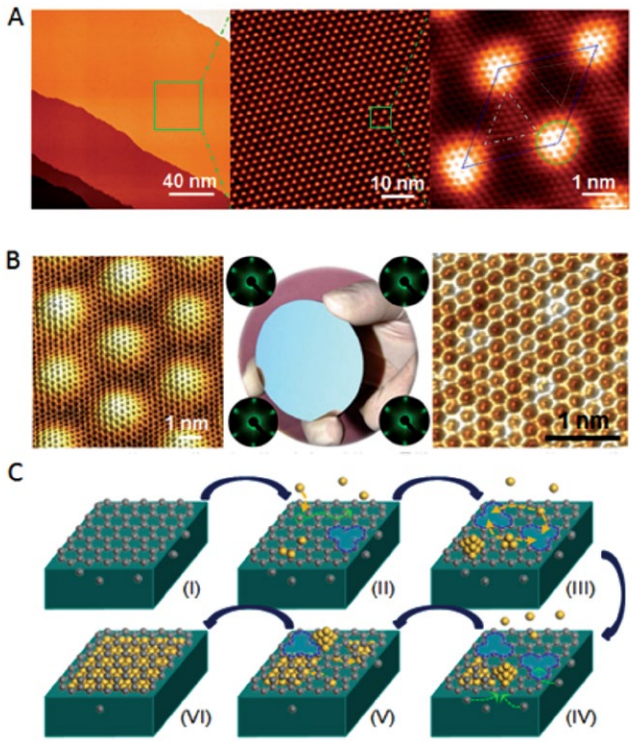

FIGURE 1. Epitaxial graphene and Si intercalation. (**A**) Scanning tunneling microscope (STM) images of graphene/ruthenium (G/Ru). (**B**) STM images of G/Ru (left) and after silicon (Si) intercalation (right). Low-energy electron diffraction (LEED) pattern (middle) of the entire sample indicates high-quality graphene over the entire surface. (**C**) Schematic of Si intercalation process.

FIGURE 2. Engineering of graphene superlattice and nanostructures. (**A**) Graphene (G) epitaxy on hexagonal boron nitride (h-BN): A 2D superlattice structure. (**B**) Fabrication of graphene nanostructure by anisotropic etching. (**C**) Transport measurements on G/h-BN superlattice.

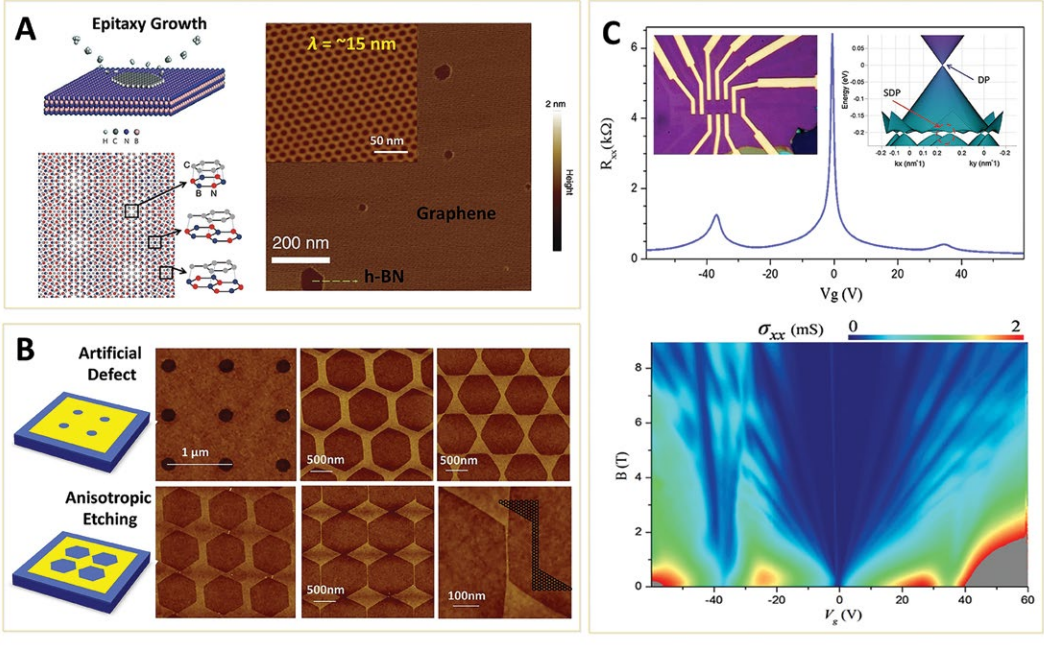

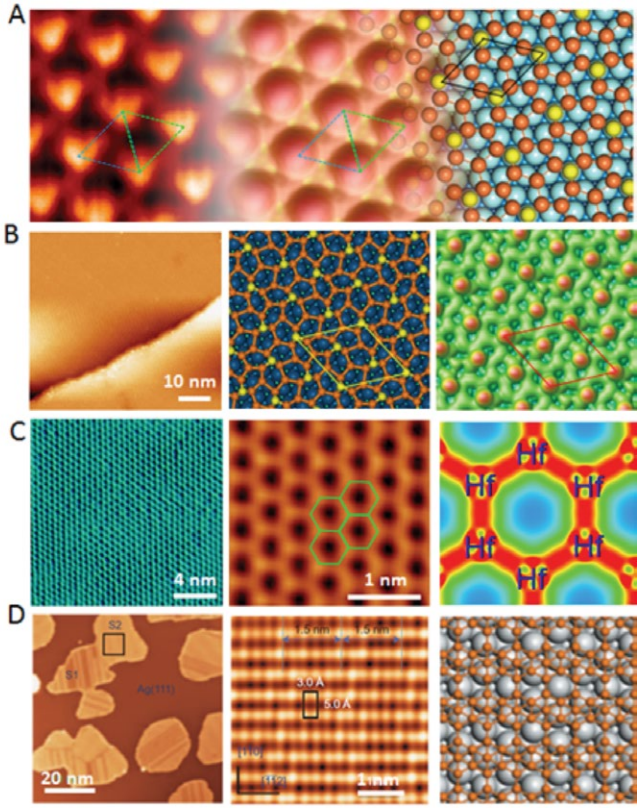

FIGURE 3. Epitaxial Xene on metal substrate. (**A**) Scanning tunneling microscope (STM) images and configuration of silicene/iridium [Ir(111)]. (**B**) STM image, configuration, and STM simulation of germanene/platinum [Pt(111)]. (**C**) STM images and charge density of hafnene/Ir(111). (**D**) STM images and configuration of borophene/silver [Ag(111)].

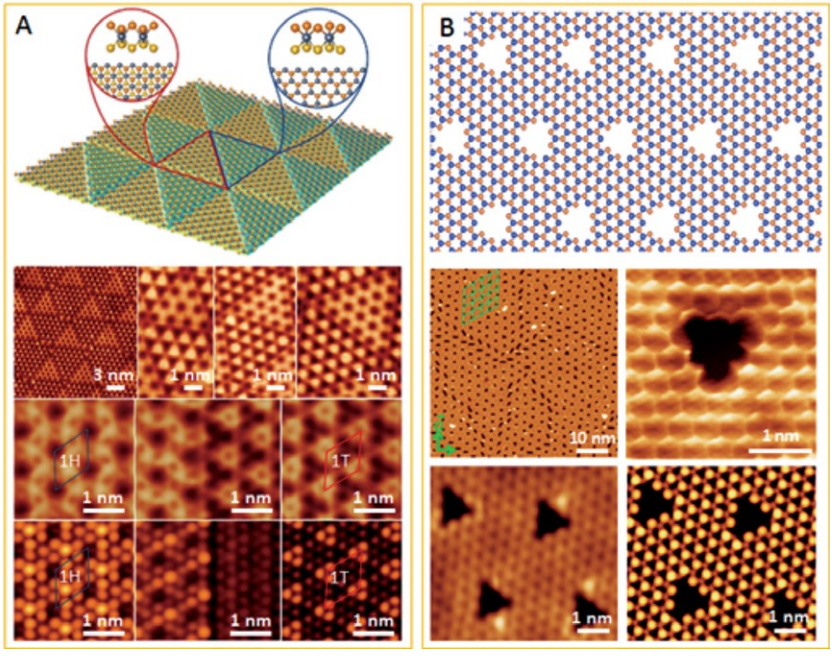

FIGURE 4. Intrinsically patterned 2D materials. (**A**) Patterned platinum diselenide (PtSe2) monolayer: schematic, scanning tunneling microscope (STM) images, and STM simulations. (**B**) Patterned copper selenide (CuSe) monolayer: schematic, STM images, and STM simulation.

Single-element 2D materials beyond graphene

Novel 2D materials can be epitaxially grown on single-crystal surfaces. Gao's and Wu's groups conducted pioneering studies on silicene with a honeycomb lattice epitaxy in ultrahigh vacuum (UHV) on iridium [Ir(111)] and silver [Ag(111)], respectively (Figure 3) (*23, 24*). Gao's group found that the growth of silicene on Ru(0001) evolves from a herringbone structure toward a buckled honeycomb lattice. Wu's group found that such a buckled honeycomb lattice could host the Dirac cone structure in the energy bands, and that hydrogenation of silicene is an effective way to protect it from oxidation (*25, 26*).

Gao's group is the first to create germanene and hafnene (Figure 3B, 3C) (*27–29*). Further experiments provide evidence of the Dirac signature in bilayer germanene on copper [Cu(111)]. The honeycomb lattice of hafnene is metallic with a spin-polarized *d*-dominated state near the Fermi level. Wu's group reported the realization of 2D boron sheets by molecular beam epitaxy (MBE) (Figure 3D). Two types of boron sheets comprising a triangular boron lattice with different arrangements of hexagonal holes have been identified and are quite stable against oxidization. Dirac cones in the energy band of 2D boron sheets were also revealed (*30, 31*).

Binary 2D materials beyond graphene

Binary 2D materials have enhanced properties and diverse materials options. Gao's group developed a direct selenization method to grow selenide monolayers in a UHV chamber by standard molecular beam epitaxy (MBE) (*32*). With this simple process, they successfully synthesized platinum diselenide ($PtSe_2$), hafnium tritelluride ($HfTe_3$), hafnium pentatelluride ($HfTe_5$), and copper selenide (CuSe) monolayers. Direct tellurization of Hf(0001) results in the spontaneous fabrication of a

$HfTe_3$-$HfTe_5$-Hf lateral heterostructure (*33*), which offers new routes for the construction of related functional heterostructures. Moreover, Gao's group found that $PtSe_2$ and CuSe monolayers are intrinsically patterned (Figure 4) (*34*), and are thus ideal templates for selective adsorptions of either molecules or magnetic metal–containing clusters. Spin-layer locking by local Rashba effect in the as-synthesized 1T-$PtSe_2$ was observed, indicating that 1T-$PtSe_2$ is a promising photocatalyst and valleytronic material.

Besides the surface reaction process, the standard chemical vapor deposition (CVD) process provides another option to grow binary 2D materials directly on insulating substrates. Zhang's group developed an oxygen-assisted CVD method for the growth of high-quality monolayer molybdenum disulfide (MoS_2) (*35, 36*). Using this method, they grew wafer-scale, highly oriented, and continuous monolayer MoS_2, representing a significant step toward the realization of wafer-scale monolayer MoS_2 devices for potential electronic and optoelectronic applications (*36*). Recently, they found that an argon (Ar)-plasma treatment could locally induce 2H-1T phase transition in monolayer MoS_2 (*37*).

Device applications based on 2D materials

Exploration of 2D materials for certain novel applications has been a driving force in this field. Zhang's group explored various 2D material-based nanodevices for electronic applications, such as graphene nanoelectromechanical system (NEMS) switch devices, ultrasensitive graphene strain sensors and electronic skin, graphene-based charge-trapping memories, and graphene nanogap multilevel memristor devices (*38–46*). They also demonstrated highly sensitive humidity sensors based on monolayer MoS_2 films with clean surfaces. Moreover, they explored graphene-contacted ultrashort channel monolayer MoS_2 field-effect transistors with channel lengths scaled down to ~4 nm, exhibiting excellent immunity to short-channel effects.

In summary, 2D materials research at IOP has rapidly developed over the past decade. A series of studies have been devoted to 2D materials with a focus on developing state-of-the-art epitaxial growth techniques by probing and manipulating their atomic, electronic, optical, and magnetic structures using advanced characterization techniques, and exploring their potential applications in electronics, optoelectronics, and spintronics.

References

1. Y. Pan, D.-X. Shi, H.-J. Gao, *Chin. Phys.* **16**, 3151 (2007).
2. Y. Pan *et al., Adv. Mater.* **21**, 2777–2780 (2009).
3. J. Mao *et al.*, *J. Am. Chem. Soc.* **131**, 14136–14137 (2009).
4. H. T. Zhou *et al.*, *Appl. Phys. Lett.* **99**, 153101 (2011).
5. H. G. Zhang *et al.*, *Phys. Rev. B* **84**, 245436 (2011).
6. G. Li *et al.*, *Appl. Phys. Lett*. **100**, 013304 (2012).
7. H. G. Zhang *et al.*, *J. Phys. Cond. Matter* **22**, 302001 (2010).
8. J. D. Ren *et al.*, *Phys. Rev. Lett*. **119**, 176806 (2017).
9. Y. Pan, M. Gao, L. Huang, F. Liu, H.-J. Gao, *Appl. Phys. Lett.* **95**, 093106 (2009).
10. J. D. Ren *et al.*, *Nano Lett.* **14**, 4011–4015 (2014).
11. G. Li *et al.*, *J. Am. Chem. Soc.* **137**, 7099–7103 (2015).
12. L. Huang *et al.*, *Appl. Phys. Lett.* **99**, 163107 (2011).
13. J. H. Mao *et al.*, *Appl. Phys. Lett.* **100**, 093101 (2012).
14. L. C. Zhang *et al.*, *Nano Res.* **4**, 315–321 (2011).
15. W. Yang *et al.*, *Nat. Mater.* **12**, 792–797 (2013).
16. W. Yang *et al.*, *Nano Lett.* **16**, 2387–2392 (2016).
17. Z. W. Shi *et al.*, *Nat. Phys.* **10**, 743–747 (2014).
18. Z. G. Chen *et al.*, *Nat. Commun.* **5**, 4461 (2014).
19. J. H. Duan *et al.*, *Adv. Mater.* **29**, 1702494 (2017).
20. X. X. Yang *et al.*, *Adv. Mater.* **28**, 2931–2938 (2016).
21. R. Yang *et al.*, *Adv. Mater.* **22**, 4014–4019 (2010).
22. Z. Shi *et al.*, *Adv. Mater.* **23**, 3061–3065 (2011).
23. B. J. Feng *et al.*, *Nano Lett.* **12**, 3507–3511 (2012).
24. L. Meng *et al.*, *Nano Lett.* **13**, 685–690 (2013).
25. L. Chen *et al.*, *Phys. Rev. Lett.* **109**, 056804 (2012).
26. J. L. Qiu *et al.*, *Phys. Rev. Lett.* **114**, 126101 (2015).
27. L. F. Li *et al.*, *Adv. Mater.* **26**, 4820–4824 (2014).
28. Z. H. Qin *et al.*, *Adv. Mater.* **29**, 1606046 (2017).
29. L. F. Li *et al.*, *Nano Lett.* **13**, 4671–4674 (2013).
30. B. J. Feng *et al.*, *Nat. Chem.* **8**, 563–568 (2016).
31. B. Feng *et al.*, *Phys. Rev. Lett.* **118**, 096401 (2017).
32. Y. Wang *et al.*, *Nano Lett.* **15**, 4013–4018 (2015).
33. Y. Q. Wang *et al., Adv. Mater.* **28**, 5013–5017 (2016).
34. X. Lin *et al.*, *Nat. Mater.* **16**, 717–721 (2017).
35. W. Chen *et al.*, *J. Am. Chem. Soc.* **137**, 15632–15635 (2015).
36. H. Yu *et al.*, *ACS Nano* **11**, 12001–12007 (2017).
37. J. Zhu *et al.*, *J. Am. Chem. Soc.* **139**, 10216–10219 (2017).
38. Z. Shi *et al.*, *Nano Res.* **5**, 82–87 (2012).
39. Y. Wang *et al.*, *ACS Nano* **5**, 3645–3650 (2011).
40. J. Zhao *et al.*, *Appl. Phys. Lett.* **101**, 063112 (2012).
41. J. Zhao *et al.*, *ACS Nano* **9**, 1622–1629 (2015).
42. R. Yang *et al.*, *Sci. Rep.* **3**, 2126 (2013).
43. C. He *et al., ACS Nano* **6**, 4214–4221 (2012).
44. C. He *et al.*, *Adv. Mater.* **25**, 5593–5598 (2013).
45. J. Zhao *et al.*, *Adv. Mater.* **29**, 1702076 (2017).
46. L. Xie *et al.*, *Adv. Mater.* **29**, 1702522 (2017).

Electron microscopy for revealing structural features at atomic scale

Xiaozhi Liu[1,2], Binghui Ge[1], Zhi Xu[1], and Lin Gu[1,2,3*]

The desire to explore the fine structural features of materials and living organisms has constantly prompted the development of various microscopic instruments. Among these, the electron microscope (EM) received the significant attention of researchers by virtue of the short wavelength of the electron. Disappointed with its spatial resolution in earlier days, Richard Feynman put out a challenge in 1959: "Is there no way to make the electron microscope more powerful?" (*1*). Fortunately, almost 60 years later, the transmission electron microscope (TEM) with subangstrom spatial resolution has become a powerful structural characterization tool for condensed matter physics, materials science, nanotechnology, and even structural biology.

TEM can collect diverse signals generated from the interactions between fast-moving incident electrons and specimens, providing important information regarding structural features and chemical characteristics. As a result, close examination of the lattice, charge, orbital, spin, and their correlations in a local sample region has become feasible. Advanced TEM can operate in various modes, including high-resolution TEM (HRTEM), scanning TEM (STEM), and energy-filtered TEM (EFTEM), among others. Owing to its versatility, TEM has become increasingly indispensable in advanced materials research concerning quantum confinement, topological systems, quantum information, strongly correlated systems, and soft matter.

The Institute of Physics (IOP) in China established the Laboratory for Electron Microscopy research in the 1950s. Since then, many new scientific discoveries have been achieved in various research fields. In 1985, the Kuo group discovered fivefold symmetry (*2*) and a metastable icosahedral phase in rapidly quenched alloys (*3*) using

[1]Beijing National Laboratory for Condensed Matter Physics, Institute of Physics, Chinese Academy of Sciences, Beijing, China
[2]School of Physical Sciences, University of Chinese Academy of Sciences, Beijing, China
[3]Collaborative Innovation Center of Quantum Matter, Beijing, China
*Corresponding author: l.gu@iphy.ac.cn

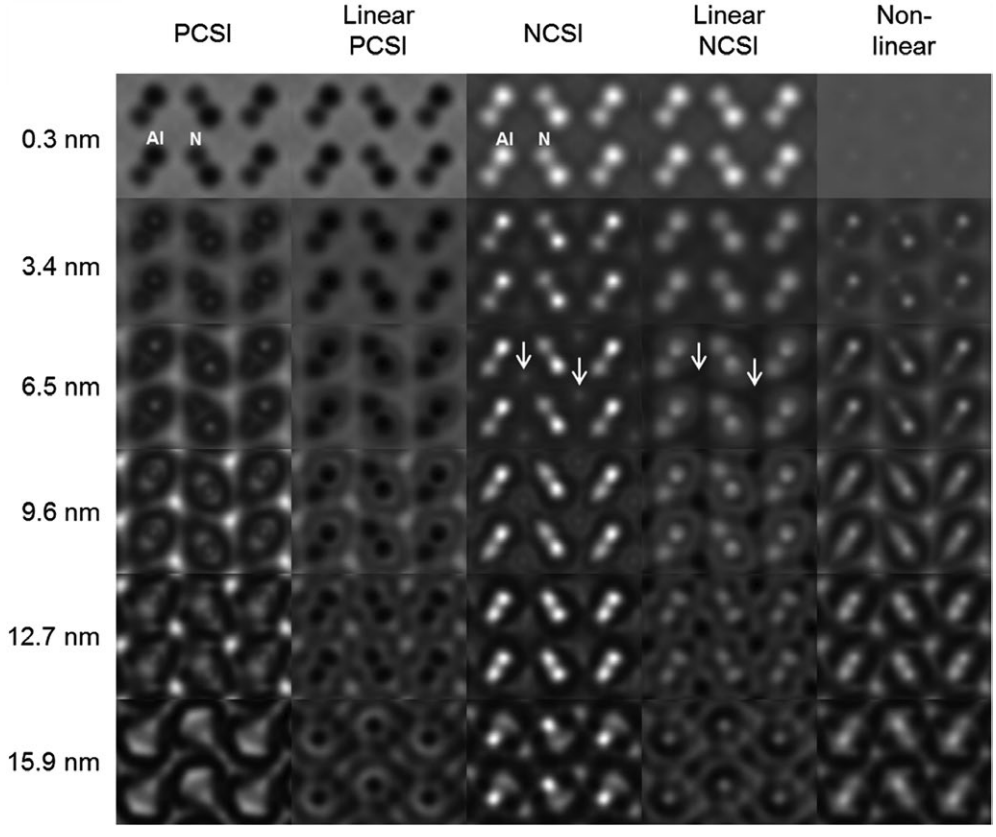

FIGURE 1. Separation between linear and nonlinear information in Cs-corrected high-resolution transmission electron microscope (HRTEM) images using the simulated results of aluminum nitride (AlN) [100] crystal with different thicknesses. PCSI, positive spherical aberration (Cs) imaging; NCSI, negative Cs imaging. This figure is reproduced from (*8*) with permission.

TEM. These works were awarded the First Prize in the National Natural Science Awards, and aroused enthusiasm for electron microscopy research at the institute. In this short review, some selected projects from IOP are highlighted to demonstrate the capabilities of TEM in revealing structural features and obtaining new physical insights.

Coherent imaging and image processing

During the last century, two scientists from IOP, Fanghua Li and Haifu Fan, developed a series of image-processing methods, including phase extension (*4*) and image deconvolution (*5*), to surpass the resolution limit of conventional TEM and restore the crystal structure from HRTEM images. Meanwhile, to explain the contrast variation in HRTEM images with increasing sample thickness due to dynamic scattering effect, the pseudo-weak-phase object approximation (PWPOA) theory was proposed (*6*). This theory would allow selecting the optimum imaging conditions for direct observation of lithium ions in Ramsdellite-type lithium titanate ($Li_2Ti_3O_7$) (*7*).

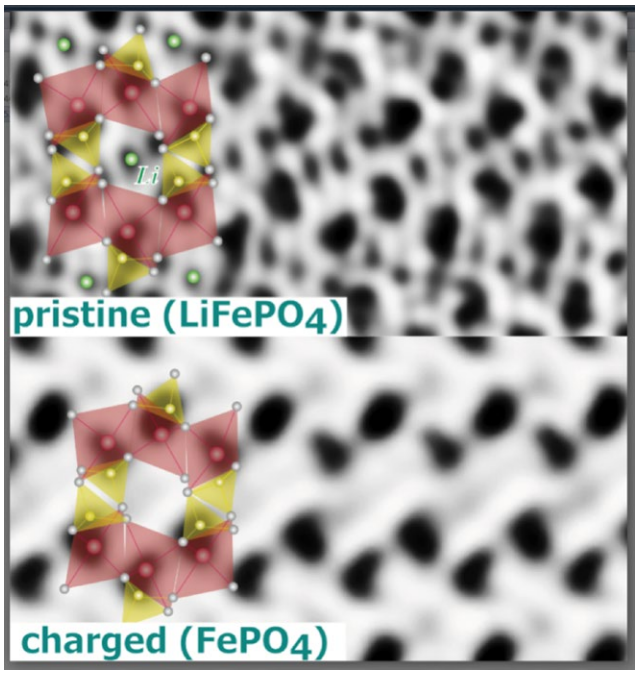

FIGURE 2. Annular bright-field (ABF) micrographs showing the atomic structure of pristine and fully charged lithium iron phosphate ($LiFePO_4$) using two corresponding superimposed atomic structure models. The Li atoms are indicated in green, Fe atoms in red, P atoms in yellow, and O atoms in grey. This figure was used as the cover picture of *Microscopy* in Volume 66 (Issue 1), and the original micrographs in this figure were adapted from (*14*).

In addition to the abovementioned dynamic scattering effect caused by sample thickness, a nonlinear effect would also occur during the imaging process. The latter was induced by the nonlinear interferences between two diffracted beams passed through the objective lens. The nonlinear effect was found beneficial for imaging light atoms (e.g., oxygen in oxides) in the negative spherical aberration (Cs) imaging (NCSI) method. On the other hand, the nonlinear component often induced complications in image contrast (first column in Figure 1), especially for thicknesses over 6.5 nm. Combination of the PWPOA theory with the transmission cross coefficient theory yielded, for the first time, the analytical expressions of linear and nonlinear imaging components in a diffractogram. Using these analytical expressions, Ge and colleagues proposed a method to separate the linear and the nonlinear components in HRTEM imaging (Figure 1) (*8*). They found that the nonlinear effect was the origin of the reversed contrast in thick samples with positive Cs imaging (PCSI) as well as the artificial white dots in NCSI (denoted by arrows). Moreover, the nonlinear component seemed analogous to linear NCSI, indicating that the nonlinear component may partially reflect the structure. The structural factor of aluminum nitride (AlN) and its separated nonlinear component were analyzed by numerical simulations under uncorrected imaging conditions (*9*). The result was beyond the linear information limit, indicating that higher-resolution structural information, even at the atomic level, can be obtained by conventional TEM using this image-processing method.

Incoherent imaging and chemical analysis

Owing to its robustness in contrast explanation, high-angle annular dark-field (HAADF) imaging became one of the most preferred techniques for revealing structural details at the atomic scale. HAADF was found to be highly sensitive to variations in the atomic number (denoted as Z) of elements in the specimen, because the image contrast varied proportionally with $Z^{1.7}$. Such dependence on the Z number became the basis for a valuable new method of elemental differentiation, which was extensively used in STEM to detect single metal atoms. Examples included detecting single palladium (Pd) and gold (Au) atoms anchored on supports as cost-effective catalysts (*10, 11*). The method was also employed to distinguish between two types of adjacent elements [e.g., zinc selenide (ZnSe) and iron nickel (FeNi)] or among several occupation states of point defects [e.g., vacancies, antisites, and adatom clusters in monolayer molybdenum disulfide (MoS_2)] (*12, 13*).

On the other hand, direct imaging of light elements [e.g., lithium (Li) or oxygen (O) atoms] was once a major challenge due to their small scattering powers. This situation totally transformed, thanks to the development of the annular bright-field (ABF) imaging technique through decreasing the collection angle of the annular detector and drastically weakening the Z-dependence of the image contrast to about $Z^{1/3}$, so that light and heavy

elements could be observed simultaneously. Gu *et al.* applied this method to lithium iron phosphate ($LiFePO_4$) electrode materials (*14*). They not only succeeded in achieving direct imaging of Li ion positions on the pristine nanowires (Figure 2), but also identified a new "staging" structure as an intermediate phase in partially delithiated $LiFePO_4$. In sodium (Na)-ion batteries, Sun *et al.* confirmed a three-phase storage mechanism in spinel lithium titanate ($Li_4Ti_5O_{12}$) anodes using ABF imaging. These interesting findings challenged the conventional Li/Na storage mechanisms and raised more interest in determining the locations of light elements in other important Li/Na -containing electrodes.

Meanwhile, chemical analysis with inelastically scattered electrons would provide supplementary information regarding the elemental composition and valence state of individual columns of atoms in crystalline materials. Regarding this capability, modern (S)TEM was now equipped with two further components: (1) electron energy-loss spectrometry (EELS) to analyze the energy distribution of electrons, and (2) X-ray energy-dispersive spectrometry (XEDS) to identify the characteristic X-rays. Liu *et al.* further combined EELS with the ALCHEMI (atom location by channeling enhanced microanalysis) technique, to examine the valence state and location of cobalt (Co) dopant atoms in ferromagnetic zinc oxide (ZnO):Co thin films (*15*). Since the assembly of an advanced Cs-corrected (S)TEM in 2010, the spatial and energy resolution of EELS were markedly improved in many subsequent studies by IOP. Recently, Gu and colleagues further advanced the spatial resolution limit to the atomic scale for both XEDS and EELS analysis and clarified how manganese (Mn) sites in tunnel-type titanium (Ti)-substituted $Na_{0.44}MnO_2$ were replaced by mixed Mn and Ti atoms (*16*).

In situ electron microscopy

In situ electron microscopy (EM) made it possible to perform dynamic imaging and spectroscopic analyses on localized regions of a sample in real time. Owing to its high spatial resolution, in situ EM was found to be more advantageous than other spatial averaging methods, including X-ray diffraction (XRD) and X-ray photoelectron spectroscopy (XPS). Moreover, various external stimuli, including beam irradiation, magnetic fields, and electric fields, could be introduced to the desired sample region during the in situ observation. Some representative in situ EM studies performed at IOP using these external stimuli are discussed below.

Electron-beam irradiation could easily be introduced into in situ TEM experiments as an external stimulus. Peng *et al.* conducted electron-beam irradiation experiments on single-walled carbon nanotubes (SWCNTs) and revealed the formation of tiny carbon tubes (with diameters of about 0.33 nm) from the parent tube, which took place without introducing much lattice distortion (*17*). By contrast, it was more difficult to introduce an external magnetic field into TEM. Wang *et al.* examined the evolution of magnetic domain walls of Co–Ni–Ga Heusler alloy ($Co_{50}Ni_{20}Ga_{30}$) using in situ Lorentz microscopy (*18*). They deliberately increased the electric current of the TEM objective lens to vary the magnetic field at sample positions. However, such an external magnetic field generated by a weakly excited TEM objective lens could only be applied parallel to the direction of an electron beam. It was still challenging to apply a controllable external magnetic field perpendicular to the direction of an electron beam. Yang and colleagues designed a novel in situ TEM holder that may generate a magnetic field as high as 100 oersteds (Oe) parallel to a thin sample foil (*19*).

The introduction of an electric field to in situ electron microscopy led to increasing interests in recent years. In 2002, Wang and Bai developed an in situ TEM holder that could apply variable electrical bias to specimens. Inspired by the scanning probe microscopy (SPM) technology, they incorporated a piezoelectric-controlled probe in the TEM holder and designed a circuit loop for in situ electrical experiments. Yu's team combined this technique with other advanced TEM operation modes, such as in situ electron holography and in situ EFTEM, to study the local charge (*20*) and oxygen vacancies (*21*) distribution in hafnium dioxide (HfO_2) insulator films under different electrical biases. Furthermore, in situ electrochemical experiments could be achieved subsequently. Wang *et al.* prepared metal lithium on the tip of a probe as a counter electrode (*22*) and used layered molybdenite (MoS_2) nanosheets as a working electrode to study the phase transition of MoS_2 during lithiation. Besides the scanning probe configuration, Wang and Bai also developed a microelectromechanical systems (MEMS) chip–based in situ holder. A slit or an electron-transparent thin membrane was fabricated on the silicon substrate of the chip. Using a similar commercial MEMS chip–based in situ TEM holder, Gong *et al.* carried out atomic-scale observation of a micro-working all-solid-state battery (*23*).

Outlook

Since the first TEM prototype was built in 1931, significant advancements have allowed better characterization of functional and structural materials. Today the spatial resolution has exceeded the limit of 0.5 Å, and the energy resolution has reached 10 meV by using state-of-the-art TEMs equipped with the latest technology, including the field-emission gun (FEG), spherical aberration corrector, and monochromator. Furthermore, using fast imaging techniques, the time resolution for dynamic video recording approached the submillisecond range. These improvements opened up new possibilities for more challenging research and technological breakthroughs using electron microscopy.

In the future, IOP researchers will use advanced TEM to gain further understanding of structure–property relationships in materials under complex working environments. Future TEM studies will surely bring about more exciting scientific discoveries in the field of advanced materials research.

References

1. R. P. Feynman, *J. Microelectromech. Syst.* **1,** 60–66 (1992).
2. H. Q. Ye, D. N. Wang, K. H. Kuo, *Ultramicroscopy* **16**, 273–277 (1985).
3. Z. Zhang, H. Q. Ye, K. H. Kuo, *Philos. Mag. A* **52**, L49–L52 (1985).
4. H. F. Fan *et al.*, *Acta Crystallogr. A Found. Crystallogr.* **41**, 163–165 (1985).
5. F. Han, H. Fan, F. Li, *Acta Crystallogr. A Found. Crystallogr.* **42**, 353–356 (1986).
6. F. H. Li, D. Tang, *Acta Crystallogr. A Found. Crystallogr.* **41**, 376–382 (1985).
7. D. Tang *et al.*, *Acta Crystallogr. B Struct. Sci.* **42**, 340–342 (1986).
8. Y. Chang *et al.*, *Microscopy* **65**, 465–472 (2016).
9. Y. Chang *et al.*, *Microscopy* **66**, 406–413 (2017).
10. P. Liu *et al.*, *Science* **352**, 797–801 (2016).
11. S. Yao *et al.*, *Science* **357**, 389–393 (2017).
12. J. Hong *et al.*, *Nat. Commun.* **6**, 6293 (2015).
13. X. Zhang *et al.*, *Nat. Commun.* **8**, 15881 (2017).
14. L. Gu *et al.*, *J. Am. Chem. Soc.* **133**, 4661–4663 (2011).
15. Y. Z. Liu *et al.*, *Appl. Phys. Lett.* **90**, 154101 (2007).
16. Y. Wang *et al.*, *Nat. Commun.* **6**, 6401 (2015).
17. L. M. Peng *et al.*, *Phys. Rev. Lett.* **85**, 3249–3252 (2000).
18. Y. Yao *et al.*, *Nat. Commun.* **4**, 2764 (2013).
19. C. Li *et al.*, *Advanced Mater.* **29**, 1602976 (2017).
20. H. Y. Wang *et al.*, *J. Chin. Electron Microsc. Soc.* **25**, 1–3 (2006).
21. X. A. Yang *et al.*, *J. Chin. Electron Microsc. Soc.* **32**, 416–419 (2013).
22. L. Wang *et al.*, *J. Am. Chem. Soc.* **136**, 6693–6697 (2014).
23. Y. Gong *et al.*, *J. Am. Chem. Soc.* **139**, 4274–4277 (2017).

Exploring surface structure and dynamics at the quantum limit

Zexian Cao, Xinghua Lu, Sheng Meng, and Jiandong Guo*

The continual development of conventional semiconductor technology depends on the miniaturization of individual units in integrated circuits. Power consumption, heat dissipation problems, the technological limit of lithography, manufacturing costs, and novel quantum behavior emerging in nanometric systems now pose a critical problem: Modern silicon technologies need to be replaced. This challenge also presents a significant opportunity for condensed matter scientists, especially for those in the field of surface physics.

In the past half century, research in surface physics has played a critical role in developing next-generation electronic devices from two perspectives. One is the precise control of growing low-dimensional surface structures at the atomic scale. In addition to the syntheses of bulk materials that are mostly dictated by thermodynamics, there is an opportunity to control growth dynamics and kinetics on surfaces. It is possible to obtain metastable artificial quantum structures that possess novel properties. For example, molecular beam epitaxy (MBE) has been employed to grow superlattices, in which band engineering can be implemented. The other perspective from which surface physics has played a crucial role in next-generation electronic devices is the precise probing capability of surface measurement techniques. For example, angle-resolved photoemission spectroscopy has proven to be a powerful method for revealing the electronic structure of condensed matter from surfaces, and scanning tunneling microscopy (STM) provides detailed information concerning the local density of states at surfaces. Exciting progress has been made by surface physicists in recent years. In this article, some recent studies conducted by a team at the State Key Laboratory for Surface Physics (SKLSP) (*1*) are reviewed.

I. Advanced instrumentation

Novel high-resolution electron energy loss spectroscopy (HREELS)

HREELS is among the most powerful techniques to measure vibrational and electronic excitations on solid surfaces. The dispersion of the excitations (i.e., energy as a function of momentum), has been conventionally measured by analyzing the loss in electron energy at different angles (momenta) by rotating the sample, monochroma-

State Key Laboratory for Surface Physics, Institute of Physics, Chinese Academy of Sciences, and Beijing National Laboratory for Condensed Matter Physics, Beijing, China
*Corresponding author: jdguo@iphy.ac.cn

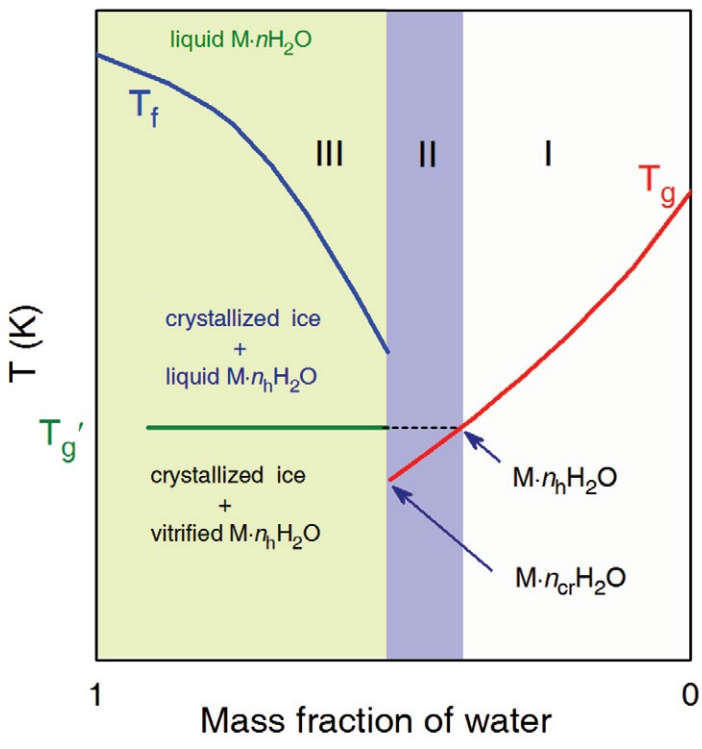

FIGURE 1. Universal vitrification and crystallization behavior, and the phase diagram thus defined, of aqueous solutions. The universal water content dependence of glass transition temperature (T_g) helps classify solutions by concentration and determine the hydration number in a convenient way.

tor, or analyzer. In our HREELS setup, by using a specially designed lens system in the electron source combined with a hemispherical electron energy analyzer, the energy and momentum of the electrons can be measured simultaneously in two-dimensional (2D) mapping. With its high detection efficiency, improved momentum resolution, and satisfactory energy resolution, HREELS is a powerful tool to study quasiparticle excitations and related interactions in low-dimensional systems (*2*).

An unusual acoustic plasmon mode was discovered on the surface of a prototypical topological insulator, bismuth selenide (Bi_2Se_3)(*3*), using HREELS. In sharp contrast to plasmon modes of ordinary metals or semiconductors, this new mode exhibits linear dispersion and remains prominent without severe damping in a large range of momentum far beyond the electron–hole-pair continuum. This behavior is related to the inherent robustness of the Dirac surface states. In addition to the Dirac surface states, collective excitations are topologically protected.

In situ transmission electron microscopy (TEM)

TEM can be used to directly measure the microstructure at the atomic scale as well as mesoscopic physical and chemical properties, and is an ideal tool to investigate their correlations. We developed an STM technique within TEM to achieve high structural resolution and highly stable operation, and realized in situ TEM high-resolution characterization and physical measurements.

By using this customer-built instrument, we studied electrical, optical, and optical–electromechanical coupling properties at the nanoscale level under various physical stimuli, including photon excitation and local strain. Furthermore, we carried out atomic-scale imaging in real time on dynamic electrochemical processes, for example, the forming, migration, and repairing of oxygen vacancies, and the transport of silver (Ag) and lithium (Li) ions. The microscopic mechanisms of their related device applications on catalysis, resistive memories, and lithium ion batteries are now better understood. In research on lithiation dynamics in silicon (Si) nanowires, we found that the "stage"-structured Si crystal remained in the nanowire core, and that lithiation was influenced by the size of the nanowires. In molybdenum disulphide (MoS_2) nanosheets, the phase transition from 2H to 1T of MoS_2 was induced by lithium intercalation (*4*).

Tip-enhanced Raman spectroscopy (TERS)

TERS provides the capability to simultaneously access structural and chemical information. However, ambient TERS systems suffer from unstable and uncertain experimental conditions. We developed TERS further by combining Raman spectroscopy and a low-temperature ultrahigh vacuum STM, with a side-illumination setup and an aspheric lens inside the ultrahigh vacuum (UHV) chamber, which could be precisely moved in 3D by a homemade miniature piezoelectric motor.

Using a 2D silicene sheet on an Ag (111) surface as a model system, we achieved a 10^9 Raman single enhancement and a spatial resolution of 0.5 nm (*5*). Due to the selective enhancement on Raman modes with vertical vibrational components in TERS, our experiment provides direct evidence of the origin of Raman modes in silicene. Furthermore, the ultrahigh sensitivity of TERS allowed us to identify different vibrational properties of silicene phases, which differed only in the bucking direction of the Si–Si bonds. Local vibrational features from defects and domain boundaries in silicene could also be identified. The further development of TERS will involve the inclusion of a femtosecond laser in the setup to provide it with a time resolution.

II. Controlled growth of low-dimensional structures

Surface growth of topological materials

The theoretical prediction and experimental confirmation of 3D topological insulators (TIs), including bismuth telluride (Bi_2Te_3) and the Bi_2Se_3 family, have

stimulated intensive research worldwide on topological phenomena in solid materials. Early experiments on Bi_2Se_3-type TIs were mostly carried out with bulk samples. We carried out pioneering work on the growth of high-quality TI films by MBE (*6, 7*). Thin Bi_2Te_3 and Bi_2Se_3 films were found to grow with a quintuple-layer (QL) unit; and high-quality thin films with controllable thickness, even down to one QL, have been obtained.

Based on these high-quality TI films, we reported many important findings—for example, the first gated transport measurement on a thin Bi_2Se_3 film, which revealed the two-channel transport property TIs involving the bulk channel and the surface channel (*8, 9*), the crossover of the 3D TI Bi_2Se_3 to the 2D limit due to the interaction between the surface states on both surfaces of a film in the thin limit (<6 QL), and the observation of the Landau quantization of TI surface states in Bi_2Se_3 revealed in STM (*10*). The high-quality TI films grown by MBE eventually led to the experimental discovery of the quantum anomalous Hall effect in magnetically doped $(Bi,Sb)_2Te_3$ on an $SrTiO_3$ substrate (*11*), which is of fundamental importance in the quantum Hall world.

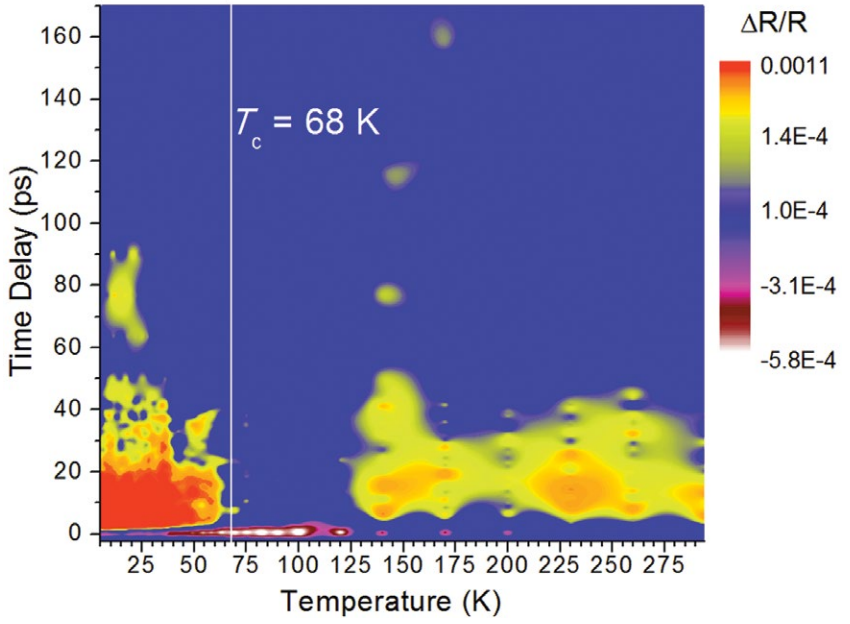

FIGURE 2. Evidence of the superconducting transition and of the constant λ, obtained in single-layer iron selenide/strontium titanate (FeSe/$SrTiO_3$) from ultrafast dynamics. Figure reproduced from PRL 116, 107001 (2016) with permission.

Universal vitrification of aqueous solution

The icing and vitrification of water in supercooled aqueous solutions are crucial issues in meteorology, cryobiology, and food science, among other disciplines. Many controversies concerning the behavior of water remain unresolved. Even data for the hydration number of simple inorganic solutes suffer from large discrepancies. For example, it was once believed that the tetrahedral coordination of water molecules in liquid comprises four equivalent hydrogen bonds, but recent studies have suggested a strongly asymmetric environment for a water molecule. A drastically different view claims that water molecules bind primarily into rings or liner chains with variable sizes.

By careful measurement of glass temperature (T_g) for aqueous solutions across a wide range of water content, it was found that for solutions of a given solute with water content above a critical value (zone III, see Figure 1), a constant T_g was measured, as spontaneous icing occurs prior to glass transition in such solutions, and the vitrification involves only the freeze-concentrated solution that has a constant concentration. The concentration of the freeze-concentrated phase refers to the solution specified by $M{\cdot}nH_2O$, where *n* is the hydration number of solute M. For solutions with water content less than that specified by the hydration number (zone I), T_g decreases monotonically with increasing water content. Spontaneous icing may or may not occur in these solutions in between (zone II), depending on the cooling/heating procedure. Such behavior is universal (*12, 13*). The fact that icing and vitrification can be manipulated in solutions in zone II explains why various controversies concerning water, such as the liquid–liquid transition of water, arise here.

III. Quantum dynamics at surfaces

Ultrafast spectroscopy

Light can interact with matter in terms of charge, lattice, spin, and orbital degrees of freedom. As advanced optical experiments are used to probe the core areas of condensed matter physics and to understand "light–matter interaction," it is essential to investigate the ultrafast spectroscopy of quantum materials.

Zhao's group investigated the time-resolved ultrafast excited-state quasiparticle dynamics of an interface high-transition temperature (T_c) superconductor, single-layer iron selenide (FeSe) on strontium titanate ($SrTiO_3$) (*14*). By directly measuring the lifetimes and densities of the photoexcited carriers, the superconducting (SC) phase transition was unambiguously identified (see Figure 2), yielding an SC T_c of 68 K and an SC gap of $\Delta(0) = 20.2$ meV. Significantly, the electron–phonon interaction constant λ was obtained, which was much larger than that of bulk FeSe. This highlighted the crucial role of λ in this interface superconductor. An acoustic coherent phonon branch at 0.05 THz in the protecting layer was also recorded, and formed an extra diminishing channel for the pairing glue.

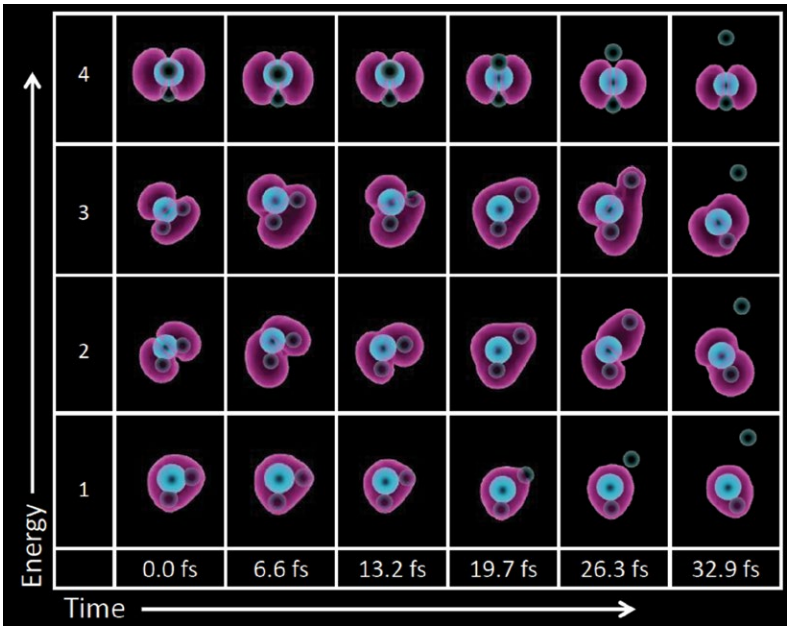

FIGURE 3. Evolution of electron orbitals of water adsorbed on gold nanoparticles, and exposed to a laser pulse.

Excited state and dynamic behavior of molecules on surfaces

The excited states and dynamic behaviors of molecules on surfaces are important for many fundamental processes in physics and chemistry. We have explored such phenomena using a combination of low-temperature STM and density functional theory (DFT).

The hydrated electron is important for interfacial chemistry on solid surfaces. Real-space imaging of hydrated electrons, however, is not yet possible, and very little is known about hydrated electrons on solid interfaces at the microscale. By injecting tunneling electrons into water clusters on a copper crystal surface, Lu's team demonstrated the excitation of a hydrated electron state (*15*). The directional diffusion path of water clusters provides profound evidence for the emergence of the hydrated electron. Based on DFT calculations and STM results, the structural transformation in the water cluster and the charging mechanism were revealed.

Quantum dynamics of water photosplitting

Water photosplitting, which is at the core of photosynthesis, occurs in ambient conditions. Despite extensive research, the microscopic mechanism of water splitting occurring in natural or artificial photosynthesis, especially its atomistic dynamics, has remained elusive.

Meng's group investigated the real-time dynamics of water photosplitting driven by femtosecond laser pulses on gold nanoparticles (*16*). Their efforts were based on the development of first-principles methods to accurately describe the ultrafast quantum dynamics of chemical systems and condensed matter. By employing parameter-free, time-dependent DFT and developing practical simulation algorithms and software, they could describe laser-induced quantum phenomena, such as water photosplitting. The ultrafast evolution of the orbitals of water in real time during laser illumination was demonstrated, as shown in Figure 3. The water molecule is rotated to align with the direction of the laser field; one hydroxide (OH) bond is then gradually elongated, and the hydrogen (H) atom is detached from the water. In this quantum dynamic simulation, the processes of generation and accumulation of hot electrons in the antibonding state of water were directly resolved. More importantly, the rate of water splitting under excitation at a low-absorption peak was found to be higher than the high-absorption peak. This finding is surprising, and has led to the discovery of mode selectivity—namely, the fact that different excitation modes couple differently with water.

IV. Conclusion

The mission of SKLSP is to explore the fundamental aspects of novel phenomena at surfaces and interfaces. The team specializes in the fabrication, characterization, and functionalization of artificial materials with potential applications in information technology, energy, and nanoscience. Current research activities include the controlled growth of low-dimensional structures with atomic precision, the development of novel instruments with high resolution in multiple degrees of freedom, and the investigation of localized phenomena as well as their collective behaviors at surfaces and interfaces, and of dynamic behavior in excited electronic states. With the steady growth of science funding in China, SKLSP has a bright future.

References

1. State Key Laboratory for Surface Physics, website, http://surface.iphy.ac.cn/eng/index.asp.
2. X. Zhu *et al.*, *Rev. Sci. Instrum.* **86**, 083902 (2015).
3. X. Jia *et al.*, *Phys. Rev. Lett.* **119**, 136805 (2017).
4. L. Wang, Z. Xu, W. Wang, X. Bai., *J. Am. Chem. Soc.* **136**, 6693–6697 (2014).
5. S. Sheng *et al., Phys. Rev. Lett.* **119**, 196803 (2017).
6. G. Zhang *et al., Appl. Phys. Lett.* **95**, 053114 (2009).
7. T. Zhang *et al., Phys. Rev. Lett.* **103**, 266803 (2009).
8. J. Chen *et al., Phys. Rev. Lett.* **105**, 176602 (2010).
9. J. Chen *et al., Phys. Rev*. B **83**, 241304R (2011).
10. P. Cheng *et al., Phys. Rev. Lett.* **105**, 076801 (2010).
11. C. Chang *et al., Science* **340**, 167–170 (2013).
12. Q. Wang *et al., Sci. Rep*. **6**, 26831 (2016).
13. L. S. Zhao *et al., Sci. Rep*. **5**, 15714 (2015).
14. Y.C. Tian *et al., Phys. Rev. Lett.* **116**, 107001 (2016).
15. Y. Guo *et al., ACS Nano* **10**, 4489–4495 (2016).
16. L. Yan *et al., ACS Nano* **10**, 5452–5458 (2016).

Quantum computation and quantum information processing

Fanming Qu[1], Zhigang Cheng[1], Shiping Zhao[1], Dongning Zheng[1], Yirong Jin[1], Lin Xia[1], Ruquan Wang[1], Gangqin Liu[1], Xinyu Pan[1], Baoli Liu[1], Duanlu Zhou[1], Li Lu[1]*, and Heng Fan[1]*

Introduction

Quantum computers are expected to help run algorithms that can solve problems with superpolynomial speedup. In addition, well-controlled quantum systems can be used to simulate exotic and complex quantum states that cannot be achieved in classical systems. In the past few years, considerable progress has been made in areas such as quantum computation and quantum simulation. Several groups of researchers from the Institute of Physics (IOP), Chinese Academy of Sciences, have been studying quantum information processing, and remarkable achievements have been made, both theoretical and experimental. The IOP research team studying quantum computing and quantum information processing is widely considered to be one of the best groups in China. In this article, we present our research highlights.

Superconducting quantum computation

IOP has considerable experience in superconductor device fabrication and weak signal measurement at ultralow temperatures. In China, IOP was the first institution to have successfully fabricated superconducting qubit (quantum bit) devices and observed their quantum coherence. Initially, devices with different superconducting materials were prepared, and various quantum phenomena were then investigated. In particular, macroscopic quantum tunneling in $Bi_2Sr_2CaCu_2O_{8+\delta}$ intrinsic Josephson junctions (*1*–*3*) and a photon-resonant escape process accompanied by microwave-induced potential barrier suppression have been observed (*4*). Using niobium (Nb)-based devices, bifurcation of nonlinear dynamical systems under strong microwave driving (*5*); quantum phase diffusion in underdamped systems (*6*); and quantum stochastic synchronization in dissipative systems (*7*) have been experimentally observed and theoretically explained. Moreover, effort has been made to develop a cryogen-free dilution refrigerator system for qubit measurement (*8*).

Recent studies at IOP have focused on aluminum (Al)-based phase, flux, and Xmon qubits as well as some new qubits, including nSQUID (negative-inductance superconducting quantum interference device). Atomic physics and quantum optics experiments, such as stimulated Raman adiabatic passage (*9*), have been performed using phase and Xmon qutrits. Gap-tunable flux qubits with high, persistent current have been fabricated, and their coupling to nitrogen-vacancy (NV) ensembles has been realized (*10*, *11*). Moreover, it has been demonstrated that a longitudinal radio-frequency (RF) field could effectively switch off/on the coupling between the qubit and a coplanar waveguide (CPW) resonator, thus establishing a new approach for controlling the coupling strength between different elements in a circuit (*12*).

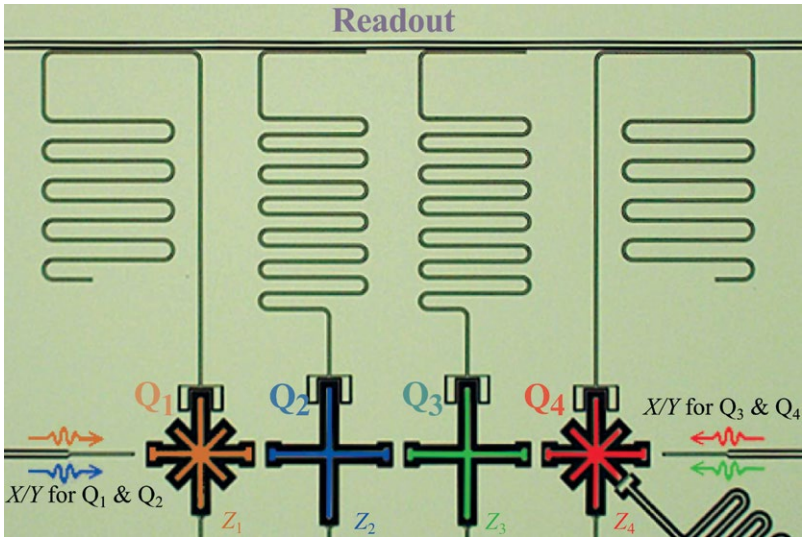

FIGURE 1. False-color photomicrograph of a superconducting quantum circuit for solving 2 × 2 linear equations. Figure reproduced with permission from (*13*).

In collaboration with Zhejiang University and the University of Science and Technology of China, several multiqubit devices have been fabricated and studied. Figure 1 shows an array of four Xmon qubits (Q1 to Q4), each of which has a Z line near the bottom controlling the qubit level spacing and the state rotation about the *z* axis. The rotation about the *x*- or *y*-axis is controlled by a microwave pulse via the left and right XY lines. Each qubit is coupled to its own readout resonator, which is in turn coupled to a common transmission line, thereby enabling simultaneous single-shot quantum nondemolition measurement. A quantum algorithm

[1]Beijing National Laboratory for Condensed Matter Physics, Institute of Physics, Chinese Academy of Sciences, Beijing, China
*Corresponding authors: lilu@iphy.ac.cn (L.L.), hfan@iphy.ac.cn (H.F.)

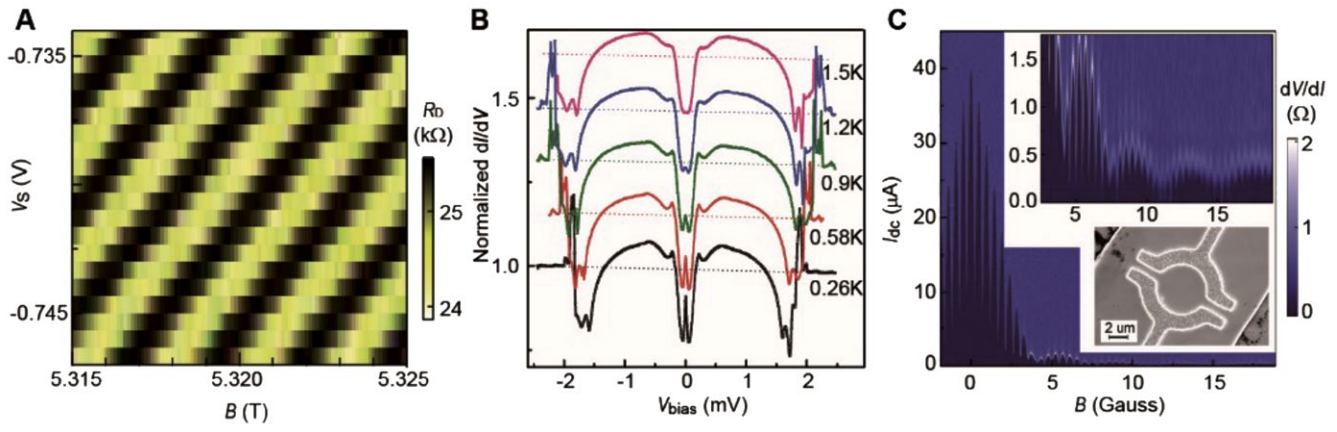

FIGURE 2. Interference and device for topological quantum computation. (**A**) Interference pattern of an interferometer fabricated on self-grown gallium arsenide/aluminum gallium arsenide (GaAs/AlGaAs) 2D electron gases (2DEGs) (*21*). (**B**) Zero-bias conductance peak at the interface between superconducting tin (Sn) and topological insulator bismuth selenide (Bi_2Se_3) (*20*). (**C**) Superconducting quantum interference device (SQUID) on bismuth telluride (Bi_2Te_3) (*23*).

for solving a two-dimensional (2D) system of linear equations was demonstrated using this device (*13*).

Furthermore, a continuous variable geometric phase has been observed using a circuit containing five qubits connected to a bus resonator, and a quantum gate protocol for the one-step implementation of *n*-qubit controlled phase gates has been realized (*14*). The production and tomography of genuinely entangled Greenberger–Horne–Zeilinger (GHZ) states with up to 10 qubits have been demonstrated (*15*). Multiqubit devices have been developed for the quantum simulation of condensed matter physics problems (*16*).

Topological quantum computation

Topological quantum computation (TQC) (*17*), which uses quasiparticles called non-Abelian anyons in (2+1)-dimensional spacetime, is an approach for realizing fault-tolerant quantum computation. A system containing a collection of non-Abelian anyons possesses topologically protected ground-state degeneracy. The exchange or braiding of such anyons helps in manipulating the quantum state, depending only on the topology of the process and not on parameters such as speed. The topological energy gap protects the quantum state (information) from weak, local perturbations. Thus, the state is immune to decoherence, which is a big challenge to other quantum computation schemes. Currently, the vigorously pursued non-Abelian anyons include Majorana zero modes (MZMs). In 2012, the first experimental signature of MZMs was discovered in semiconducting nanowires coupled with s-wave superconductors (*18*). Subsequently, progress has been made in ferromagnetic iron atomic-chain superconductor and topological insulator (TI) superconductor structures (*19*, *20*).

At IOP, the roadmap for TQC started in 2006, with the establishment of the Daniel Chee Tsui Laboratory, named after the Nobel laureate Dr. Tsui. Thereafter, the focus was on achieving ultralow temperatures by implementing adiabatic nuclear demagnetization and ultrahigh mobility gallium arsenide/aluminum gallium arsenide (GaAs/AlGaAs) 2D electron gases (2DEGs), using state-of-the-art molecular beam epitaxy. The lowest electron temperature in the 2DEG was ~4 mK, which is among the best worldwide. On the material side, the mobility of 2DEGs in GaAs/AlGaAs heterostructures exceeded 5×10^6 cm^2/Vs, which is also a record in China. Stable and repeatable interference of the integer quantum Hall edge states has been successfully realized on our self-grown 2DEGs (*21*).

Besides the 5/2 fractional quantum Hall state, this rapidly developing field requires MZMs in hybridized systems with topological superconductivity. In 2008, Fu and Kane constructed MZMs by combining the spin-momentum-locked helical surface states of TIs and s-wave superconductors (*22*). Since then, step-by-step progress has been made at IOP, as shown in Figure 2. In a preliminary study, Josephson junctions and SQUIDs based on TIs have been analyzed (*23*). At a very early stage, zero-bias conductance peaks at the interface between the surface of a TI and an s-wave superconductor have been observed (*20*), similar to the first signature of MZMs in semiconducting nanowires (*18*). Furthermore, based on TIs, ongoing experiments showed evidence of full transparency in the Josephson junctions resulting from the helical nature of the surface state and the parity switches in radio-frequency SQUIDs, probably because of quasiparticle poisoning. This was consistent with the existence of MZMs.

Given the unique advantage of topological protection, researchers across the globe should focus on TQC, including the teams in IOP. However, it is uncertain

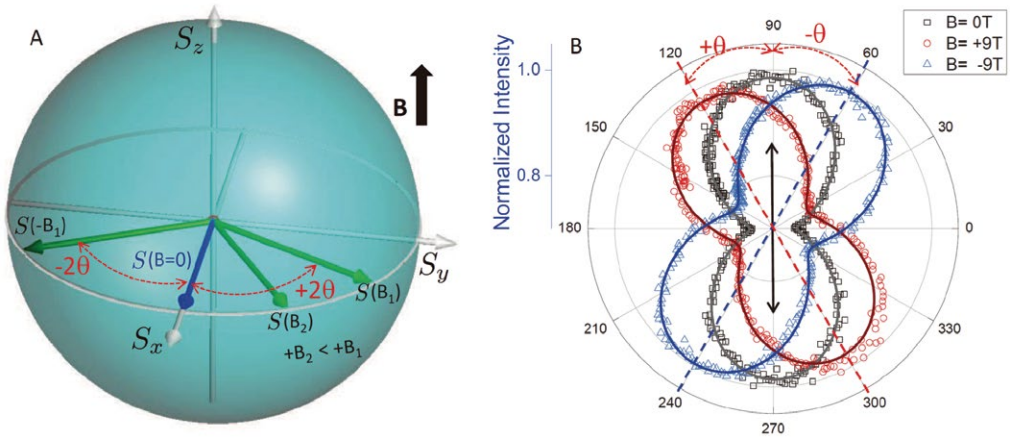

FIGURE 3. Control of exciton valley superposition states. (**A**) Bloch sphere representation of the manipulation of valley superposition states. The valley superposition states can be tuned to different points on the equator by changing the amplitude and direction of the magnetic field in the *Z* direction. (**B**) Normalized angle-dependent intensity of neutral exciton emission for $B = 0$ (black), $B = +9$ T (red), and $B = -9$ T (blue) with polar plots. The maximum intensity indicates the direction of the valley superposition states.

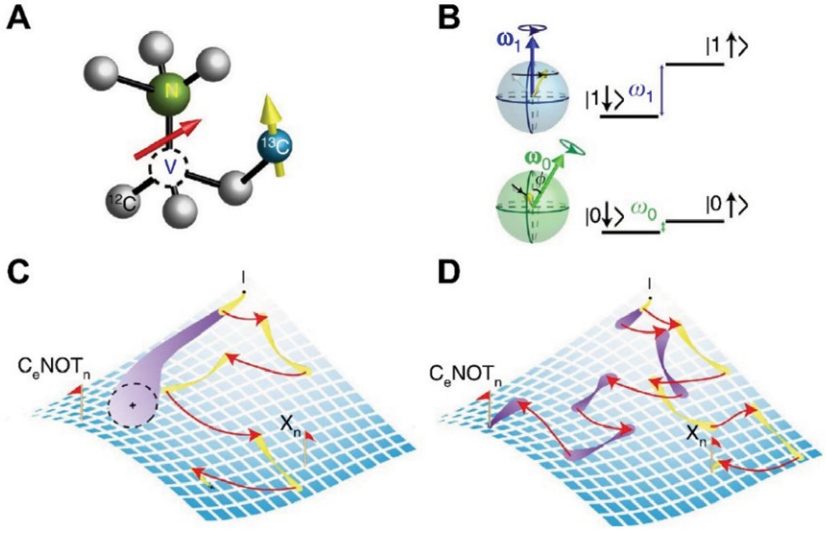

FIGURE 4. Nitrogen-vacancy (NV) center in diamond. (**A**) Atomic structure. (**B**) Energy levels of an NV center and a nearby ^{13}C nuclear spin. (**C**) and (**D**) Steering the quantum evolution of the two-qubit system in its operator space. A conventional dynamical decoupling (DD) sequence only protects the center spin coherence, whereas an engineered DD implements the quantum gate and coherence protection simultaneously (*26*).

when exactly the first topological quantum computer would be developed, in consideration of the challenges from both hardware (qubits) and software (algorithms) viewpoints. Nevertheless, the braiding of MZMs and the demonstration of non-Abelian statistics may be realized soon in the laboratory.

Quantum control of valleytronics

2D layered transition-metal dichalcogenide semiconductors [MX_2, M = molybdenum (Mo), W and X = sulfur (S), selenium (Se)] have emerged as an exciting platform for valleytronics, a technology that investigates the control over the valley degree of freedom (a local maximum/minimum on the valence/conduction band) of certain semiconductors (*24*). A valley degree of freedom termed the "valley pseudospin" is observed in hexagonal MX_2 monolayers (MLs) because of their strong spin–orbit interactions along with inversion symmetry breaking. The circularly and linearly polarized photoluminescence studies show that valley pseudospin and its coherent superposition states in MX_2 can be initialized and detected optically by taking advantage of the optical coupling between the valley pseudospins and the helicity of the excitation photons. The manipulation of the superposition states associated with valley pseudospins is one of the important steps toward the application of valley pseudospins in the field of valleytronics. Here, the ability to control the coherent superposition of the valley pseudospin was demonstrated via the Zeeman effect of the valley neutral exciton states with different valley indices using an external magnetic field applied perpendicular to the ML plane (*25*), as shown in Figure 3. The coherent superposition rotation of the valley states demonstrates a pronounced manipulation of the valley pseudospins in the applied magnetic field. This work could significantly help the physics community, as well as those aiming to integrate such materials for future applications that involve harnessing the valley degree of freedom.

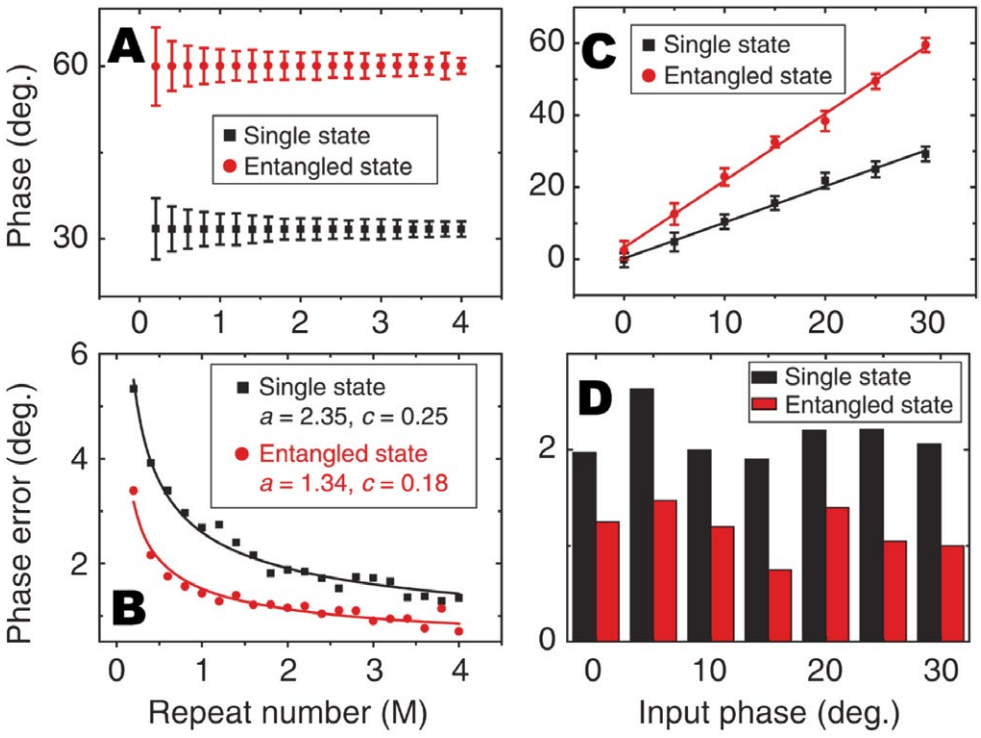

FIGURE 5. Entanglement-enhanced phase estimation. Different methods by two individual qubits and two entangled qubits are used to show that the entanglement can help reduce the uncertainty in the phase estimation. Figure reproduced from Ref [*27*].

associated with the entangled state is always lower than that associated with the independent states. We used a two-spin system (an NV electron spin and its nearby ^{13}C nuclear spin) to demonstrate this protocol (*27*).

Cold-atom quantum simulation and entanglement in many-body systems

We studied ultracold molecules with a sodium-potassium (NaK) alloy (*28*). A high-performance Na^{23} and K^{40} sympathetic cooling apparatus was designed and built. Using a Zeeman slower, we captured 2×10^{10} Na atoms in the magneto-optical trap (MOT). The evaporative cooling in the hybrid trap produced largely pure condensates of 1×10^{7} atoms. With a 2D+ cooling stage, we successfully captured 5×10^{6} K^{40} atoms from a naturally abundant K source. Our second experiment was a tunable spin–orbit coupling (SOC) with the rubidium Bose–Einstein condensate (Rb^{87} BEC) (*29*). We created synthesized SOC for ultracold Rb^{87} atoms with a gradient magnetic field (GMF). The strength of the SOC can easily be tuned by changing the amplitude of the GMF. Our experiment opens a new avenue for synthesizing SOC with atom species such as lithium (Li), Na, and K; this would have otherwise been impossible with the Raman scheme. The third experiment involved an optically pumped spin-exchange relaxation-free (SERF) magnetometer (*30*). A potassium atomic SERF magnetometer was set up, and a single-channel sensitivity of 8 $fT/Hz^{1/2}$ was achieved in a shielded environment, which is one of the best worldwide. The spin precession frequency and relaxation time were measured to verify the working of our magnetometer in the SERF regime. In addition, we studied many-body physics of bosons in optical lattices. Currently, we are building an experimental setup to study many-body physics of bosons in optical lattices. Rb^{87} atoms are captured and cooled to a Bose–Einstein condensate. The many-body system is formed by adiabatically loading atoms to 3D lattices. This system can be used to study many-body physics, condensed matter physics, and the quantum information process. We plan on

Quantum information processing by nitrogen-vacancy center

The nitrogen-vacancy (NV) center in diamond (Figure 4A) is a promising physical system for the implementation of room-temperature quantum computing. The unique spin-dependent optical transitions provide an efficient way to achieve the polarization and readout of the electron spin, and the relatively isolated spin environment ensures the excellent coherence time of the spin qubit, even under ambient conditions. We designed and experimentally implemented a noise-resilient quantum gate [controlled NOT, (CNOT)], which is the element block of the quantum circuit model, to a hybrid spin system comprising an NV electron spin and a nearby ^{13}C nuclear spin (*26*). As shown in Figure 4, the quantum gate is implemented by applying only dynamical decoupling (DD) pulses to the center electron spin, simultaneously suppressing its decoherence and steering the quantum evolution of the nearby nuclear spin. This scheme has been generalized to other remote nuclear spins, which are large in number and have good coherence.

As shown in Figure 5, an entanglement-enhanced phase estimation is demonstrated by comparing the phase errors in the two measurements. The error

studying the dynamics of many-body systems and quantum distillation of states (*31*).

Recently, we theoretically investigated how quantum information interacts with quantum many-body physics (*32*), wherein the many-body entanglement structures (*33*, *34*) played an essential role in characterizing different quantum phases.

Conclusion

We expect that more researchers will join the quantum information and computation groups of IOP. In fact, several national programs have been organized to promote the research of quantum information processing. IOP will be a crucial part of these projects. In addition, we plan to play a more important role both in China and worldwide in developing quantum computation and quantum information processing for industrial and scientific applications.

References

1. S. P. Zhao *et al.*, *Phys. Rev. B* **72**, 184511 (2005).
2. X. B. Zhu *et al.*, *Phys. Rev B* **73**, 224501 (2006).
3. S. X. Li *et al.*, *Phys. Rev. Lett.* **99**, 037002 (2007).
4. H. F. Yu *et al.*, *New J. Phys.* **15**, 095006 (2013).
5. H. F. Yu *et al.*, *Phys. Rev. B* **81**, 144518 (2010).
6. H. F. Yu *et al.*, *Phys. Rev. Lett.* **107**, 067004 (2011).
7. G. M. Xue *et al.*, *Phys. Rev. B* **90**, 224505 (2014).
8. Y. Tian *et al.*, *Rev. Sci. Instrum.* **83**, 033907 (2012).
9. H. K. Xu *et al.*, *Nat. Commun.* **7**, 11018 (2016).
10. W. Yu-Lin *et al.*, *Chin. Phys. B* **22**, 090312 (2013).
11. H. Deng *et al.*, *IEEE Trans. Appl. Supercond.* **25**, 1–4 (2015).
12. Y. L. Wu *et al.*, arXiv:1605.06747 (2016).
13. Y. R. Zheng *et al.*, *Phys. Rev. Lett.* **118**, 210504 (2017).
14. C. Song *et al.*, *Nat. Commun.* **8**, 1061 (2017).
15. C. Song *et al.*, *Phys. Rev. Lett.* **119**, 180511 (2017).
16. K. Xu *et al.*, *Phys. Rev. Lett.* **120**, 050507 (2018).
17. C. Nayak *et al.*, *Rev. Mod. Phys.* **80**, 1083–1159 (2008).
18. V. Mourik *et al.*, *Science* **336**, 1003–1007 (2012).
19. S. Nadj-Perge *et al.*, *Science* **346**, 602–607 (2014).
20. F. Yang *et al.*, *Phys. Rev. B* **85**, 104508 (2012).
21. Y.-Y. Zhu *et al.*, *Chin. Phys. Lett.* **34**, 067301 (2017).
22. L. Fu, C. L. Kane, *Phys. Rev. Lett.* **100**, 096407 (2008).
23. F. Qu *et al.*, *Sci. Rep.* **2**, 339 (2012).
24. Cao, T. *et al.*, *Nat. Commun.* **3**, 887 (2012).
25. Wang, G. *et al.*, *Phys. Rev. Lett.* **117**, 187401 (2016).
26. G. Q. Liu *et al.*, *Nat. Commun.* **4**, 2254 (2013).
27. G. Q. Liu *et al.*, *Nat. Commun.* **6**, 6726 (2015).
28. Z. Feng *et al.*, *Chin. Phys. Lett.* **32**, 123701 (2015).
29. X. Y. Luo *et al.*, *Sci. Rep.* **6**, 18983 (2016).
30. J. Q. Fu *et al.*, *Chin. Phys. B* **25**, 010302 (2016).
31. L. Xia *et al.*, *Nat. Phys.* **11**, 316–320 (2015).
32. B. Zeng, X. Chen, D. L. Zhou, X. G. Wen, arXiv:1508.02595 (2015).
33. D. L. Zhou, *Phys. Rev. Lett.* **101**, 180505 (2008).
34. J. Cui *et al., Nat. Commun.* **3**, 812 (2012).

Light–matter interactions

Ling Lu*, Rongjuan Liu, Xiulai Xu, Chen Ge, Kuijuan Jin, Li Wang, and Guozhen Yang

Here, we highlight a few directions of research being pursued at the Key Laboratory of Optical Physics, on light–matter interactions between microwave, terahertz, and subwavelength structures as well as optical photons, quantum emitters, oxide films, and biological samples.

Topological photonics

Topology, a branch of mathematics that recently found wide applications in science, is concerned with the invariant properties of an object undergoing continuous transformation. Consequently, any physical quantity expressed by discrete topological invariants is unprecedentedly robust against large perturbations. The 2016 Nobel Prize in physics was awarded for research on topological physics. Likewise, photonics is also benefiting from band topologies—discrete global configurations of wave-functions in the Brillouin zone of periodic systems such as photonic crystals. Using topological photonics, photon transport without any localization and scattering loss is now feasible.

Since the concept of photonic crystals was first proposed in 1987, Group L01 has been working on experiments with periodic dielectric materials. In 1994, our group reported laser-assisted crystallization of polystyrene spheres and strontium titanate ($SrTiO_3$) particles (n = 2.5) with lattice constants of ~1.5 μm (*1*). Such photonic crystals are characterized by their band structures, while the hidden freedom of band topology was only unveiled in 2005. Topological photonics started with the proposal of a one-way waveguide as the edge state of a two-dimensional (2D) photonic crystal, which was experimentally demonstrated in 2009. In the following year, our group published the second set of experimental results (*2*) on this topic in the context of microwave frequencies. The idea is illustrated in Figure 1A. The edge mode of a magnetic photonic crystal has a gapless dispersion curve traversing the whole bandgap, connecting the bulk bands above and below. The group velocity of the edge mode has only one sign and propagates in one direction only, without scattering from arbitrary defects. Such a one-way edge state is analogous to the chiral edge state in the quantum Hall effect, providing a novel mechanism for planar integration of nonreciprocal photonic devices.

In three dimensions, optical fibers are the best light guides and are ubiquitous in modern technologies. Using high-dimensional band topologies, we have shown that one-way fibers can be designed using 3D magnetic photonic crystals (*3*), as illustrated in Figure 1B. These

Key Laboratory of Optical Physics, Institute of Physics, Chinese Academy of Sciences/ Beijing National Laboratory for Condensed Matter Physics, Beijing, China
*Corresponding author: linglu@iphy.ac.cn

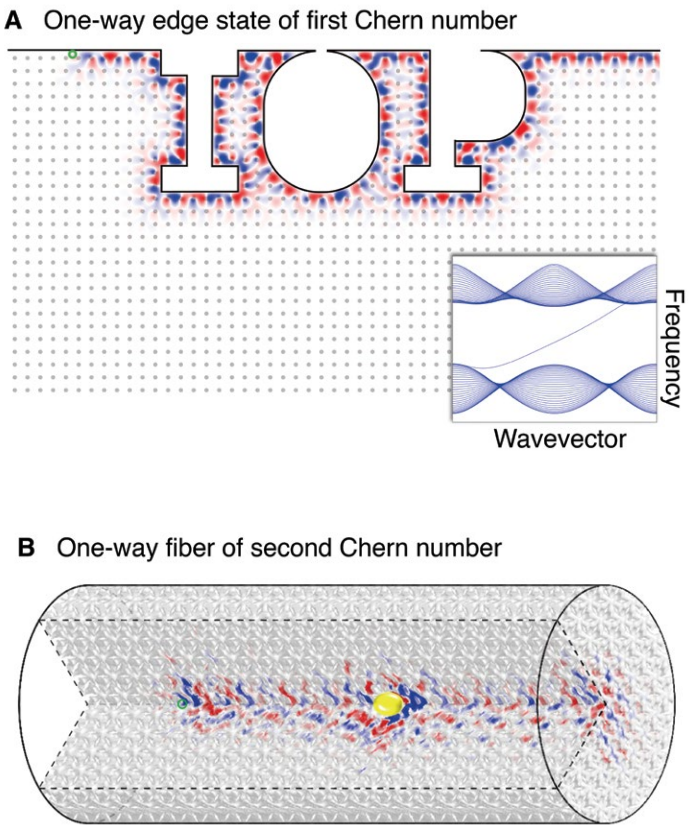

FIGURE 1. Topological one-way waveguides in two and three dimensions. (**A**) Simulation of a one-way edge state, in a two-dimensional magnetic photonic crystal, immune to backscattering from arbitrary defects. The band structure is plotted as the inset. (**B**) Simulation of wave propagation around a metallic sphere inside a one-way fiber, designed using a topological line defect in a three-dimensional magnetic photonic crystal. The green circles indicate continuous-wave point sources.

one-way fiber modes were realized by introducing a topological line defect within a fully gapped topological photonic crystal. Unlike the one-way edge states protected by the first Chern numbers defined in the 2D Brillouin zone, our one-way fiber modes are protected by the second Chern numbers defined in the four-dimensional (4D) parameter space, including the 3D momentum space and the winding angle associated with the helical line defects.

The above one-way edge states and fiber modes are only two intuitive examples of the potential of topological photonics (*4*). Topological band structures in three dimensions remain largely unexplored. For example, nodal lines can have nontrivial connectivity, such as the nodal chains that we demonstrated experimentally (*5*). Useful device designs and applications are anticipated in many areas of photonics using topology.

Solid-state quantum optics

Solid-state quantum optics has encouraged pronounced advances in the implementation of quantum information processing. Group L02 focuses primarily on the quantum-state control of single quantum dots (QDs), QD-cavity coupling for cavity quantum electrodynamics (CQED), and scaling up for quantum photonic networks. Self-assembled QDs, such as InAs/GaAs QDs, are 3D-confined nanostructures grown by molecular-beam epitaxy. Owing to quantum confinement, the QDs have atom-like discrete energy levels and are key elements for solid-state quantum optics.

The spins of electrons and holes in a single QD have long coherence time at low temperatures, which makes QDs one of the best candidates for quantum bits (qubits). With a single QD embedded in the intrinsic region of a Schottky photodiode, the charge states in the QD can be controlled precisely by applying DC electric and magnetic fields. For example, we demonstrated that the dipole moment of an exciton in a QD can be inverted, when the carrier wave functions shrink with the applied magnetic field (*6*). In addition, the diamagnetic energy shifts of excitons can be greatly enhanced when the carrier wave functions extend into the underlying wetting layer. Figure 2A shows the magneto-photoluminescence of a single QD. With a bias voltage of 0.5 V, additional weak emission lines appear to have much larger energy shifts, compared with the normal exciton emissions (X^-, XX^-, and X^{2-}) labeled in the left panel. This may offer a novel platform to control the interactions between QDs and the surrounding environment (*7*).

An advantage of semiconductor QDs is their monolithic integration with optical cavities as a CQED system. One potential application of CQED is nonclassical photon sources. As shown in Figure 2B, we proposed a two-beam scheme to implement a strong photon blockade with a single QD in a nanocavity (*8*). By driving the cavity and the QD simultaneously by two laser fields with frequency ω_L and ω_p of specific phases, the photon blockade can be substantially enhanced because of the destructive quantum interference of the two-photon excitation in the cavity. In this scenario, the calculated second-order correlation function $g^{(2)}(0)$ is lower by over two orders of magnitude than the traditional values.

Experimentally, the Purcell enhancement of colloidal QDs in a microdisk was demonstrated at room temperature in the weak coupling regime (*9*). To achieve strongly coupled exciton–polariton states, we designed and fabricated the L3 photonic crystal cavity embedded with a single QD. Figure 2C shows a scanning electron microscopy image of the cavity as well as the corresponding optical modal profile. The measured quality factor of the cavity is around 11,000, as shown in Figure 2D. As illustrated in Figure 2E, an integrated device with coupled photonic crystal cavities and waveguides has been designed to implement ultrafast

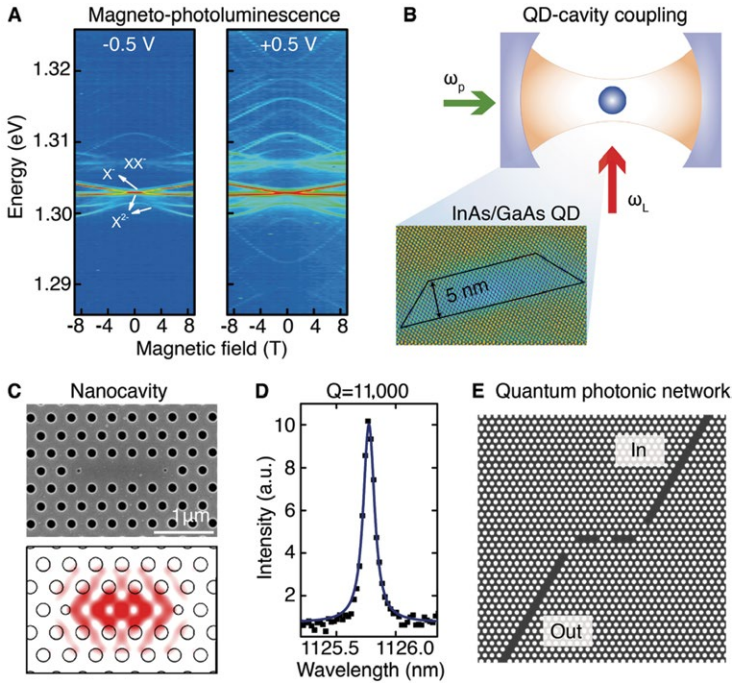

FIGURE 2. Physical mechanism and devices of quantum dots (QDs). (**A**) Photoluminescence spectra as a function of magnetic fields and different bias voltages. Much larger energy shifts of the excitons were observed with weaker emission intensities compared to the regular excitons labeled as X^-, XX^-, and X^{2-}, known as the negatively charged exciton, negatively charged bi-exciton, and double negatively charged exciton, respectively. (**B**) A new scheme for photon blockade. The cavity and the QD are driven simultaneously by two laser fields with frequency ω_L and ω_p. A transmission electron microscope image of the QD is shown as the inset. (**C**) A scanning electron microscope image and calculated mode profile of the L3 photonic crystal cavity embedded with QDs. (**D**) Cavity quality factor or Q factor=11,000. (**E**) An integrated device with coupled nanocavities and waveguides to implement ultrafast laser switching for a solid state–based photonic network.

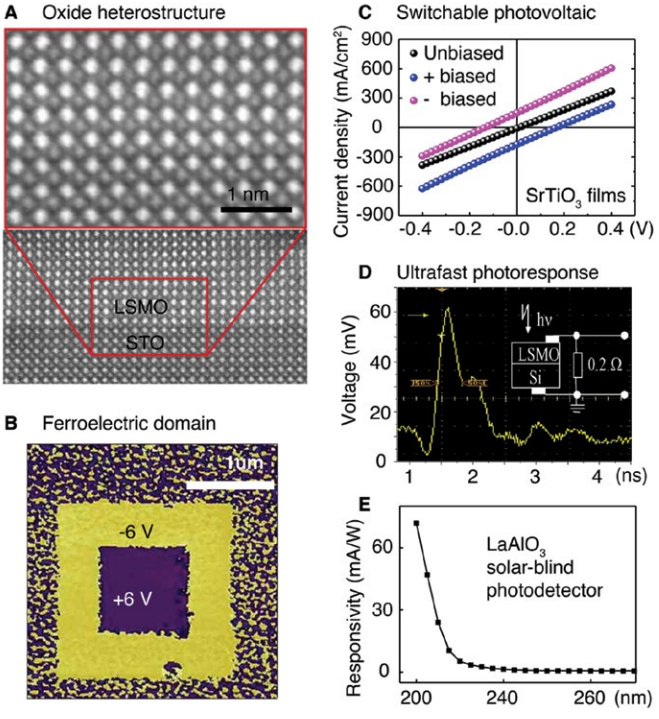

FIGURE 3. Multifunctional perovskite-oxide films. (**A**) Transmission-electron-microscopy image of lanthanum strontium manganite/strontium titanate ($La_{0.8}Sr_{0.2}MnO_3/SrTiO_3$) interface. (**B**) Out-of-plane piezoresponse force microscopy phase map of an 8-nm bismuth ferrite ($BiFeO_3$) film. (**C**) Photocurrents of the pristine, positively and negatively biased strontium titanate photovoltaic devices based on $SrTiO_3$ films under the illumination of a 375-nm laser. (**D**) Ultrafast photoresponse of an $La_{0.7}Sr_{0.3}MnO_3$/silicon (Si) heterojunction. (**E**) Spectral response of the lanthanum aluminum oxide ($LaAlO_3$) photodetector under a 10-V bias. LSMO, lanthanum strontium manganite; STO, strontium titanate.

optical switching with a time scale of a few picoseconds due to energy oscillation between the two cavities (*10*).

Perovskite-oxide optoelectronics

The well-known perovskite structure, ABX_3, is a rich platform in materials science. For example, solution-based perovskite solar cells with an organic A-site and halide X-site were recently reported to have substantial increase in efficiencies (>20%). In the past few decades, epitaxial perovskite oxide (ABO_3) films and heterostructures have attracted considerable attention for their physical properties as well as their potential device applications. Laser molecular beam epitaxy (LMBE) is one of the most popular methods to deposit high-quality perovskite oxide

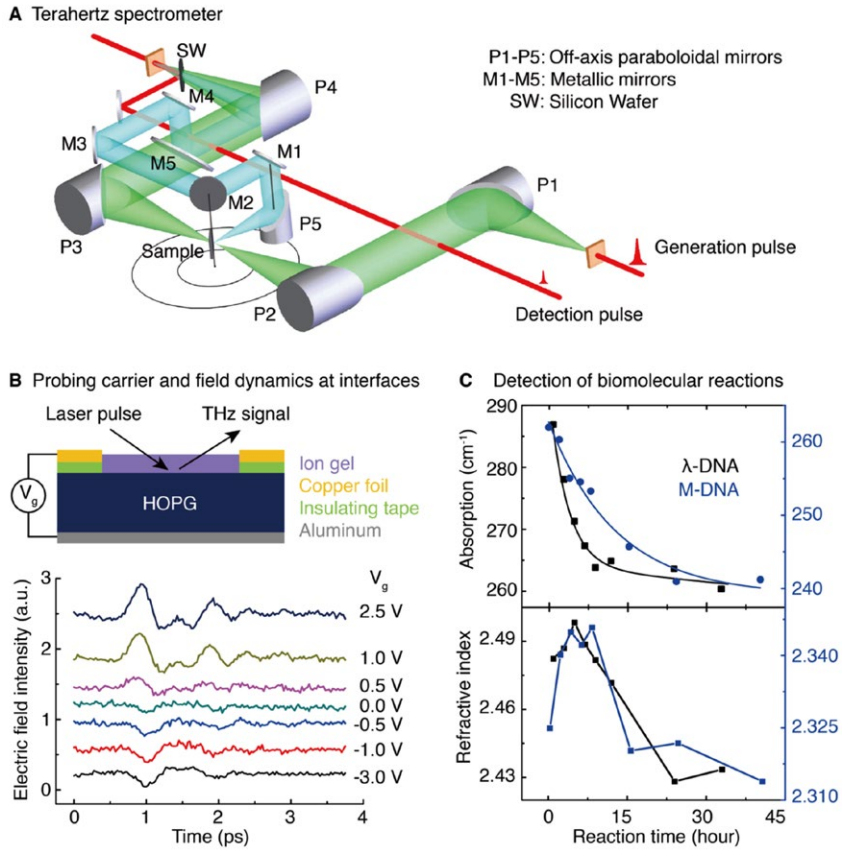

FIGURE 4. Applications of terahertz time-domain spectroscopy. (**A**) The patented terahertz time-domain spectroscopy (THz-TDS) system for angle-varying transmission–reflection measurements that can easily switch the detection mode between transmission and reflection by flipping mirror M5. In the reflection mode, M1 and P5 are on the same axis rotating around the vertical axis of the sample and M2. (**B**) THz generation from the highly ordered pyrolytic graphite (HOPG) and the waveforms as a function of bias. (**C**) Time evolution of THz responses of the λ-DNA and M-DNA reactions with oxaliplatin in aqueous solutions.

films due to its outstanding performance and ease of use. Briefly, the deposition of perovskite oxide film via LMBE is achieved by vaporization of target materials using a pulsed laser in a reactive environment.

Group L03 designed China's first LMBE equipment about three decades ago, and has successfully demonstrated many functional films such as ferromagnetic, ferroelectric, and optoelectronic perovskite-oxide heterostructures with atomically sharp interfaces (Figure 3A) (*11*, *12*). For instance, the lanthanum strontium manganite/strontium niobium titanate ($La_{0.9}Sr_{0.1}MnO_3/SrNb_{0.01}Ti_{0.99}O_3$) interfaces exhibited a colossal positive magnetoresistance under low magnetic fields (*13*). As another example shown in Figure 3B, good ferroelectricity of our bismuth ferrite ($BiFeO_3$) films was confirmed by local measurements using a piezoresponse force microscope (*14*, *15*). A switchable diode effect, diode direction reversible by switching ferroelectric polarization, was observed in the $BiFeO_3$ ferroelectric thin films, in which the polarization-modulated interfacial barrier played an important role (*14*, *15*). Furthermore, by using the migration of oxygen vacancies in strontium titanate ($SrTiO_3$) oxides (*16*), we proposed another strategy to produce the switchable diode and photovoltaic effect without using ferroelectric materials. The results are shown in Figure 3C. We revealed that the band bending induced by the motion of oxygen vacancies is the driving force for the switch between the two states. Based on this strategy, one could design switchable photovoltaic devices.

In Figure 3D, an ultrafast photoelectric effect was observed in the $La_{0.7}Sr_{0.3}MnO_3$/Si heterojunction (*11*, *12*). When this junction was irradiated by a 1064-nm laser pulse of 25 ps duration, the rise time was ~210 ps, and the full width at half-maximum was ~650 ps for the photovoltaic pulse. An unusual lateral photovoltage induced by the Dember effect was discovered in this structure (*17*). Recently, much attention has been paid to perovskite oxides with wide bandgaps, because they are natural candidates for photoabsorption materials for next-generation ultraviolet (UV) photodetectors. We fabricated a solar-blind UV photodetector employing lanthanum aluminum oxide ($LaAlO_3$) perovskite oxide with a bandgap of 5.6 eV for the first time (*18*). The response showed a sharp cutoff at ~220 nm. The photocurrent response reached 71.8 mA/W at 200 nm (Figure 3E), and the quantum efficiency reached 44.6%, indicating a unique potential in deep-UV detection.

Terahertz spectroscopy

Since the invention of femtosecond titanium (Ti):Sapphire all-solid-state lasers in the early 1990s, coherent terahertz sources developed rapidly (*19*), and terahertz time-domain spectroscopy (THz-TDS) emerged as a powerful tool for exploring light–matter interactions. In 1994, group L04 built the first THz-TDS measurement system in mainland China, as illustrated in Figure 4A.

When photocarriers are excited at the interface of semiconductors, THz radiation can be generated through current transients, carrying important information such as carrier mobility, field evolution, and modulated material responses. For example, the gold/gallium arsenide (Au/GaAs) Schottky interface excited by a femtosecond laser

pulse results in fast Fermi-level bending due to carrier accumulation in the depletion layer. We revealed this mechanism by temperature-dependent pump-probe measurements with picosecond time resolution (*20*). As shown in Figure 4B, the radiation was produced from a bulk highly oriented pyrolytic graphite (HOPG) excited by femtosecond laser pulses at 800 nm. By varying the incident angle of the pumping laser and applying an external bias, it was confirmed that the photocarriers driven by the built-in field within the first few carbon atomic layers were responsible for the THz generation (*21*).

The THz vibrational modes in biomolecules are very sensitive to molecular configuration and conformation. We used THz-TDS measurements to investigate the absorption and dispersion of polycrystalline α- and γ-glycine in the spectral region of 0.5 THz–3.0 THz (*22*). On the other hand, biomolecular reactions in a physiological condition are very important in many biological and medical studies, but quite difficult to detect. After overcoming the issue of water absorption using our highly sensitive THz-TDS system, we successfully observed the molecular reactions in aqueous solutions of anticancer drug oxaliplatin with λ-DNA and M-DNA extracted from mouse liver. As shown in Figure 4C, the half-life of the reaction was about 4.0 h for λ-DNA and 12.9 h for M-DNA, which can be attributed to their differences in strand length, composition, and sequence of nucleic acids (*23*).

References

1. B. Y. Cheng *et al.*, *Acta Phys. Sin.* 3, 861 (1994).
2. J. X. Fu, R. J. Liu, Z. Y. Li, *Appl. Phys. Lett.* **97**, 041112 (2010).
3. L. Lu, Z. Wang, arXiv:1611.01998.
4. L. Lu, J. D. Joannopoulos, M. Soljačić, *Nat. Phys.* **12**, 626–629 (2016).
5. Q. H. Yan *et al.*, *Nat. Phys.* (2016), www.nature.com/articles/s41567-017-0041-4.
6. S. Cao *et al.*, *Sci. Rep.* **5**, 8041 (2015).
7. S. Cao *et al.*, *Nano Res.* **9**, 306–316 (2016).
8. J. Tang, W. Geng, X. Xu, *Sci. Rep.* **5**, 9252 (2015).
9. Y. Sun *et al.*, *ACS Photonics* **4**, 369–377 (2017).
10. Y. Zhao *et al.*, *Opt. Express* **23**, 9211–9220 (2015).
11. K. J. Jin *et al.*, *Adv. Mater.* **21**, 4636–4640 (2009).
12. Y. Q. Feng *et al.*, *Sci. Rep.* **6**, 22382 (2016).
13. K. J. Jin *et al.*, *Phys. Rev. B* **71**, 184428 (2005).
14. A. Q. Jiang *et al.*, *Adv. Mater.* **23**, 1277–1281 (2011).
15. C. Wang *et al.*, *Appl. Phys. Lett.* **98**, 192901 (2011).
16. C. Ge *et al.*, *ACS Appl. Mater. Interfaces* **8**, 34590 (2016).
17. K. J. Jin *et al.*, *Appl. Phys. Lett.* **91**, 081906 (2007).
18. J. Xing *et al.*, *Opt. Lett.* **34**, 1675–1677 (2009).
19. L. Wang, in *Encyclopedia of Modern Optics*, vol. 5, G. Steel, B. D. Guenther, Eds. (Elsevier, New York, 2004), pp. 163–168.
20. Y. L. Shi *et al.*, *Appl. Phys. Lett.* **88**, 161109 (2006).
21. T. Ye *et al.*, *Sci. Rep.* **6**, 22798 (2016).
22. Y. L. Shi, L. Wang, *J. Phys. D* **38**, 3741–3745 (2005).
23. X. J. Wu *et al.*, *Ap pl. Phys. Lett.* **101**, 033704 (2012).

Ultrafast intense laser technology and physics

Yutong Li, Zhiyi Wei*, Bingbing Wang, and Jie Zhang*

The pursuit of ultrashort laser pulses and ultraintense laser power has attracted interest from a wide range of disciplines since the creation of lasers. The invention of chirped pulse amplification (CPA) technology and the discovery of Kerr-lens mode locking (KLM) for the titanium (Ti) sapphire laser in 1985 and 1991, respectively, have enabled us to generate ultrahigh intensity laser pulses at tabletop scale. With remarkable progress in recent years, peak power up to several petawatts (PW) has been reported, and pulse durations of shorter than 50 attoseconds have been demonstrated, which not only provide unprecedented extreme conditions for exploring emerging physics and phenomena, but also open a new era for revealing the ultrafast dynamics of electrons. Since the National Research Institute of Physics, Academia Sinica, was founded in 1928, optics has been studied as one of the main disciplines, and considerable achievements in laser science and technology have been made in the past 90 years. Inheriting these developments and innovations in optical physics,the Institute of Physics (IOP), Chinese Academy of Sciences, has been working toward ultrafast lasers and intense laser–matter interactions since 1997. Until now, only carrier-envelope phase (CEP)-controlled few-cycle lasers have been capable of realizing low-noise frequency comb generation and attosecond laser pulses; however, intense laser power—up to 1.16 PW—has now been generated from the in-house Ti-sapphire laser facility [XL-III (eXtreme Light)]. These laser systems have provided an experimental platform for research on laser-driven particle acceleration, novel laser-driven X-ray and THz radiation sources, laboratory astrophysics, fundamental physical processes relevant to advanced nuclear fusion concepts, long-distance propagation of femtosecond (fs) laser pulses in air (*1, 2*), and ultrarelativistic laser–matter interactions. Below, we briefly review some previously published results.

CEP control of few-cycle femtosecond lasers

It has been challenging work generating the shortest laser pulse. By using chirped mirrors to compensate for dispersion, we have generated 6-fs pulses from an in-house Ti-sapphire laser oscillator (*3*). An ultrabroad saddle-shaped spectrum was designed to enable superior results in CEP measurements, based on the difference fre-

Key Laboratory of Optical Physics, Institute of Physics, Chinese Academy of Sciences/Beijing National Laboratory for Condensed Matter Physics, Beijing, China
*Corresponding authors: zywei@iphy.ac.cn (Z.W.), jzhang@iphy.ac.cn (J.Z.)

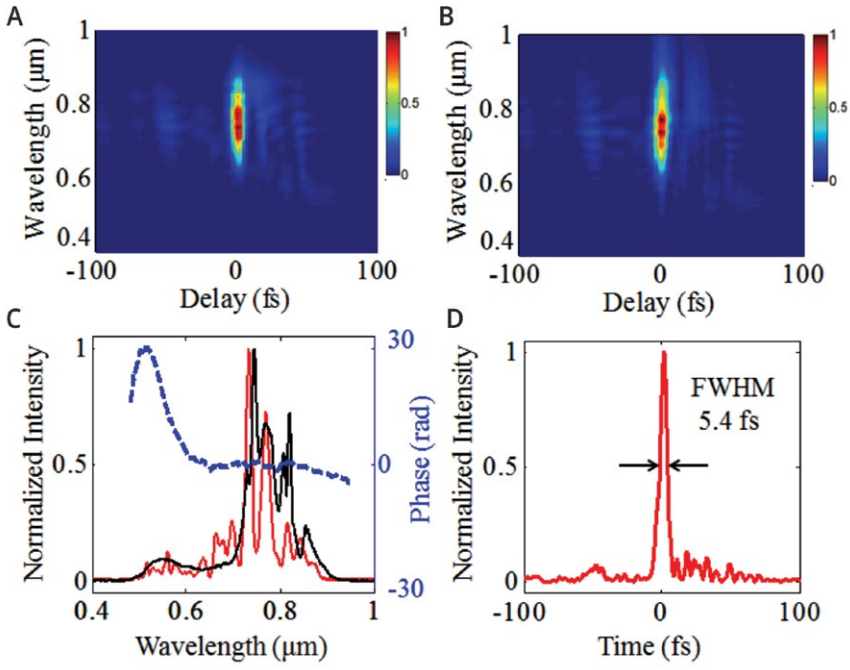

FIGURE 1. Frequency-resolved optical gating (FROG) characterization of a 5.4-fs pulse compressed from the supercontinuum.

quency generation (DFG) scheme—CEP frequencies with signal-to-noise ratios of up to 58 dB have been obtained. By locking the CEP and laser repetition rate to a microwave reference, we established an optical frequency comb with low noise (*4*).

The development of CPA technology has also attracted wide interest for its ability to compress intense laser pulses to a few cycles and stably lock the CEP. For this purpose, we injected a 30-fs laser pulse from a CPA Ti-sapphire laser (Femtopower Pro) into a hollow fiber to broaden the spectrum. Following a set of chirped mirrors that compensate for the dispersions, laser pulses as short as 3.8 fs with 0.5 mJ of energy were generated at a repetition rate of 1 kHz, corresponding to about 1.5 optical cycles. More recently, we replaced the hollow fiber with a set of thin silica plates to broaden the spectrum—transmittance of up to 85% was demonstrated in comparison with the 50% transmittance in the hollow fiber scheme—and the laser pulses were compressed to 5.4 fs with 0.68 mJ of energy, corresponding to a peak power higher than 0.1 terawatts (TW) (*5*). Figure 1 shows frequency-resolved optical gating (FROG) traces that characterize the pulse. The CEP could be continuously locked within a 75.2-mrad root mean square (RMS) for many hours.

Generation of isolated attosecond laser pulses

With the intense femtosecond laser–gas interaction, high-order harmonic generation (HHG) occurs on the attosecond timescale in the extreme ultraviolet (XUV) range. Since the first measurement of attosecond laser pulses by Drescher *et al.* (*6*), numerous studies on attosecond physics have been performed throughout the world. To generate isolated attosecond laser pulses for applications in condensed matter physics, we used the aforementioned CEP-controlled 5-fs CPA laser to induce interactions with noble gases, such as neon (Ne) and argon (Ar)—HHG events with discrete and continuous distributions were measured. By accurately controlling the CEP of the driving laser, we observed the arrowlike HHG spectrum—corresponding to the long and short trajectories of the ionized electrons (Figure 2)—for the first time; the contribution to HHG spectra can be easily recognized, which agrees well with the full quantum explanation (*7*).

To further measure the pulse duration of the HHG, we recorded the photoelectron energy spectrum with a time-of-flight detector. By scanning the delay between the attosecond XUV and femtosecond infrared (IR) pulses, the fringe-resolved streaking spectrogram was obtained, as shown in Figure 3. The pulse duration and phase can be retrieved from the spectrogram by FROG for complete reconstruction of attosecond bursts (FROG-CRAB), which showed attosecond laser pulses as short as 160 as, centered at a photon energy of 82 eV (*8*).

Amplification of the femtosecond laser to 1.16 PW with a high contrast ratio

To generate femtosecond laser pulses for even higher-energy laser–matter interactions, we developed a series of Ti-sapphire lasers with improved regenerative and multipass schemes based on CPA technology. For laser–matter interaction experiments at petawatt level, a contrast ratio of higher than 10^{10} in the temporal domain is required, to avoid preplasma formation before the arrival of the main pulse. Defined as the ratio of main laser intensity to background intensity, the contrast has been greatly enhanced by 5 or 6 orders of magnitude with some novel techniques. To generate ultraintense femtosecond laser pulses with high contrast from our XL-III facility, we proposed a new scheme that combines a doubled CPA system and a femtosecond noncollinear optical-parametric amplifier (NOPA)—its schematic diagram is shown in Figure 4; a sub-10 fs in-house Ti-sapphire oscillator was used as the seeding source. After amplification by a two-stage NOPA, which was pumped by the laser pulse from the CPA I, a 26-μJ signal with a contrast ratio of 10^{10} was obtained at a central wavelength of 800 nm. Seeding the high contrast signal into the CPA II and suppressing the parasitic lasing with a special liquid material surrounding the Ti-sapphire crystal, a 32.3-J

laser pulse with a duration of 27.9 fs—corresponding to a peak power of 1.16 PW—was measured using a commercial FROG device (*9*). To our knowledge, this is the first laser pulse of larger than 1 PW from a Ti-sapphire laser facility.

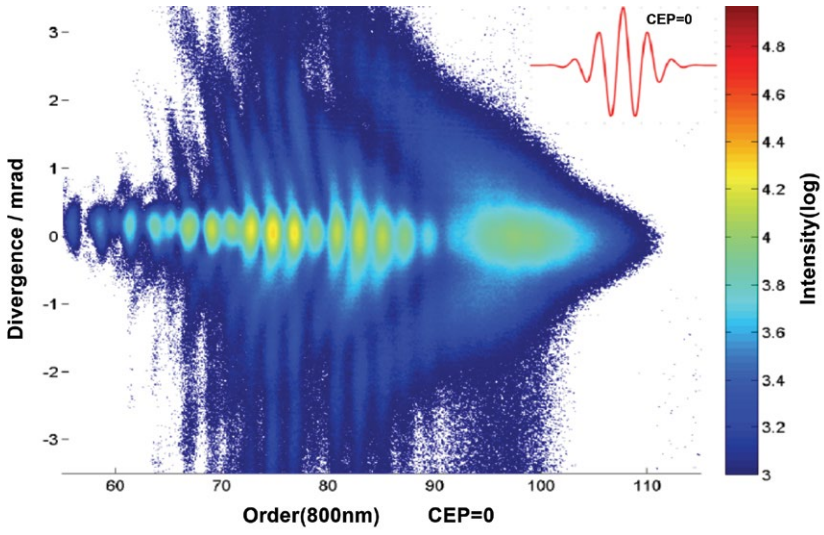

FIGURE 2. Arrowlike high-order harmonic generation (HHG) spectrum.

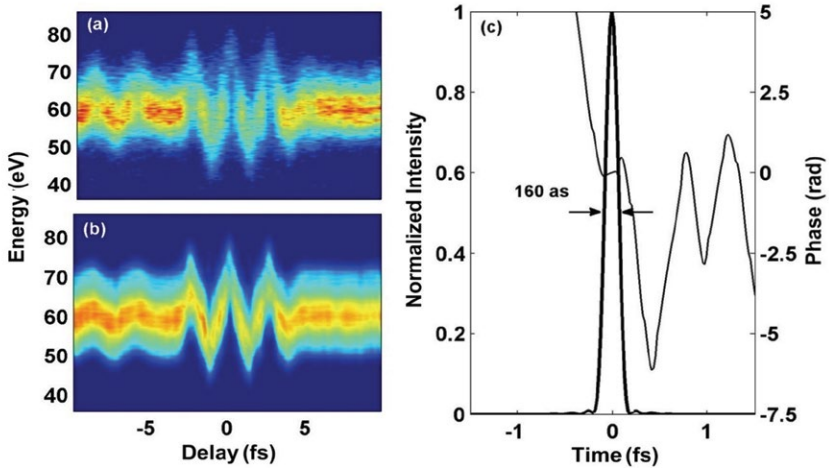

FIGURE 3. Fringe-resolved streaking spectrogram.

Generation and transport of intense laser–produced energetic (fast) electrons

The generation and transport of fast electrons are fundamental physical processes that are important for applications such as fast ignition (FI) of inertial confined fusion. We have comprehensively studied the physics of fast electrons within laser durations ranging from femtoseconds to picoseconds, and intensities ranging from 10^{16} W/cm^2 to 10^{20} W/cm^2. We demonstrated a stable, collimated fast electron beam along the target surface in intense laser interactions with planar solid foils at large incident angles (Figure 5)—the confinement being due to the surface quasistatic electromagnetic fields (*10*). The effects of laser polarization on emission direction of fast electrons from solid targets have been identified (*11*). For the first time, we observed the directional emission of fast electrons from water plasma (*12*). A two-dimensional Fokker–Planck code was developed, and we found that the well-known Spitzer–Harm model is no longer held under field strength, which prompted us to propose a new theoretical model (*13*). We have demonstrated bulk ion acceleration in low-density foam targets with the electrostatic fields induced by the fast electron transport among the multiple lamellae inside the foam (*14*). A key issue with the FI scheme is enhancing the heating efficiency of high-intensity lasers; for this purpose, we proposed a magnetically assisted FI scheme (*15*), which could enhance efficiency by up to 14% with an external magnetic field of 20 megagauss (MG).

Laser-driven novel radiation sources

Hard X-ray sources based on femtosecond laser–driven plasmas have numerous interesting applications owing to their ultrashort duration and small sizes. Using high-contrast laser–cluster target interactions, we have generated quasi-monoenergetic hard X-ray radiation with a peak brightness of 10^{21} photons/(s mm^2 mrad^2). We further proposed a new oscillation injection scheme and obtained a high yield of 5×10^8 photons with a peak brilliance of 10^{23} photons/(s mm^2 mrad^2)/[0.1% bandwidth (BW)] in a corresponding experiment (*16, 17*). In view of the big challenge of intense THz radiation generation, we have extended plasma radiation to the THz regime; THz sources stronger than hundreds of μJ were generated with intense lasers. A linear mode conversion mechanism was proposed, and it was demonstrated through picosecond laser interactions with large-scale inhomogeneous plasmas (*18, 19*). In addition, we demonstrated coherent THz radiation from a foil due to transition radiation of the laser-produced electron beams (Figure 6); the THz radiation energy (of up to 400 μJ) is comparable to that from linear accelerators (*20*).

Laboratory astrophysics

The extreme conditions created by high-power lasers

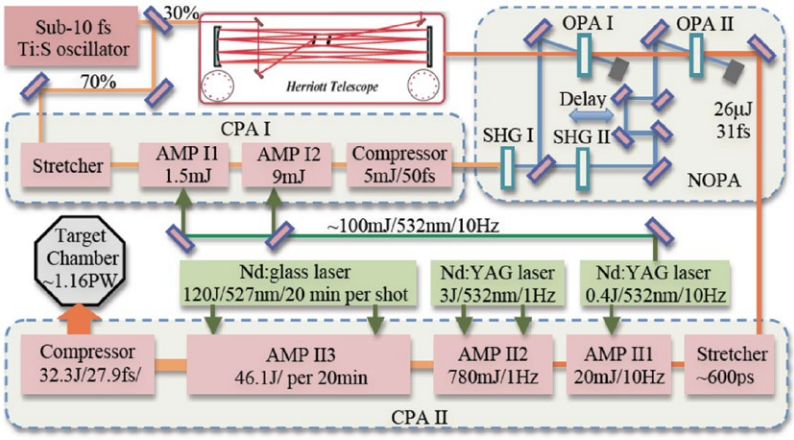

FIGURE 4. Schematic setup of the XL-III (eXtreme Light) facility. AMP, amplifier; CPA, chirped pulse amplifier; OPA, optical parametric amplifier; SHG, second harmonic generation.

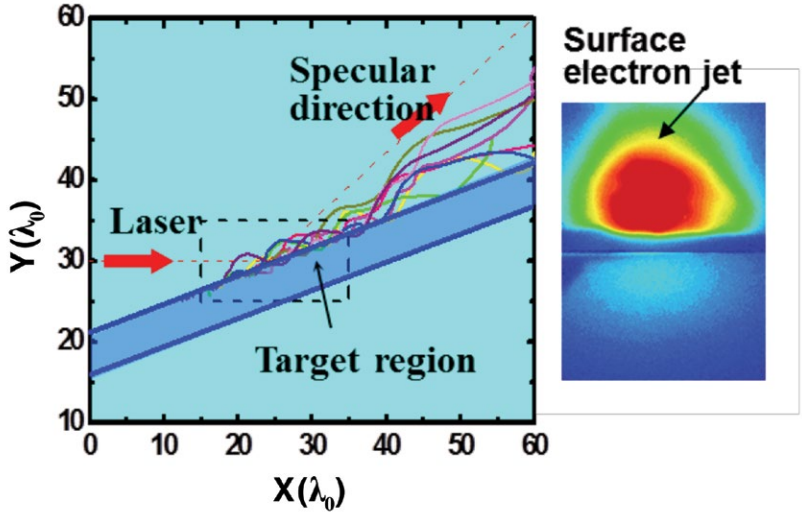

FIGURE 5. Fast electron beam emission along the surface of a target irradiated by intense laser pulses.

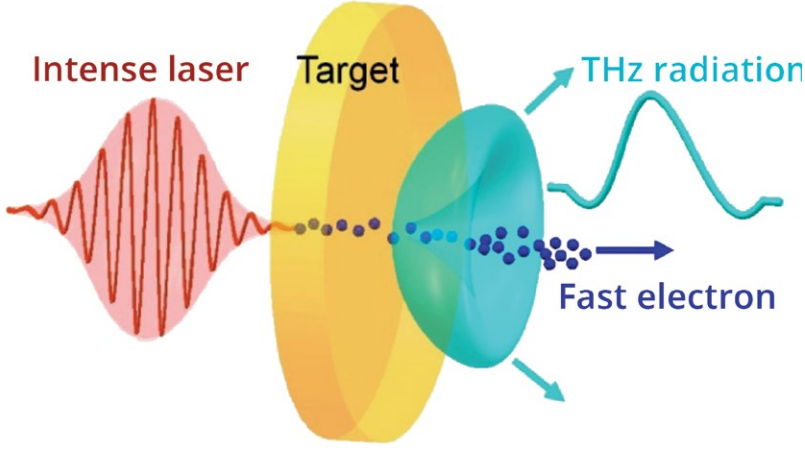

FIGURE 6. Schematic diagram illustrating THz generation via coherent transition radiation from the rear surface of a foil target.

can be used to simulate astronomical phenomena and processes. Magnetic reconnection (MR) is important in many astrophysical phenomena, such as solar flares. We reconstructed MR outflows and the loop-top X-ray source in solar flares at the laboratory. The electron-diffusion regions (EDR) in MR were resolved, and electron acceleration was observed (*21, 22*). Collisionless shock waves, responsible for the generation of high-energy cosmic rays, were demonstrated with two counterstreaming laser-produced plasmas (*23*). By heating a simple open-ended coil with a high-power laser, a 200-T pulsed strong magnetic field was generated (*24*). Herbig–Haro (HH) objects associated with newly born stars are of great interest in astrophysics. We generated a laser-produced supersonic jet deflected by 55 degrees when colliding with a nearby orthogonal side flow, which well represented the jet deflection in the HH object (*25*).

Strong-field atomic and molecular physics

We revealed the effect of a static electric field on HHG in research on strong-field atomic and molecular physics in 1998 (*26*). Since then, we have focused on the dynamic processes of intense laser–matter interaction, including the excitation, ionization, and emission of atoms and molecules in intense laser fields. We have been long-engaged in developing the frequency-domain theory of the recollision processes in intense laser fields. In contrast with conventional time-domain theory, there are many advantages offered by frequency-domain theory. For example, all dynamic processes can be decoupled into two steps: (1) above threshold ionization (ATI) and (2) laser-assisted collision (LAC) or laser-assisted recombination (LAR), so that one can investigate separately the roles of these subprocesses; additionally, all recollision processes—including HHG, high-order ATI (HATI), and nonsequential double ionization (NSDI) (*27*)—can be solved under a unified theoretical frame, where the relationships among all these processes can be conveniently studied. Progress has also been made on

numerical approaches for solving the time-dependent Schrodinger equation based on the Hylleraas and B-spline methods. For the first time, we found the CEP effect in the laser-driven atomic bound–bound transition for a long laser pulse containing tens of laser cycles (*28*).

Perspectives

Studies of ultrashort intense laser–matter interactions have been performed worldwide during the past decades. In the future, we will concentrate on demonstrating some important applications for laser-driven radiation sources. The Synergetic Extreme Condition User Facility (SECUF) will be built in five years in Beijing; there we will build ultrafast radiation and electron beamlines for studying the dynamics of many disciplines, including condensed matter, biology, and chemistry.

References

1. T. T. Xi, X. Lu, J. Zhang, *Phys. Rev. Lett.* **96**, 025003 (2006).
2. X. Lu *et al.*, *Sci. Rep.* **5**, 15515 (2015).
3. Y. Y. Zhao, P. Wang, W. Zhang, J. R. Tian, Z. Y. Wei, *Sci. China Ser. G* **50**, 261–266 (2007).
4. W. Zhang, H. Han, Y. Zhao, Q. Du, Z. Wei, *Opt. Express* **17**, 6059–6067 (2009).
5. P. He *et al.*, *Opt. Lett.* **42**, 474–477 (2017).
6. M. Drescher *et al.*, *Science* **291**, 1923–1927 (2001).
7. P. Ye *et al.*, *Phys. Rev. Lett.* **113**, 073601 (2014).
8. M. J. Zhan *et al.*, *Chin. Phys. Lett.* **30**, 093201 (2013).
9. Z. Wang *et al.*, *Opt. Lett.* **36**, 3194–3196 (2011).
10. Y. T. Li *et al.*, *Phys. Rev. Lett.* **96**, 165003 (2006).
11. L. M. Chen *et al.*, *Phys. Rev. Lett.* **87**, 225001 (2001).
12. Y. T. Li *et al.*, *Phys. Rev. Lett.* **90**, 165002 (2003).
13. S. M. Weng *et al.*, *Phys. Rev. Lett.* **100**, 185001 (2008).
14. Y. T. Li *et al.*, *Phys. Rev. E* **72**, 066404 (2005).
15. W. M. Wang, P. Gibbon, Z. M. Sheng, Y. T. Li, *Phys. Rev. Lett.* **114**, 015001 (2015).
16. L. M. Chen *et al.*, *Phys. Rev. Lett.* **104**, 215004 (2010).
17. W. Yan *et al.*, *Proc. Nat. Acad. Sci. U.S.A.* **111**, 5825–5830 (2014).
18. Z. M. Sheng, K. Mima, J. Zhang, H. Sanuki, *Phys. Rev. Lett.* **94**, 095003 (2005).
19. G. Q. Liao *et al.*, *Phys. Rev. Lett.* **114**, 255001 (2015).
20. G. Q. Liao *et al.*, *Phys. Rev. Lett.* **116**, 205003 (2016).
21. J. Zhong *et al.*, *Nat. Phys.* **6**, 984–987 (2010).
22. Q. L. Dong *et al.*, *Phys. Rev. Lett.* **108**, 215001 (2012).
23. X. Liu *et al.*, *New J. Phys.* **13**, 093001 (2011).
24. B. J. Zhu *et al.*, *Appl. Phys. Lett.* **107**, 261903 (2015).
25. D. Yuan *et al.*, *Astrophys. J.* **815**, 46 (2015).
26. B. Wang, X. Li, P. Fu, *J. Phys. B* **31**, 1961–1972 (1998).
27. B. Wang, Y. Guo, J. Chen, Z. C. Yan, P. Fu, *Phys. Rev. A* **85**, 023402 (2012).

Research on magnetism and magnetic materials

Young Sun*, Fangwei Wang, Xiufeng Han, Zhaohua Cheng, Fengxia Hu, Wenhong Wang, Jianwang Cai, and Baogen Shen

The Institute of Physics (IOP) has a long history of research on magnetism and magnetic materials, beginning in 1934, when Ruwei Shi began studying magnetism at the Institute of Physics of the Academia Sinica. In 1950, a magnetism research group was established within the Institute of Applied Physics at the Chinese Academy of Sciences (CAS). This group was expanded to form a magnetism laboratory in 1959, and later developed into the CAS Open Laboratory of Magnetism in 1987. Finally, it became the State Key Laboratory of Magnetism (SKLM) in 1995. Historically, the magnetism laboratory at IOP has been regarded as the national center for magnetism studies. It has educated many young researchers who later found staff and faculty positions at various universities and institutions around China. At present, SKLM consists of seven research groups (M01–M07) that cover diverse research topics ranging from traditional magnetic materials to frontiers in modern magnetism (Figure 1).

Magnetic functional materials

Since the 1960s, the exploration of advanced rare-earth permanent magnets has had a traditional research direction. The magnetism laboratory has been accumulating data on permanent magnets for many years, achieving fruitful results in this field, including the successful fabrication of new melt-spun Nd-Fe-B permanent magnets with a single-phase hard magnetic behavior, the first synthesis of $Sm_2(Fe,Ga)_{17}C_y/\alpha$-Fe nanocomposites, and the confirmation of the origin of enhanced remanence in $Sm_2Fe_{17-x}M_xC_y$ nanopermanent magnets. The discovery of SmFeGaC permanent magnets is believed to have opened a new research direction for permanent magnets. Related works have won the first prize for Science and Technology in Beijing, and the second prize for Natural Sciences at the Chinese Academy of Sciences. In 1985, some faculty members of the magnetism laboratory founded the Beijing Zhong Ke San Huan Hi-Tech Company, based on previous achievements in the field of permanent magnets. After more than 30 years of rapid development, it is now among the top three permanent magnet companies in the world.

The refrigeration technique based on the magnetocaloric effect (MCE) has obvious advantages over the conventional gas-compression technique in

State Key Laboratory of Magnetism, Institute of Physics, Chinese Academy of Sciences
*Corresponding author: youngsun@iphy.ac.cn

terms of environmental protection and energy conservation. We have been focusing on the MCE since 1998. One important discovery has been the giant magnetic entropy change in $La(FeSi)_{13}$-based materials (*1*); this change is twice that in the rare-earth metal gadolinium. Our work revealed the close relationship between a large MCE and a sudden change in the lattice volume induced by phase transition and itinerant-electron metamagnetic transition. Moreover, we proved that the Maxwell relations—commonly adopted to determine magnetic entropy changes—cannot be directly applied to first-order phase transitions, and established an appropriate method for determining entropy changes in phase-separated systems. Recently, a large MCE was found at room temperature in the Heusler alloy Ni–Mn–Ga, revealing the close relationship between magnetoelasticity and the MCE (*2*). These research achievements have been awarded the first prize for Science and Technology in Beijing in 2011, the second prize for National Natural Sciences in China in 2012, and the Tan Kah Kee Award in 2014.

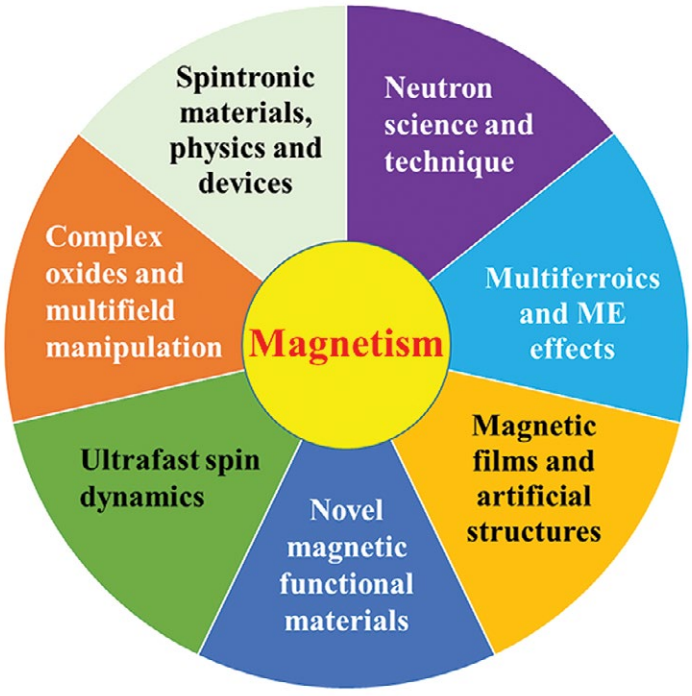

FIGURE 1. Current research topics at the State Key Laboratory of Magnetism (SKLM). ME, magnetoelectric.

Magnetostructural transition materials provide a rich resource for searching various functional magnetic materials, such as highly spin-polarized ferromagnetic materials, magnetic refrigerators, nanoscale magnetic skyrmions, and topological magnetic quantum materials. Since 1998, three new Heusler-type magnetostructural transition materials have been discovered in this laboratory. In 2012, an important physical effect, a Curie temperature window, was found in MM'X alloys with hexagonal structures (Figure 2A), in which the stable coupling of magnetic and structural transitions was realized (*2*). In 2015, a novel magnetic alloy family known as all-d-metal Heusler alloys, which include $Ni_{50}Mn_{50-y}Ti_y$ and $Ni_{50-x}Co_xMn_{35}Ti_{15}$, was developed based on d-d covalent bonding; these alloys exhibit excellent mechanical and martensitic transformation properties.

Complex oxides and multiferroics

Complex oxides with coupled degrees of freedom exhibit many emergent phenomena, which have been a source for finding novel physical effects. In the past two decades, we focused on the design and fabrication of heteroepitaxial multilayers/superlattices of complex oxides with strongly coupled degrees of freedom, and the quantum manipulation of their distinct magnetic and spin–charge transport behaviors. The main achievements include the discovery of electronic phase separation in colossal magnetoresistive manganites, magnetic-field-tunable rectifying behavior in manganite-based p–n junctions, a novel cooperative tuning of photoexcitation and the gate field to the two-dimensional electron liquid at the $LaAlO_3/SrTiO_3$ interface (*3*), and efficient spin-to-charge conversion at the conducting $LaAlO_3/SrTiO_3$ interface (Figure 2B).

Multiferroics and magnetoelectric (ME) effects have been studied extensively because of their intriguing fundamental physics as well as significant potential in device applications. We discovered several new types of multiferroic materials with strong ME effects. Record-breaking giant ME effects were achieved in Y-type hexaferrite $Ba_{0.4}Sr_{1.6}Mg_2Fe_{12}O_{22}$ single crystals (*4*). Meanwhile, we proposed and demonstrated that the fourth fundamental circuit element defined according to the charge–magnetic flux relationship can be realized by implementing ME effects. The fourth element is called the transtor, and its corresponding nonlinear memelement is called the memtranstor. Thus, a complete diagram of the fundamental circuit elements was obtained (Figure 2C). Moreover, we developed a new type of nonvolatile memory based on the memtranstor, which has outstanding practical advantages, such as a simple structure, easy writing and reading operations, low power consumption, high speed, and availability of diverse materials.

Magnetic heterostructures and spintronic devices

SKLM has been working in the field of spintronic physics and developing spintronic materials and prototype devices for a long time. Spintronic devices and information storage technology are being developed

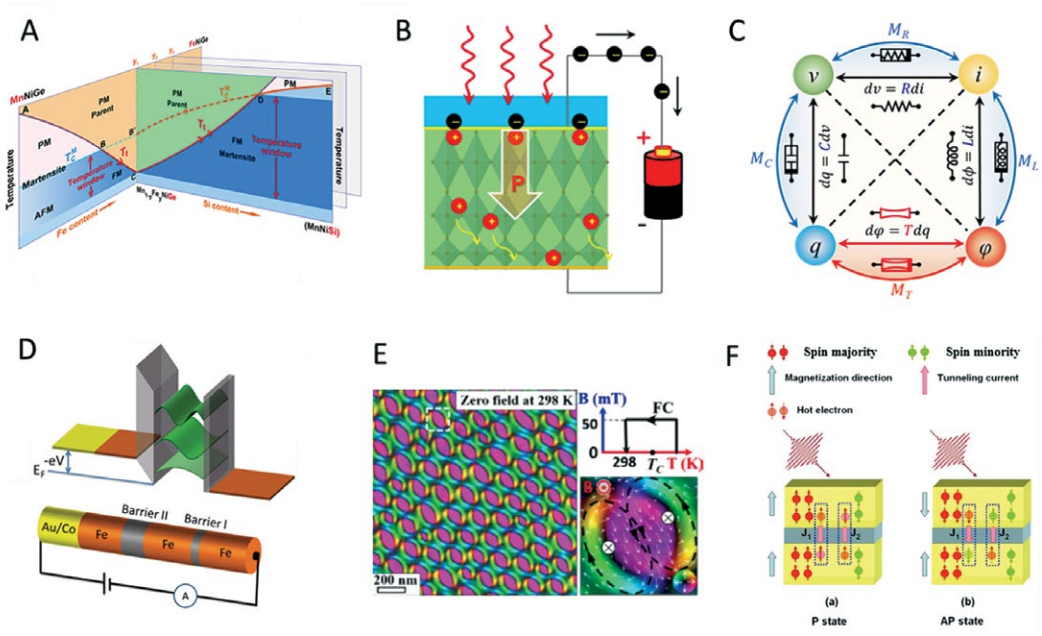

FIGURE 2. Recent representative achievements in magnetism R&D. (**A**) Designing magnetic phase-transition materials based on the Curie-temperature window method and the isostructural alloying principle. (**B**) Visible-light-enhanced gating effect at the LaAlO3/SrTiO3 interface. (**C**) Complete diagram of fundamental circuit elements. (**D**) Long-range phase coherence in double-barrier magnetic tunnel junctions (DBMTJs). (**E**) Real-space observation of nonvolatile zero-field biskyrmion lattice in a MnNiGa magnet. (**F**) Ultrafast demagnetization enhancement in a CoFeB/MgO/CoFeB magnetic tunnel junction. PM, paramagnetic; FM, ferromagnetic; AFM, antiferromagnetic; P, parallel; AP, antiparallel.

to achieve higher speed, higher density, and lower energy consumption than current models and methods. Magnetic random-access memory (MRAM) is a type of nonvolatile memory that was developed based on magnetic tunnel junction (MTJ) unit cells. We fabricated a nanoring-shaped MTJ, based on an aluminum oxide (AlO_x) barrier with ring widths between 25 nm and 30 nm, and designed a demo MRAM device based on the nanoring MTJ. This MTJ can avoid stray fields between cells because of its closed shape, and can improve thermal stability, making it a superior candidate for high-density MRAM. Resonant tunneling through spin-dependent quantum well (QW) states formed in the middle layer of double-barrier MTJs (DBMTJs) can result in extremely high tunneling magnetoresistance (TMR). We clarified the relationship between QW energy and the thickness of the middle iron (Fe) layer. Furthermore, we fabricated single-crystal DBMTJs with a Fe/$MgAlO_x$/Fe/$MgAlO_x$/Fe core structure (Figure 2D), and their conductance was unambiguously observed to oscillate as a function of the bias due to the QW states in the middle Fe layer (*5*).

Considering the surface/interface effect, quantum confinement, and interface exchange interaction as well as other factors, magnetic heterostructure films exhibit features such as interlayer exchange coupling, exchange bias, magnetic proximity, interfacial perpendicular magnetic anisotropy (PMA), and interfacial Dzyaloshinskii–Moriya interaction. We considerably improved the PMA of Ta/CoFeB/MgO films by replacing tantalum (Ta) with a thin hafnium (Hf) or molybdenum (Mo) layer, and developed thermally robust Mo/CoFeB/MgO-based perpendicular MTJs with a high TMR of 120%. We also demonstrated that platinum (Pt) exhibits magnetic proximity in $Y_3Fe_5O_{12}$/Pt heterostructures (*6*). Moreover, our recent study showed that four types of magnetoresistance (MR) correlations could be reproduced in Fe thin films depending on the film thickness, texture, interface, and morphology. In magnetic heterostructures with modulations for the constituent physical parameters, interface, and external fields, we will explore the spin Hall effect, interfacial spin current transparency, and interfacial spin memory loss to efficiently utilize various spin current effects.

Topological magnetism

Topological magnetic textures have drawn considerable interest because of their potential applications in high-density, energy-efficient information storage. By focusing on discovering new topological magnetic states, we found two types of bulk materials hosting magnetic skyrmions/biskyrmions—$(Mn_{1-x}Ni_x)_{65}Ga_{35}$ (*7*) and Fe_3Sn_2 (*8*)—with a remarkably wide temperature range and high-temperature stability, respectively. Moreover, by employing simple field-cooling manipulation, we demonstrated the generation and sustainability of a robust biskyrmion lattice in a zero magnetic field over a wide temperature range (16 K–338 K) in a $(Mn_{0.5}Ni_{0.5})_{65}Ga_{35}$ alloy. Alternatively, in perpendicularly magnetized platinum/cobalt/tantalum (Pt/Co/Ta) multilayers, we used an in situ Lorentz microscope to generate and tune the skyrmions via a

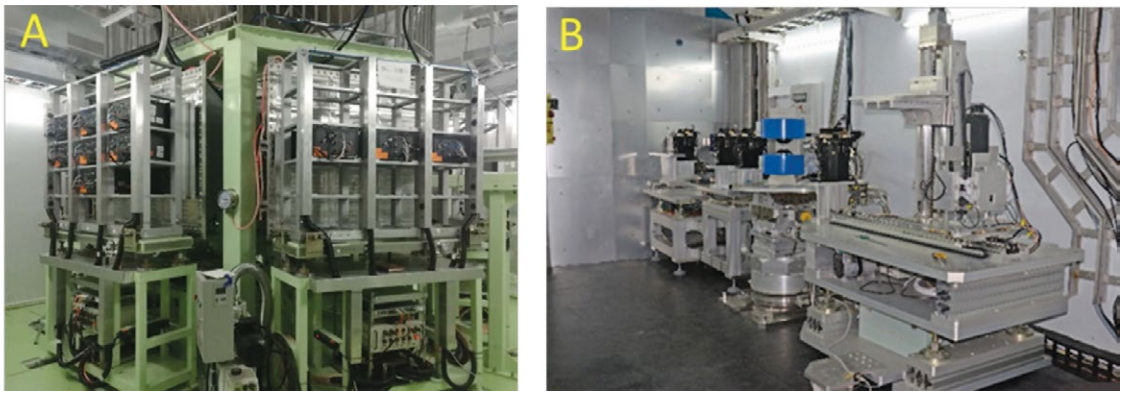

FIGURE 3. (A) Detector banks of general-purpose powder diffractometer. (B) Scattering chamber of multipurpose reflectometer.

preset in-plane current and perpendicular magnetic field, confirming that the high-density skyrmions persisted after the current and magnetic field were switched off (Figure 2E).

Development of advanced techniques and facilities

The neutron-scattering group of the SKLM established the Engineering Center for Target Station and Neutron Instruments of the China Spallation Neutron Source (CSNS) in 2006, focusing on neutron instrumentation and neutron scattering applications in condensed matter, particularly in magnetically related systems. From 1979 to 2000, the group built three instruments around the reactor at the China Institute of Atomic Energy. From 2000, the team began designing, constructing, and commissioning the target station and three day-one neutron instruments for CSNS. After a 10-year prototype study and six-year construction phase, the first neutron pulse bombardment took place on August 28, 2017, with the expected energy spectrum and high proton–neutron transfer efficiency. The first "hot" commissioning of neutron instruments was performed, the first diffraction pattern was collected on a standard silicon (Si) sample, and a resolution of 0.23% was realized without further data reduction analysis in November 2017. All the CSNS day-one instruments are expected to be open to users after their commissioning in March 2018 (Figure 3).

Femtosecond (fs) laser pulses offer the intriguing possibility of probing a magnetic system on a timescale corresponding to the exchange interaction responsible for the existence of the magnetic order, while also having a considerably shorter timescale than that of a spin–orbit interaction or magnetic precession. Laser-induced femtosecond magnetism opens a new frontier for faster magnetic storage devices, but probing such a fast magnetization change is a big challenge (Figure 2F). Recently, we designed and set up a time-resolved magneto-optical Kerr microscope and magnetometer with a temporal resolution of 100 fs and spatial resolution of 500 nm. In a magnetic system, spin–orbit coupling influences the optical transition rates, leading to magnetic dichroism (MCD). By using a deep ultraviolet laser, we can employ magnetism to analyze the spin chirality and the dynamics of the spin and orbital angular momentum down to the pico- or femtosecond timescale. Angle-resolved photoemission spectroscopy (ARPES) has been proven to be the most powerful technique to investigate electronic structures. A combined deep-ultraviolet MCD and ARPES technique is under development; it will provide deep insight into the electronic structure, spin structure, and spin–orbit coupling of magnetic nanostructures and magnetic topological insulators.

Outlook

Magnetism is a broad field that overlaps with many subfields in condensed matter and materials physics, such as superconductivity, semiconductors, surface science, and topological states. SKLM intends to broaden its scope to include new topics, such as proximity effects in ferromagnet/superconductor heterostructures, exotic quantum states of frustrated spin systems, molecular magnetism, bio/chemical magnetism, magnetic microscopy, and imaging. Talented young scientists interested in magnetism are encouraged to apply for faculty positions at SKLM.

References

1. B. G. Shen, J. R. Sun, F. X. Hu, H. W. Zhang, Z. H. Cheng, *Adv. Mater.* **21**, 4545–4564 (2009).
2. E. Liu *et al.*, *Nat. Commun.* **3**, 873 (2012).
3. Y. Lei *et al.*, *Nat. Commun.* **5**, 5554 (2014).
4. K. Zhai *et al.*, *Nat. Commun.* **8**, 519 (2017).
5. B. S. Tao *et al.*, *Phys. Rev. Lett.* **115**, 157204 (2015).
6. Y. M. Lu *et al.*, *Phys. Rev. Lett.* **110**, 147207 (2013).
7. W. Wang *et al.*, *Adv. Mater.* **28**, 6887–6893 (2016).
8. Z. Hou *et al.*, *Adv. Mater.* **29**, 1701144 (2017).

Phase problem in X-ray crystallography and electron microscopy

Hai-Fu Fan*

Since 1980, a research group led by Hai-Fu Fan at the Institute of Physics (IOP) has been dedicated to the "phase problem" in X-ray crystallography and electron microscopy (EM) (http://cryst.iphy.ac.cn). The group collaborated for two papers published in 1965, both of which focus on "direct methods" in crystallography (*1, 2*). The first paper (*1*) extended the Sayre equation (*3*) by considering the existence of heavy atoms with known positions. A subsequent systematic study on pseudosymmetries and phase ambiguities (*4*) led to the development of the program SAPI (structure analysis programs with intelligent control—or, read backwards, "Institute of Physics, Academia Sinica") (*5–7*), which is the first direct-method computer program that can detect and solve superstructures. SAPI was adopted by the Rigaku Corporation (Japan) and the Molecular Structure Corporation (United States), from 1986 until the early 1990s, as the main structure-solving program for small crystal structures. The second paper (*2*) proposed a method to break the phase ambiguity intrinsic in SAD (single-wavelength anomalous diffraction) or SIR (single isomorphous replacement) experiments, marking one of the earliest attempts to introduce direct methods to protein crystallography. The results of the research have been successfully applied in numerous disciplines, including materials and life sciences. Since its inception, the group has focused on exploring new applications for direct methods outside of their traditional fields.

1. Direct methods as a tool of image processing in EM

A two-stage image processing procedure that combines information from an EM image and the corresponding electron diffraction (ED) pattern has been proposed (*8*). Tests using the EM image of the high-critical-temperature (Tc) superconductor Bi-2212 showed that the resolution of the original EM image is enhanced by a factor of two (*9*), as shown in Figure 1. Hopefully, this technique may also be useful in improving the resolution of cryo-EM images. The program package VEC (visual computing in electron crystallography) was written for the automation of two-stage EM image processing (*10*).

2. Incommensurate modulated structures and composite structures solved by multidimensional direct methods

Multidimensional direct methods (MDDM) were proposed for the determination of incommensurate crystal structures without relying on a preassumed model (*11, 12*). The application of MDDM to the *0klm* ED pattern of the high-Tc superconductor Bi-2223 revealed incommensurate modulation, which was reported by Zhong-Xian Zhao during the Nobel Jubilee Symposium of 1991 (*13*). The program DIMS (direct methods in multidimensional space) was written for the implementation of these methods (*14*), and it was later incorporated in the VEC package (*15, 16*).

3. Combining direct methods with protein crystallographic methods

The P_+ probability formula (*17*) was derived by

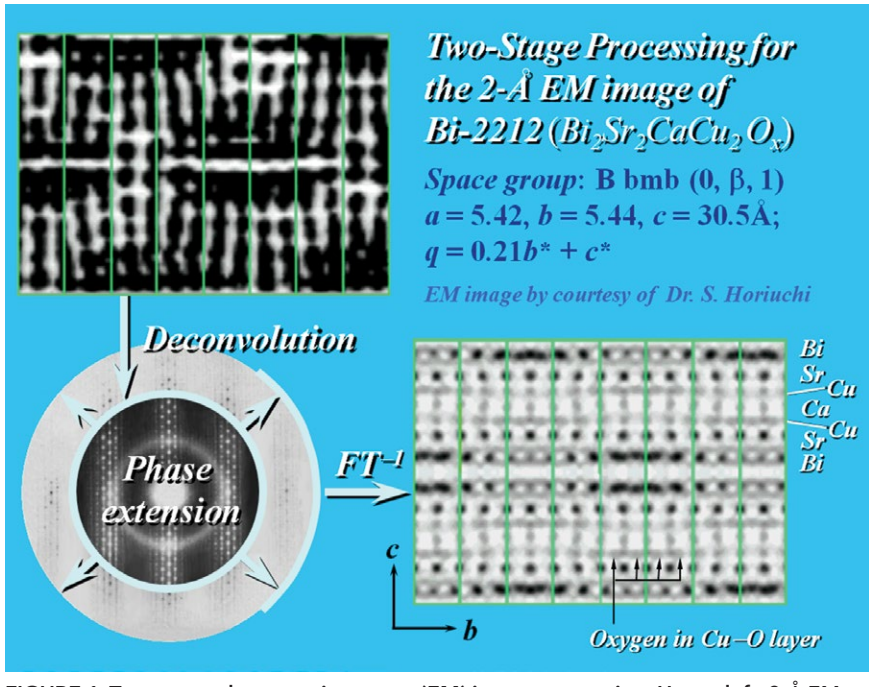

FIGURE 1. Two-stage electron microscopy (EM) image processing. Upper left: 2-Å EM image of the high-critical-temperature (Tc) superconductor Bi-2212. **Lower left:** 1-Å electron diffraction pattern plus 2-Å diffraction phases; the latter resulted from stage 1 (deconvolution). **Lower right:** 1-Å structure image, the inverse Fourier transform (FT) of the result from stage 2 (phase extension).

Beijing National Laboratory for Condensed Matter Physics and Key Laboratory of Soft Matter Physics, Institute of Physics, Chinese Academy of Sciences, Beijing, China
*Corresponding author: fan@iphy.ac.cn

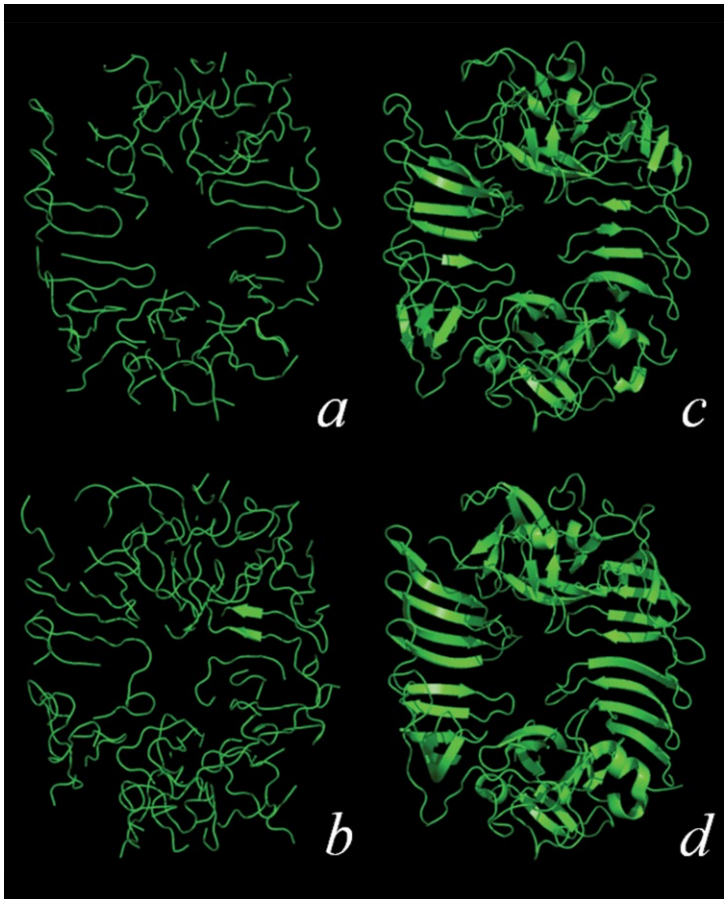

FIGURE 2. Direct-method-aided model completion. (*a*) The starting model obtained by PHENIX.AutoBuild with 5.3-Å 1h3i (PDB code) MAD data. (*b*) Result obtained by IPCAS running in Model Extension mode with 2.8-Å 1h3i SAD (at high-remote wavelength) data. (*c*) Result obtained by IPCAS running in Phase/Model Extension mode with 2.8-Å 1h3i SAD high-remote data. (*d*) The final 1h3i model. IPCAS, Iterative Protein Crystal structure Automatic Solution; MAD, multiwavelength anomalous diffraction; PDB, Protein Data Bank; SAD, single-wavelength anomalous diffraction. (Models in this figure were plotted by PyMOL in the cartoon mode.)

combining the Cochran distribution in the direct methods, the bimodal distribution of SAD and SIR experiments in protein crystallography, and the Sim distribution in small-molecule crystallography. The program OASIS (one-wavelength anomalous scattering and single isomorphous substitution) (*18*) was written based on the P_+ formula. OASIS has been adopted by CCP4 (Collaborative Computational Project No. 4, United Kingdom) since 2000 as the only direct-method program capable of breaking the SAD/SIR phase ambiguity for diffraction data far below the 1.2-Å atomic resolution. The pipeline IPCAS (Iterative Protein Crystal structure Automatic Solution) (*19*) has been developed, in which OASIS and several world-renowned programs are involved. Two features of IPCAS are iterative direct-method SAD phasing and direct-method-aided model completion (*20, 21*). An example of the latter is shown in Figure 2, where a set of 5.3-Å MAD (multiwavelength anomalous diffraction) phases has been successfully extended to a set of 2.8-Å SAD (at high-remote wavelength) data, leading to more than 90% of the complete structure. With this technique, a set of cryo-EM phases at about 6 Å resolution could readily be extended to a set of X-ray native protein data at a resolution higher than 3 Å.

References

1. H. F. Fan, *Acta Phys. Sin*. **21**, 1105–1114 (1965); in Chinese; English translation available in *Chinese Phys*. 1418–1428 (1965).
2. H. F. Fan, *Acta Phys. Sin*. **21**, 1114–1118 (1965); in Chinese; English translation available in *Chinese Phys.* 1429–1435 (1965).
3. D. Sayre, *Acta Cryst*. **5**, 60–65 (1952).
4. H. F. Fan, *Rigaku Journal* **1**, 15–21 (1984).
5. H. F. Fan, J. X. Yao, J. Z. Qian, *Acta Cryst*. **A44**, 688–691 (1988).
6. H. F. Fan *et al., Acta Cryst*. **A44**, 691–692 (1988).
7. H. F. Fan *et al*., *Acta Cryst*. **A46**, 99–103 (1990).
8. H. F. Fan, F. H. Li, in *Direct Methods, Macromolecular Crystallography and Crystallographic Statistics*, Proceedings of the IUCr Winter School, Madras, India, December 9–19,1985, H. Schenk, A. J. C. Wilson, and S. Pathasarathy, Eds. (World Scientific, Singapore, 1987), pp. 400–409.
9. Z. Q. Fu *et al*., *Ultramicroscopy* **54**, 229–236 (1994).
10. Z. H. Wan *et al*., *Z. Krist*. **218**, 308–315 (2003).
11. Q. Hao, Y. W. Liu, H. F. Fan, *Acta Cryst*. **A43**, 820–824 (1987).
12. H. F. Fan, S. van Smaalen, E. J. W. Lam, P. T. Beurskens, *Acta Cryst*. **A49**, 704–708 (1993).
13. Y. D. Mo *et al*., in *Low Dimensional Properties of Solids*, Proceedings of the Nobel Jubilee Symposium, Gothenburg, Sweden, December 4–7, 1991, M. Jonson, T. Claeson, Eds., Physica Scripta, The Royal Swedish Academy of Sciences (World Scientific, Singapore, 1992), pp. 18–19.
14. Z. Q. Fu, H. F. Fan, *J. Appl. Cryst*. **27**, 124–127 (1994).
15. H. F. Fan, *CompComm Newsletter* **5**, 16–23 (2005).
16. H. F. Fan, *CompComm Newsletter* **5**, 24–27 (2005).
17. H. F. Fan, Y. X. Gu, *Acta Cryst*. **A41**, 280–284 (1985).
18. Q. Hao, Y. X. Gu, C. D. Zheng, H. F. Fan, *J. Appl. Cryst.* **33**, 980–981 (2000).
19. T. Zhang *et al*., IPCAS 1.0, Institute of Physics, Chinese Academy of Sciences, People's Republic of China (2012).
20. D. Q. Yao *et al*., *Acta Cryst*. **D70**, 2686–2691 (2014).
21. H. F. Fan *et al*., *Acta Cryst*. **A70**, 239–247 (2014).

Soft matter and biological physics

Ke Chen, James D. Farrell, Ming Li, Pengye Wang, Yuxiang Weng*, and Fangfu Ye

Overview

Highlights of recent advancements in soft matter and biological physics research at the Institute of Physics, Chinese Academy of Sciences—particularly studies on protein dynamical structures and dynamics, dynamics of chromatin fibers, electrorheological fluids, and bifurcation behavior in dilute granular systems—are herein reviewed.

Protein dynamical structure revealed by temperature-jump time-resolved infrared spectroscopy

Many static protein structures have been resolved at the atomic level via X-ray crystallography, two-dimensional nuclear magnetic resonance spectroscopy, and cryo-electron microscopy. However, protein structures in vivo are generally different from those of a "frozen" crystal structure. To understand protein structure–function relationships in the corresponding biological contexts, it is imperative to develop physical methods to solve dynamical protein structures under physiological conditions.

Temperature-jump time-resolved infrared (T-jump TRIR) transient-absorbance-difference spectroscopy is a method designed to address the above objective. It employs a pulsed near-IR laser as the heating source and a mid-IR laser as the probe source in the amide I fingerprint region of proteins. With the most recent advancement of the home-built holmium: yttrium-aluminum-garnet (Ho:YAG) heating laser combined with the home-built continuous wave carbon monoxide (cw CO) probe laser, a detection limit of $10^{-4}\Delta$OD (optical density) was achieved (*1*). With this instrument, thermally induced structural changes have been revealed in several important proteins.

Thermal breaking pathway for cytochrome c

Cytochrome *c* contains a heme group with the iron (Fe) atom binding to the methionine sulfur (Met S) atom of a loop structure. It was believed that the breaking of the Fe–S bond (which has a time constant of 300 ns) is the precipitating factor of thermally induced unfolding in this protein. T-jump TRIR results showed that the loop structure unfolds earlier and faster than the Fe–S bond breaks, leading to the breaking of the Fe–S bond, and subsequently, the unfolding of cytochrome *c* (*2*).

"Proteinquake" in DegP hexamer

The *Escherichia coli* (*E. coli*) DegP protein belongs to the heat-shock protein family and possesses both chaperone and protease activities. When in a resting state, DegP exists as a hexamer, consisting of two trimeric units linked by interfacial β-strands, with its protease active sites blocked. Upon binding with a substrate, the hexamers dissociate and form larger oligomers that include the substrate. The protease activity of DegP increases as the temperature rises. Hence, an important question is whether the DegP hexamer activation is triggered by the substrate binding or the temperature increase. T-jump TRIR spectroscopy shows that the disassembly of the DegP hexamer proceeds in the manner of a "proteinquake," which eventually leads to the dissociation of the hexamer into two trimeric units (Figure 1). The sequential unfolding/disassembly process initiated by the interfacial β-sheets serves as a temperature sensor and epicenter. The process is complete within approximately 134 ns at room temperature. The thermal dissociation even occurs at room temperature, suggesting that temperature is not the key factor that triggers the activation process of DegP (*3*).

Dual contradictory functions of DsbC

Homodimeric disulfide bond isomerase (DsbC) primarily serves as a reductase responsible for opening mismatched disulfide bonds. However, it has been found that a DsbC dimer can also acquire a puzzling activity as an oxidase. According to its crystal structure, a DsbC dimer consists of two monomers linked via nine pairs of hydrogen bonds. T-jump TRIR spectroscopy reveals that the hydrogen bonds at the dimeric interface break within a period of approximately 30 ns when subjected to heat shock (Figure 2).

This thermally induced dissociation was verified via biochemical methods, and the temperature-dependent oxidase activity of DsbC both in vivo and in vitro were determined. The results confirmed that the DsbC dimer does have an abnormal activity as an oxidase, which increases with temperature. Thus, the thermally induced dissociation of the DsbC dimer enables it to have an unexpected oxidase activity owing to the monomer formation, which accounts for the puzzle at the molecular level (*4*).

Surface-induced fluorescence attenuation method to visualize membrane-protein 3D dynamics

Research on the dynamics of membrane proteins is stagnant because of a lack of experimental methods that can extract real-time information about protein localization in lipid membranes. To address this shortfall, we developed a single-molecule visualization method—termed surface-induced fluorescence attenuation (SIFA)—to track both vertical and lateral motions of membrane proteins in supported lipid bilayers (*5*). The attenuation is a result of strong electromagnetic coupling between a fluorescing molecule and an absorbing surface, obeying a quenching equation,

$$I/I_0 = [1+(d_0/d)^4\,]^{-1}, \quad (1)$$

where I_0 is the fluorescence intensity of a free fluorophore, I denotes the intensity near the surface, and d_0 is the characteristic quenching distance at which $I/I_0 = 1/2$. For studying proteins in lipid bilayers, a good choice of d_0 is ~4 nm. We used graphene oxide monolayers on a glass surface to fulfill this requirement. The in-plane position can be directly read in the images, and the transmembrane position can be derived from the fluorescent intensity according to Equation 1. Lateral motion and the vertical insertion of proteins are hence decoupled in our approach, which is important because membrane proteins should be

Beijing National Laboratory for Condensed Matter Physics and Key Laboratory of Soft Matter Physics, Institute of Physics, Chinese Academy of Sciences, Beijing, China
*Corresponding author: yxweng@iphy.ac.cn

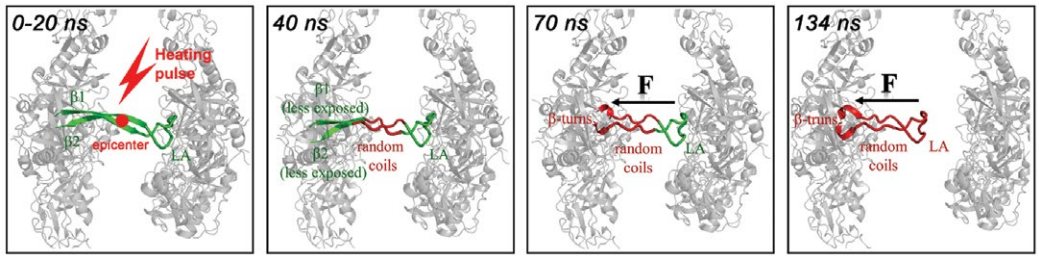

FIGURE 1. Schematic illustration of the proteinquake mechanism for the thermal-induced dissociation of the DegP hexamer with four typical snapshots at the indicated time points. Only one of the six β1-LA-β2 structures at the interface of the trimeric units is displayed (green ribbons). Unfolded sequences are colored red. The epicenter (red circle) is located at the fully exposed part of the interfacial β-sheet. The black arrows denote the direction of the motion of the LA loop, and F denotes the tension.

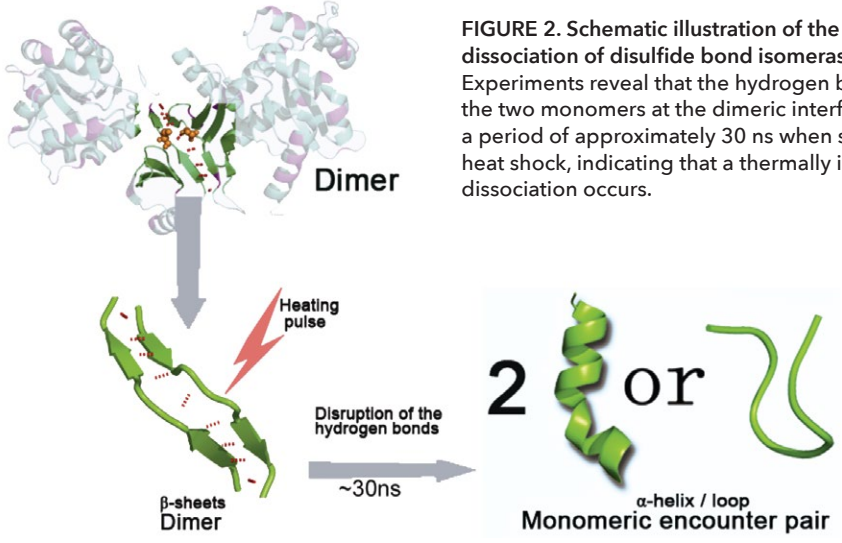

FIGURE 2. Schematic illustration of the thermally induced dissociation of disulfide bond isomerase (DsbC dimer). Experiments reveal that the hydrogen bonds linking the two monomers at the dimeric interface break within a period of approximately 30 ns when subjected to heat shock, indicating that a thermally induced dimeric dissociation occurs.

allowed to freely diffuse in the membrane to mimic natural conditions.

SIFA is a powerful method of tracking the insertion depth of single-membrane proteins. It distinguishes the part of a protein that inserts into a supported lipid bilayer and the extent of its depth. We applied the method to study the pore-forming peptide LL-37 (Figure 3). Our results suggest that the pores induced by LL-37 are dynamic, and the LL-37 monomers in the pores dynamically transfer between five transmembrane positions: the surface, upper leaflet, center, lower leaflet, and bottom. The ability to distinguish five transmembrane positions in a space as thin as ~4 nm indicates that SIFA has an unprecedented precision for studies of protein–membrane interactions. On the other hand, our results suggest that the dynamics of the toroidal pores are unexpectedly complex.

Nucleosome grouping revealed by force spectroscopy

Compact chromatin fibers in eukaryotes must unfold during gene activation to expose genomic DNA to transcription factors and RNA polymerases. However, the dynamic organization of chromatin fibers and its regulatory mechanisms remain poorly understood. We used single-molecule force spectroscopy to investigate the dynamics of chromatin fibers reconstituted in vitro by applying a continuously increasing force on a single chromatin fiber (*6*). The results reveal that the chromatin fiber first unfolds into an intermediate "tetranucleosomes-on-a-string" structure by disrupting the interactions between tetranucleosomal units. This unfolding is followed by another one, which disrupts nucleosome–nucleosome interactions within the units and produces a completely open "beads-on-a-string" structure.

As a structural intermediate of chromatin, the tetranucleosomal unit must function as a regulatory platform in genome-associated processes. We found that the stability of the tetranucleosomal unit is attenuated by the histone-chaperone FACT (facilitates chromatin transcription complex), which plays essential roles in nucleosome remodeling during DNA transcription, replication, and repair (Figure 4). In addition, we found that the peptide of the U-turn motif of Spt16 alone—which weakens the nucleosome–nucleosome interactions within tetranucleosomal units by interacting with the N-terminal α_1 helix of H2B—can mimic the function of FACT. However, the peptide structure may differ from that in the native FACT complex.

Electrorheological fluids

Electrorheological (ER) fluids are a class of suspensions whose rheological properties can be controlled by applying an external electric field, spanning free-flowing liquid states to solid states that can withstand certain shear stresses before yielding. Recently, we developed a new type of ER fluid, termed polar molecule–dominated ER (PM-ER) fluid, which has yield stresses much higher than the theoretical upper-bound of conventional ER fluids (*7*). The key of developing PM-ER is to introduce polar molecules to an otherwise nonpolar solvent. Titanium dioxide (TiO_2), calcium titanium oxide (Ca-Ti-O), lanthanum titanium oxide (La-Ti-O), and strontium titanium oxide (Sr-Ti-O) particles

with C–O/H–O polar groups adsorbed were synthesized by using either the sol-gel method or the coprecipitation process. The ER fluids were prepared by dispersing the particles in silicone oil or hydraulic oil with different volume fractions. The yield stress of such PM-ER fluids can easily reach above 100 kPa under an applied DC electric field. The yield stress of these fluids can be as high as 500 kPa. We anticipate attaining MPa-scale yield stresses by increasing the volume fraction of particles.

Bifurcation behavior in dilute granular systems

Granular materials are ubiquitous, and their dynamics are critical to many industrial processes. A remarkable property of these materials is that particles of different kinds often tend to segregate. We studied segregation due to interstitial air and identified negative buoyancy in the presence of air (*8*). The oscillatory clustering behavior in bidispersed compartmentalized dilute granular systems was experimentally studied (*9*); a phase diagram of the oscillatory clustering in terms of the driving velocity and number ratio of the two types of particles in the system was obtained. By examining the oscillation amplitude when close to the transition points, we determined that the system transition from the homogeneous state to the oscillatory state is via a Hopf bifurcation. Our two-temperature model captures the essential features of this oscillatory phenomenon. Further bifurcation behavior of this phenomenon was experimentally, theoretically, and computationally studied and reported (*10*); the nonequilibrium dynamics of the system were so enriched that a homoclinic gluing bifurcation was observed for the first time, potentially making ours a model system for nonlinear dynamics.

Research prospects

In addition to the above studies, recent efforts included studies on colloidal glasses (*11*), intracellular diffusion (*12*), multivalent targeting (*13*), and other areas. In the coming years, efforts will be devoted to the development of new physical techniques for biological studies and to the elucidation of emergent phenomena in complex living systems. We anticipate that more international scientists will join in these efforts and that further advancements will be made.

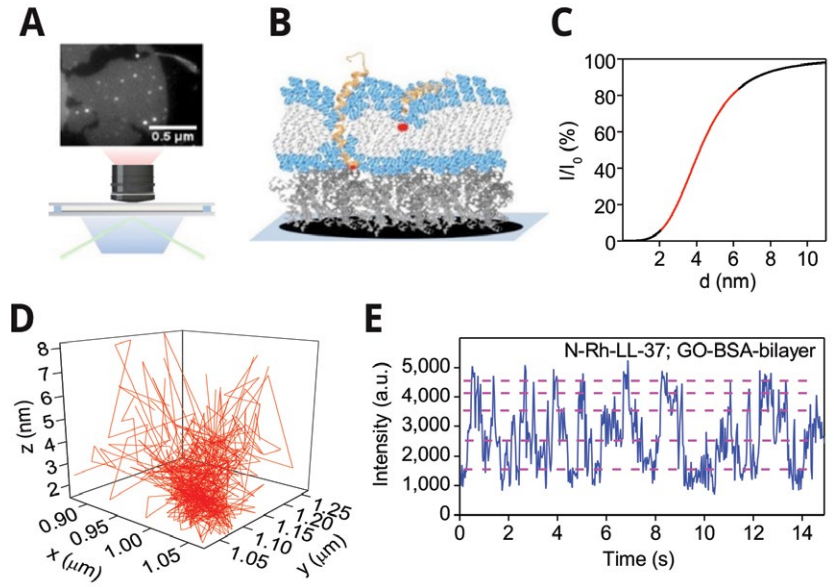

FIGURE 3. Surface-induced fluorescence attenuation (SIFA) method. (**A**) Experimental setup. (**B**) Sketch of a lipid bilayer with the helices representing the peptides at different depths. (**C**) Degree of attenuation of a dye as a function of dye–surface distance, where the red segment on the curve represents the most sensitive SIFA range. (**D**) 3D trace of a dye in the bilayer. (**E**) Fluorescence trace of an LL-37 molecule in the bilayer.

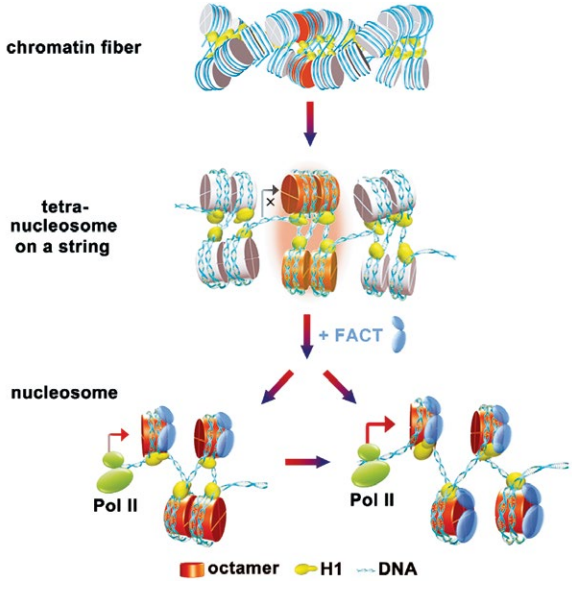

FIGURE 4. Tetranucleosomes-on-a-string structure and its regulation by the protein–histone complex known as "facilitates chromatin transcription" (FACT), which attenuates the chromatin fibers by binding the tails of histone H2B.

References

1. D. Li *et al.*, *Rev. Sci. Instrum.* **86**, 053105 (2015).
2. M. Ye *et al.*, *Biophys. J.* **93**, 2756–2766 (2007).
3. S. Li *et al.*, *Sci. Rep.* **4**, 4834 (2014).
4. H. Li *et al.*, *Biophys. J.* **97**, 2811–2819 (2009).
5. Y. Li *et al.*, *Nat. Commun.* **7**, 12906 (2016).
6. W. Li *et al.*, *Molec. Cell* **64**, 120–133 (2016).
7. R. Shen *et al.*, *Adv. Mater.* **21**, 4631–4635 (2009).
8. X. Yan *et al.*, *Phys. Rev. Lett.* **91**, 014302 (2003).
9. M. Hou *et al.*, *Phys. Rev. Lett.* **100**, 068001 (2008).
10. Y. Li *et al.*, *Phys. Rev. Lett.* **109**, 198001 (2012).
11. X. Yang *et al.*, *Phys. Rev. Lett.* **116**, 238003 (2016).
12. H. Li *et al.*, *J. Am. Chem. Soc.* **137**, 436–444 (2015).
13. T. Curk *et al.*, *Proc. Natl. Acad. Sci. U.S.A.* **114**, 7210–7215 (2017).

Renewable energy conversion, storage, and efficient utilization

Xuejie Huang, Qingbo Meng, Hong Chen, Xiaolong Du, and Liquan Chen*

The Renewable Energy Laboratory (REL) was founded on August 17, 2009, by merging four research groups. The launch of energy-related research dates back to the late 1970s, when research on solid-state lithium (Li) batteries and related fundamental studies of solid-state ionics were initiated and pioneered in China for the first time (*1*). At that time, a series of promising ionic conductors, including solid solution ionic conductors [$Li_{14}Zn(GeO_4)_4$, $Li_{3.3}V_{0.7}Si_{0.3}O_4$, $Li_{3.6}V_{0.4}Ge_{0.6}O_4$], amorphous fast ionic conductors (LiB_2O_4, B_2S_3-Li_2S-LiI), polymer ionic conductors (PECH-PEO-$LiClO_4$), and composite ionic conductors were investigated (*2*). Particular attention was paid to revealing the intrinsic nature of fast-ion diffusion. The achieved ionic conductivity of 10^{-4}–10^{-3} Siemens (S)/cm realized by using a mixed-phase ionic conductor paved the way for the development of solid electrolytes for solid-state batteries, and initiated experimental and theoretical research in energy-related fields. Since then, REL has focused on ionic conductors while expanding the frontiers of clean energy by attracting scientists with wide-ranging expertise to conduct fundamental research on novel concepts, undiscovered mechanisms, new materials, and new techniques for realizing clean energy, with the goal of providing ideal scientific solutions and developing core technologies in energy harvesting (solar cells), storage (rechargeable batteries), and utilization (solid-state lighting).

Energy harvesting

Photovoltaics represent a promising way to solve the foreseeable worldwide energy crisis, by converting solar energy into electricity. So far, the relatively higher price of photovoltaics compared to conventional energy sources is a major drawback. Improving the cost-effectiveness of photovoltaics is still a great challenge for scientists and engineers. At REL, efforts have been focused primarily on two aspects. One is the precise control of the silicon (Si) surface texture for maximizing light trapping and photocarrier collection. The other is the development of emerging solar cells, including dye-sensitized solar cells (DSCs), quantum dot solar cells (QDSCs), and perovskite-sensitized solar cells (PSCs), especially to determine and control the charge processes in these solar cells. The related achievements in recent years are discussed below.

1. Black silicon solar cells

We developed two techniques to prepare large-area black silicon solar cells: silver (Ag)-catalyzed chemical etching (ACCE) (*3*) and copper (Cu)-catalyzed chemical etching (CCCE) (*4*–*7*). By using silver nitrate ($AgNO_3$) instead of the much more expensive chloroauric acid ($HAuCl_4$), a low-cost, one-step ACCE process for large-area black silicon fabrication on both crystalline silicon (c-Si) and multicrystalline silicon (m-Si) has been developed. In the double-layer passivation technique, the silicon dioxide (SiO_2) layer is formed via thermal oxidation before the silicon nitride (SiN_x) layer is deposited as usual (*3*). This results in a significant

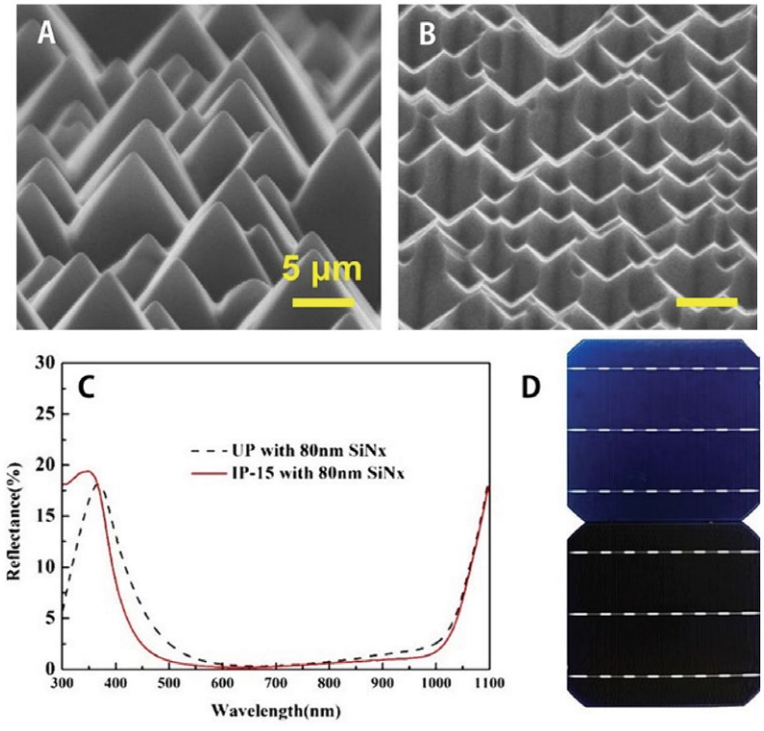

FIGURE 1. Scanning electron microscope (SEM) images of (A) the conventional upright-pyramid (UP) texture, and (B) the random inverted-pyramid (IP) texture obtained by using the alkaline etching and the copper-catalyzed chemical etching (CCCE) methods, respectively. (**C**) The reflectance of the IP-textured wafer covered with an 80-nm-thick silicon nitride (SiNx) layer, in comparison with that of the UP texture. (**D**) Photographs of UP (up) and IP solar cells (down).

Renewable Energy Laboratory, Beijing Key Laboratory for New Energy Materials and Devices, Beijing National Laboratory for Condensed Matter Physics, Institute of Physics, Chinese Academy of Sciences, Beijing, China
*Corresponding author: lqchen@iphy.ac.cn

increase in the conversion efficiency of nanotextured solar cells. c-Si texturing with microscale-inverted-pyramid arrays is achieved by using the CCCE process. Inverted pyramids with heights of 2 μm–6 μm appear randomly distributed over the whole wafer. The detailed mechanisms are then revealed: The dynamic activity of Cu nanoparticles, which depends on the concentration of the etchant, finally determines the silicon surface morphology. The inverted-pyramid textures outperform conventional pyramid textures with a lower average reflectivity, better surface passivation, and higher-quality ohmic contacts, resulting in a higher solar-cell efficiency, which is increased by 0.47% (Figure 1). These one-step ACCE and CCCE techniques help to realize reproducible microscopic/submicroscopic texture and structures, and have been applied to the mass production of diamond-wire-sawn m-Si and c-Si solar cells, respectively, with an average efficiency increase of 0.3%–0.5% absolute.

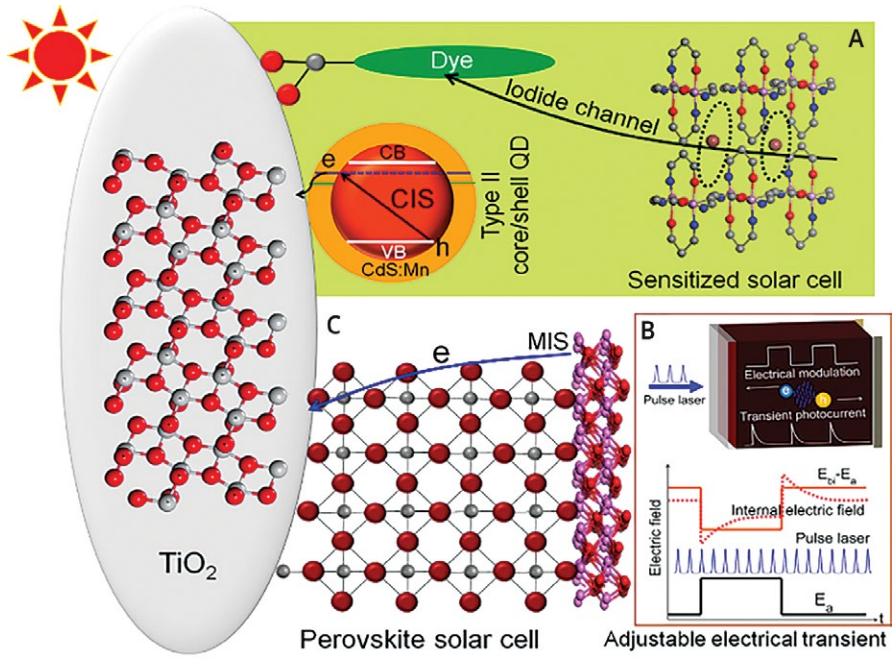

FIGURE 2. Schematic diagram of our work in controlling and determining the charge processes in emerging solar cells, including (A) designing the iodide transport channel for dye-sensitized solar cells (DSCs), (B) regulating charge transfer in quantum dot solar cells (QDSCs), and (C) probing and controlling charge diffusion in perovskite-sensitized solar cells (PSCs). Reprinted with permission from (*13*).

2. Developing new materials for highly efficient and stable emerging solar cells

A solid-state LiI/3-hydroxypropionitrile (HPN) electrolyte with large 3D iodide ion transport channels has been successfully designed to improve the ionic conductivity of the DSC (*8*). The mesoporous filling and interface charge transfer are further enhanced by introducing SiO_2 nanoparticles to suppress electrolyte crystallization, leading to better cell performance. Further, in order to reduce the quantum dot (QD) defects and improve charge transfer in QDSCs, copper indium disulfide ($CuInS_2$) (CIS)/cadmium sulfide-manganese (CdS:Mn) core-shell QDs with a type-II energy structure were developed, and the In_{Cu} substitution and Cu vacancy defects in the CIS core were controlled by composition regulation (*9*–*11*). (Figure 2A). In addition, the cell efficiency of QDSCs was boosted to 11.3% via systematic controlling charge processes. By introducing polystyrene to stabilize the perovskite composition, grains, and microstructure and by composition regulation, PSCs with over 20% efficiency were realized (*12*).

3. Determining and controlling the charge dynamic processes in PSCs

A modulated transient photoelectrical system [modulated transient photovoltage (M-TPV)/transient photocurrent (M-TPC)] and a time-dependent "modulation-probe" method have been developed, which provide an effective approach to elucidate microscopic charge processes within a cell, as shown in Figure 2B. Ion migration and stabilization in the dynamic functioning of PSCs have been systematically investigated. An intrinsic hysteresis behavior was further revealed due to ion migration in the perovskite absorber by the built-in electric field of the heterojunction, external bias voltage, and ion migration–induced polarization electric field. The most important aspect of this development is that our M-TPV/M-TPC system is not only applicable for PSCs, but also for other emerging solar cells and even conventional Si-based solar cells. Moreover, the interplays between electron and ion transportation have been clarified by performing dynamics measurements (e.g., using impedance spectra and TPV) (*14*). And the boundary conditions for charge diffusion have been controlled to avoid carrier loss by designing a metal–insulator–semiconductor (MIS) structure and adjusting the conduction band offset (*15*), as shown in Figure 2C.

Energy storage

Increasing awareness of environmental pollution has led to the development of electric vehicles to

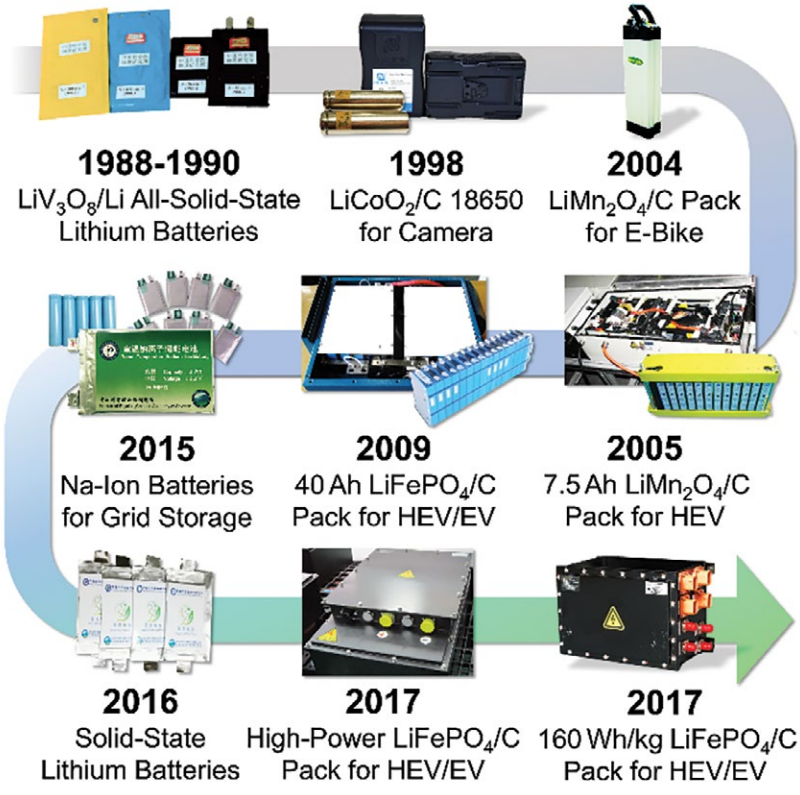

FIGURE 3. Prototype and commercialized batteries developed the Renewable Energy Laboratory from 1988 to 2017. HEV, hybrid electric vehicle; EV electric vehicle.

replace those with conventional internal combustion engines. In addition, advanced energy storage systems have been developed to integrate with renewable and clean energy sources. With the widespread use of electricity, rechargeable batteries play a key role in modern society: Portable handheld electronics, electric vehicles, and even aircrafts all require reliable energy storage devices. Over the past several decades, the energy storage team at REL has realized impressive advancements in rechargeable batteries by exploring new materials, investigating ionic and electronic transport mechanisms, modeling based on first-principle calculations and molecular dynamics simulations, developing advanced energy storage devices (Figure 3), and so on. In 1998, Li-ion battery commercialization was realized using homemade equipment, domestic raw materials, and our own Chinese technology. Our previous work (performed prior to 2000) has been well documented in a recent interview (*2*). Here, we focus on our recent original contributions to this field.

1. Stabilizing the cathodes via surface modification strategy

We propose the use of a surface coating of gamma-aluminum oxide (γ-Al_2O_3) on layered cathodes to attain good cycling performance when charged to 4.5 V or even higher (*16*).

2. Developing a high-capacity Nano-Si anode

The Tianmu Energy Anode Material Co., Ltd. has been established to commercialize this technology by utilizing knowledge gained through our efforts over 20 years in understanding the Li storage mechanism in Nano-Si that we proposed in 1997 (*17*).

3. Revealing the degradation mechanism of the spinel cathode

A degradation mechanism in spinel lithium nickel manganese oxide ($LiNi_{0.5}Mn_{1.5}O_4$) at the atomic level has been revealed: The distortion of the surface structure is due to the rearrangement of transitional metal ions during high-voltage and high-temperature cycling (*18*). The surface modification of $LiNi_{0.5}Mn_{1.5}O_4$ with oxides [i.e., titanium dioxide (TiO_2)] is an effective means to improve cycling performance via stabilization of the surface structure by migration of coating ions into the surface structure.

4. Accelerating the Materials Genome Initiative

By using high-throughput, multiscale computation, as well as data-mining technology that is part of the Materials Genome Initiative, a new oxysulfide solid electrolyte, lithium aluminum oxysulfide (LiAlSO), is predicted to exhibit high ionic conductivity (*19*).

5. Proposing highly concentrated electrolytes for metallic Li batteries

We propose highly concentrated electrolytes with a high Li^+ transference number for high-energy metallic Li batteries (*20*), which can effectively suppress the growth of Li dendrite and significantly improve cycling efficiency during Li plating/stripping.

6. Promoting solid-state Li batteries

We recently proposed a strategy of "in-situ solidification" for solid-state batteries, which can minimize the use of liquid electrolytes and thus enhance the energy density, stability, and cyclic performance of lithium batteries. The Beijing Welion New Energy Technology Co., Ltd. has been founded to promote the industrial advancement of solid-state batteries.

7. Developing Na-ion batteries for grid energy storage

We designed a low-cost, environmentally friendly Na_x[Cu-Fe-Mn-M]O_2-layered oxide cathode using a novel

copper ion (Cu^{2+}/Cu^{3+}) redox couple (*21*), and proposed a superior low-cost soft carbon anode made from anthracite (*22*). We also fabricated prototype sodium (Na)-ion pouch cells with a capacity of 1–12 Ah (12 Ah cell exhibits an energy density of 117 Wh/kg), using our own developed kilogram-scale cathode and anode materials, which have passed a series of safety tests.

Energy-efficient utilization

Light-emitting diodes (LEDs) have shown great potential in many lighting applications due to their many advantages over traditional light sources, including longer lifetime, greater efficiency, and smaller size, factors which will help to save a tremendous amount of electrical power and help to hold the promise for a more sustainable future. Taking advantage of our extensive research on the epitaxial growth of semiconductors and the design of relevant devices, the REL research team has made significant progress in the development of gallium nitride (GaN)-based LEDs for next-generation lighting technology, as summarized below and shown in Figure 4.

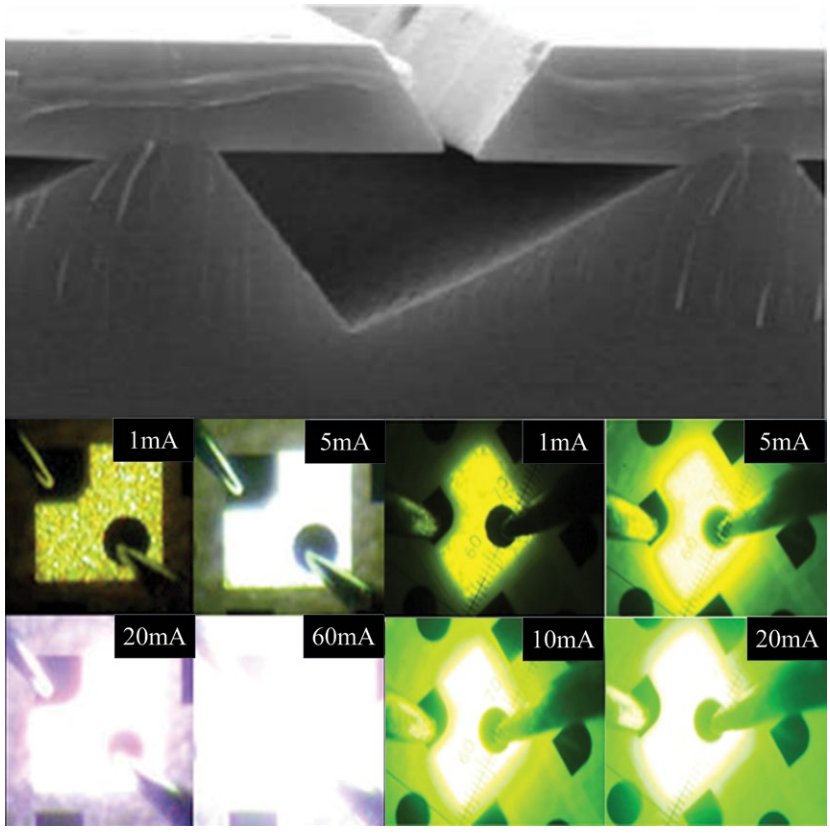

FIGURE 4. Gallium nitride (GaN) growth on maskless, chemically etched grooved sapphire substrate and different-colored LED chips with white and yellow-green light.

1. GaN growth on maskless, chemical-etched grooved sapphire substrate (23)

The performance of near-ultraviolet GaN-based LEDs has been dramatically enhanced threefold due to lowering of the dislocation density of III-nitride films to 5×10^7 cm^{-2}, by developing a wet-etching process that realizes a maskless, chemically etched, V-grooved sapphire substrate without any damage and selective growth as a result of the Ga atom migration.

2. GaN-based, single-chip, phosphor-free white LEDs (24, 25)

By inserting an indium gallium nitride (InGaN) underlying layer (UL), a GaN-based, single-chip, phosphor-free, white LED with indium-rich quantum dots emitting yellow light and a low-indium-content region emitting blue light can be realized via a simple process. Thus, the limitations of current commercial white LEDs with phosphor, such as multiple packaging steps, a low color-rendering index, and different color temperatures at different visual angles, are overcome.

3. High-luminous efficiency InGaN "green gap" LEDs (26)

A high-brightness LED in the "green gap" range has been developed. It is based on hybrid InGaN/GaN multi-quantum wells (MQWs) in which high-indium QWs, in the wavelength region of 535 nm–570 nm near the p-type GaN side, rest above low-indium-content QWs, resulting in a 2.4-fold enhancement of the 540-nm light output power at an injection current of 20 mA. This can effectively move the efficient InGaN LED emission toward longer wavelengths, thus providing an LED product line with sufficient luminous efficacy covering the entire visible spectra.

Envisioning our future

Considering our important achievements in research on energy conversion, storage, and utilization in terms of solar cells, rechargeable batteries, and solid-state lighting, we are confident in our ability to continue generating the best and most innovative results. With the persistent endeavors of our scientists, we will continue the strong tradition of fundamental research on energy conversion, storage, and utilization, and at the same time, push to maintain cutting-edge discovery and innovation. We will attract China's bright young minds to this exciting field of renewable clean energy, foster them in their endeavors, and welcome world-class scientists to collaborate with us to promote the progress of science and technology.

Since May 31, 2017, the Center for Clean Energy (CCE) has been under construction in Huairou Science City, thanks to a joint undertaking by the Beijing municipal government and the Institute of Physics, Chinese Academy of Sciences. REL is responsible for participating in the construction and personnel recruitment for CCE. CCE will be the first professional user-facility center for clean energy materials and devices in China. It will enable comprehensive analysis and tests, ranging from the atomic scale to macroscale dimensions, from ex situ to in situ, from 1D to 3D, from inert atmospheres to ambient conditions, from normal to extreme conditions, and from materials to systems. CCE will generate high-level scientific research with reliable data, promote original and creative discovery, uncover failure mechanisms, and accelerate technology transfer. Scientists and engineers from across the world are welcome to come here and realize their scientific and technological dreams. We would like to take this opportunity to invite global talent to apply for tenure-tracked positions in multiple research areas. New ideas, directions, methods, and techniques in clean energy are our first priority. We believe that CCE is the right place for distinguished young people to promote a technological revolution that benefits human society by applying their groundbreaking ideas. We look forward to working with you to make greater contributions to the development of clean energy. Our goal must be achieved—and our goal can be achieved!

References

1. L. Q. Chen *et al.*, *Acta Phys. Sin.* **29**, 661–666 (1980).
2. H. Li, *Natl. Sci. Rev.* **4**, 106–110 (2017).
3. Y. P. Liu *et al.*, *Small* **8**, 1392–1397 (2012).
4. Y. Wang *et al.*, *Sci. Rep.* **5**, 10843 (2015).
5. Y. Wang *et al.*, *Nanoscale* **9**, 907–914 (2017).
6. L. Yang *et al.*, *Sol. Energy Mater. Sol. Cells* **166**, 121–126 (2017).
7. L. Yang *et al.*, *ACS Appl. Mater. Interfaces* **8**, 26–30 (2016).
8. B. Xue *et al.*, *J. Am. Chem. Soc.* **128**, 8720–8721 (2006).
9. J. Luo *et al.*, *Chem. Commun.* **49**, 3881–3883 (2013).
10. G. Wang *et al.*, *Nano Energy* **35**, 17–25 (2017).
11. H. Wei *et al.*, *J. Mater. Chem. A* **4**, 14194–14203 (2016).
12. H. Zhang *et al.*, *Nano Energy* **43**, 383–392 (2018).
13. J. Shi *et al.*, *Rev. Sci. Instrum.* **87**, 123107 (2016).
14. J. Dong *et al.*, *Appl. Phys. Lett.* **107**, 073507 (2015).
15. J. Shi *et al.*, *Appl. Phys. Lett.* **107**, 163901 (2015).
16. Z. Wang *et al.*, *Solid State Ionics* **148**, 335–342 (2002).
17. H. Li *et al.*, *Electrochem. Solid-State Lett.* **2**, 547–549 (1999).
18. M. Lin *et al.*, *Chem. Mater.* **27**, 292–303 (2014).
19. X. Wang *et al.*, *Phys. Rev. Lett.* **118**, 195901 (2017).
20. L. Suo *et al.*, *Nature Commun.* **4**, 1481 (2013).
21. L. Mu *et al.*, *Adv. Mater.* **27**, 6928–6933 (2015).
22. Y. Li *et al.*, *Energy Storage Mater.* **5**, 191–197 (2016).
23. Y. Jiang *et al.*, *Energy Environ. Sci.* **4**, 2625–2629 (2011).
24. X. Wang *et al.*, *Appl. Phys. Lett.* **91**, 161912 (2007).
25. X. Wang *et al.*, *Appl. Phys. Lett.* **94**, 111913 (2009).
26. Y. Jiang *et al.*, *Sci. Rep.* **5**, 10883 (2015).

Silicon carbide: A wide-bandgap semiconductor and beyond

Gang Wang[1], Wenjun Wang[1], Tonghua Peng[2], Liwei Guo[1], and Xiaolong Chen[1*]

Silicon carbide (SiC) has attracted intense research interest due to its wide bandgap (WBG), high-carrier saturation velocity, high electric-field breakdown strength, and other interesting properties. From as early as the mid-20th century, it has been believed to be an excellent semiconductor. SiC has found increasing applications in optoelectronic, high-temperature, and high-power/high-frequency devices in recent decades. Its single-crystal growth is, however, problematic when compared to semiconductors grown from either melts or solutions, as stoichiometric melting occurs only at pressures higher than 10 GPa and temperatures exceeding 3,200°C. The extreme growth temperatures pose a challenge to the control and monitoring of the process. SiC has over 200 polytypes possessing similar formation energies, a factor that increases the demand for accurate control of the thermodynamic and kinetic conditions, in order to avoid simultaneous crystallization of two or more polytypes during crystal growth. Defects, such as micropipes, dislocations, etc., are commonly observed, and they deteriorate the performance of SiC-based devices. In 1955, Lely obtained flakelike SiC single crystals using the so-called Lely method, in which SiC sublimated into species such as Si, SiC_2, and Si_2C under high temperatures, and randomly nucleated at the slightly colder parts of a carbon crucible (*1*). Tairov and Tsvetkov (*2*) demonstrated a physical vapor transport (PVT) method in 1978, in which a seed was used to achieve better-controlled nucleation. In the early 1990s, Cree, Inc. presented a tremendous breakthrough in the growth of SiC (*3*), which initialized the commercialization of SiC wafers.

Efforts in SiC single-crystal growth started from scratch at the Institute of Physics (IOP), Chinese Academy of Sciences, in the late 1990s. Many new techniques, from furnace design to wafer processing, were developed. Novel properties of SiC were unraveled in the hope of expanding its applications. The existence of defect-induced magnetism in SiC was confirmed, enabling the use of WBG semiconductors as diluted magnetic semiconductors (DMS). A mid-infrared (MIR) laser with a wavelength ranging from 3.90 μm to 5.60 μm was generated using SiC as a nonlinear optical (NLO) crystal, opening a new avenue for the practical use of WBG semiconductors as new-generation NLO crystals. Other novel properties of SiC, such as surface polarity and photocatalysis, were also unraveled. Our research on SiC will not only improve the crystallization of the substrate further, but also widen its future applications.

[1]Beijing National Laboratory for Condensed Matter Physics, Institute of Physics, Chinese Academy of Sciences, Beijing, China
[2]TankeBlue Semiconductor Co., Ltd., Beijing , China
*Corresponding author: chenx29@iphy.ac.cn

SiC single-crystal growth

In 1999, we attempted SiC single-crystal growth using Acheson crystals as seeds and a resistance furnace with a graphite heater (*4*). The design of a new induction-heating furnace with an induction coil in a vacuum chamber followed shortly; this furnace was different from existing commercial ones featuring a double-wall, water-cooled quartz tube inside an induction coil. Improvements continued, leading to four generations of furnaces. The fourth-generation furnace could achieve a maximum temperature of 2,600°C with temperature accuracy within ±1°C. It could also achieve a vacuum of less than 5×10^{-5} Pa and decrease power consumption by more than 15%. It could be used for growing 2 in.–6 in. boules. In addition to the furnace, we consistently modified the seeding technology, source material, process control, defects, doping, and wafer processing (*5–9*). The relationships among the temperature profiles and partial pressures of the Si, Si_2C, and SiC_2 species were established during the growth process, which was optimized accordingly. The polytypic transformations, micropipes, inclusions, and dislocations induced by fluctuations in the temperature profiles and pressures of the gaseous species were controlled to very low levels. The growth of 4H- and 6H-SiC single crystals of 2 in.–6 in. is now state-of-the-art technology.

In 2006, based on our research, a spin-off (TankeBlue Semiconductor Co., Ltd.) was launched, which became the first manufacturer and marketer of SiC substrates in China. Now, after over 10 years of investments and expansions, TankeBlue is one of the major worldwide suppliers of SiC and a leading Chinese company. Figure 1 shows n-type 2-, 3-, 4-, and 6-in. 4H-SiC wafers grown by TankeBlue. The 6-in. wafers have a resistivity of approximately 0.02 Ω cm, a micropipe density of less than 0.5 cm^{-2}, a warp of less than 40 μm, and a total thickness variation of less than 6 μm. The SiC substrates are sold in more than 20 countries including the United States, Japan, and Europe. Many of the customers are big players in the global electronic device market, such as Mitsubishi Electric and Denso. TankeBlue became a listed company on China's National Equities Exchange and Quotations on April 10, 2017, and is planning to expand its production capacity in the next few years.

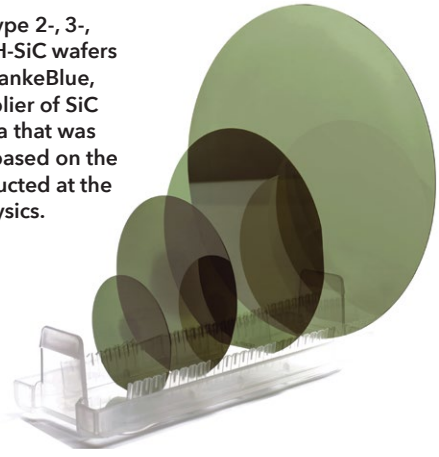

FIGURE 1. N-type 2-, 3-, 4-, and 6-in. 4H-SiC wafers produced by TankeBlue, a leading supplier of SiC wafers in China that was founded and based on the research conducted at the Institute of Physics.

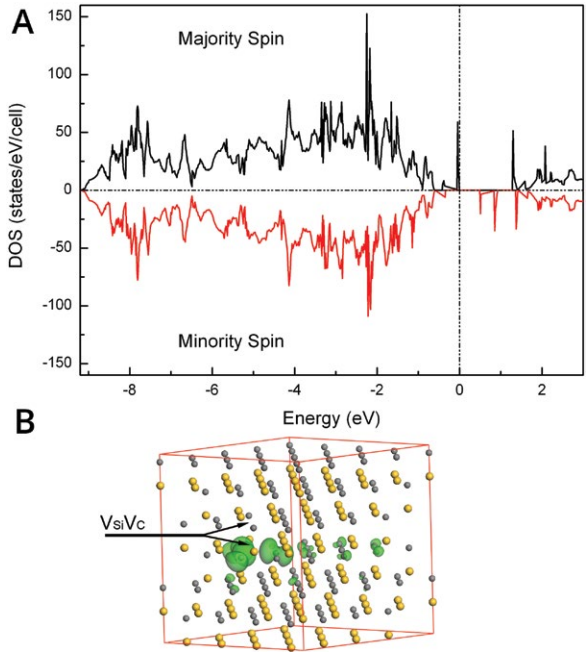

FIGURE 2. (A) Spin-resolved density of states of a neutral Si-C divacancy in a 192-atom SiC supercell. (B) Isosurface charge density plot (isovalue is 0.02 e/Å^3) of the total spin states about a neutral Si-C divacancy in a 192-atom SiC supercell. Silicon atoms are shown in yellow and carbon atoms in gray. Arrows indicate the location of the Si-C divacancy (*13*).

Magnetism of SiC

In 2000, the prediction of ferromagnetism (FM) at temperatures above 300 K in some semiconductors and oxides (*10*) brought focus onto DMS, as it raised hopes of applications combining logic functionalities with information-storage capabilities. Since then, much effort has been devoted to finding evidence of room temperature (RT) FM in WBG semiconductors. The origin of magnetism in WBG semiconductors remains a controversial issue despite numerous studies.

Our investigations on the magnetism of SiC began with transition-metal–doped SiC polycrystals. In manganese (Mn)-doped SiC, an FM order emerged at approximately 250 K at 10^{-4} mol % Mn, which was speculated to be more related to the defects than to the Mn content (*11*). To investigate the role of defects in the observed FM of SiC, we selected aluminum (Al) (with no partially filled *d* and *f* subshells) as a dopant (*12*). Hysteresis loops were observed for single-phase Al-doped SiC with Al of 0.75 atomic percent at 200 K and 300 K, whereas, they were not observed in undoped SiC even at 4 K. Under 1,000 oersteds (Oe), the zero-field-cooled and field-cooled temperature-dependent dc magnetization showed a clear irreversibility at 16.4 K, which was suppressed at 5,000 Oe. Moreover, both the real and imaginary parts of the complex susceptibility were frequency dependent. Thus, SiC showed a glassy FM state with Al doping. Then, we carefully investigated the magnetism of SiC single crystals irradiated with neutrons (*13*). Raman spectra showed there was no secondary phase; only a weakening of intensity was observed

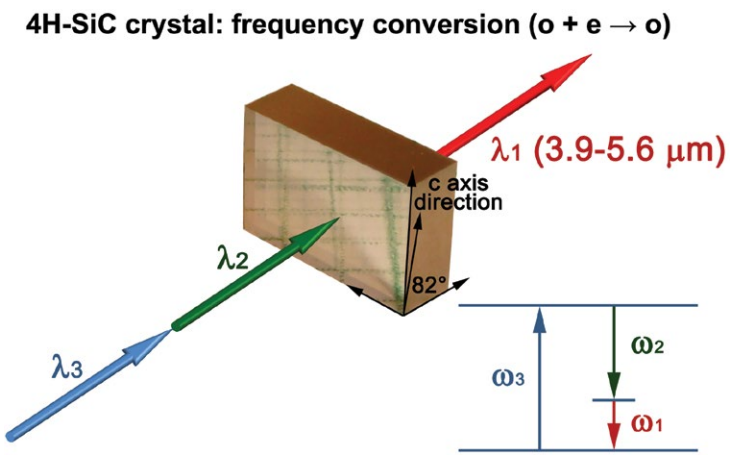

FIGURE 3. Schematic of mid-infrared (MIR) laser generated by difference-frequency generation (DFG) using 4H-SiC as a nonlinear optical (NLO) crystal (*15*).

in each mode. Meanwhile, the concentration of the Si-C divacancies induced by neutron irradiation was enhanced by increasing the dose. It was also found that the magnetic order was enhanced on increasing the neutron dose. At a neutron dose of 2.29×10^{18} n cm^{-2}, a distinct hysteresis with FM features was observed and the saturated magnetization reached 1×10^{-4} electromagnetic units (emu)/g at 5 K. A similar increasing trend was observed in the Si-C divacancy concentration and saturated magnetization with increase in the irradiation dose, suggesting a correlation between magnetism and divacancy. The first-principles calculations (Figure 2) showed that the localized nature of the divacancy state fostered the formation of a local moment [2.0 Bohr magnetons (μ_B)], whereas the extended tails of the defect wave functions induced long-range coupling between these local moments (*13*). The FM was further correlated to the *p* electrons of the nearest-neighbor carbon atoms around the Si-C divacancy (*14*). These results confirmed the origin of intrinsic magnetism in SiC and implied the possibility of magnetism tuning for WBG semiconductors, which shed light on the practical application of DMS.

SiC: A new nonlinear crystal

MIR lasers are crucial for both science and technologies such as spectroscopy, materials processing, and chemical and biomolecular sensing. The NLO technology is well suited for generating MIR lasers, owing to its high efficiency, wide tuning range, ability to operate at RT, and compact and low-cost setups. However, the NLO crystals such as $LiNbO_3$, $AgGaS_2$, and $ZnGeP_2$ all suffer from low laser damage threshold (LDT), and new NLO crystals with high LDT are highly desired.

4H- and 6H-SiC crystallize in the $P6_3mc$ space group and should exhibit the second-order NLO effect. They can act as new NLO crystals, considering their high LDT, high thermal conductivity, high quality, and large size. The transmittance of semi-insulating (SI) 4H- and 6H-SiC was higher than 50% in the wavelengths ranging from 0.37 μm to 5.60 μm and 0.40 μm to 5.60 μm (*15*). No damage was observed up to a power density of 3.0 gigawatts (GW)/cm^{-2} (*15*). Index data ranging from the visible region to 5.00 μm were measured carefully (*15*). In the visible region, the measured refractive indices were consistent with those reported previously, whereas, in the MIR region, they deviated from those obtained by extrapolation based on the data measured in the visible and near-infrared regions. From 293 K to 493 K, the thermo-optic coefficients decreased quickly in the visible region and remained quite steady in the infrared region (*16*). The small temperature-dependent birefringence variation was helpful for maintaining phase-matching conditions (PMCs) for NLO frequency conversion.

The PMCs of SiC were calculated based on the new measured refractive indices. Within the transparency range, PMCs were not available for 6H-SiC. As 4H-SiC had a larger birefringence, phase-matched DFG and optical parametric oscillation were possible. Broadband MIR radiation, with wavelength ranging from 3.90 μm to 5.60 μm and an average power of 0.2 mW, was generated (*15*) by DFG using a SI 4H-SiC crystal, cutting at an angle of 82 degrees with respect to the optical axis as an NLO crystal (see Figure 3). Then, we used two-stage optical parametric amplification and generated a 17-μJ MIR pulse with a duration of 70 fs and bandwidth of 550 nm centered at 3.75 μm at a repetition rate of 1 kHz (*17*). Recently, a 100-mW pulse of 4.03 μm was realized, showing the great potential of using WBG semiconductors practically as new-generation NLO materials for high-power-output MIR lasers.

More novel properties

According to our studies, SiC exhibits other interesting properties. We found that the contact angle of deionized water on the carbon face was larger than that on the silicon face, induced by the charge agglomeration on the carbon and silicon faces (*18*). Such wetting behavior offers a reliable method to determine the polarity of polar materials and is important for developing processing techniques for devices. The spatial charge separation on the Si-{0001} and {10−10} facets and its induced selective photodeposition could improve photocatalytic activity for the water splitting of SiC approximately fivefold, by effectively enhancing the separation of the photogenerated charges. In addition, we prepared graphene-covered SiC particles by in situ thermal decomposition (ISTD) of SiC and found that its photocatalytic activity was remarkably enhanced for both the degradation of rhodamine (greater than 100%) and efficient hydrogen evolution (over 33 times, reaching 472.4 μmol g^{-1} h^{-1}) compared to those of pristine SiC particles (*19, 20*). ISTD was used to prepare epitaxial graphene (EG) on SiC wafers, for use in graphene-based devices and vertically aligned graphene sheets (VAGS) (*21, 22*). The wafer-scale EG thus obtained had good uniformity, an average sheet resistance of 720 Ω/square with a nonuniformity of 7.2%, and a carrier mobility of approximately 450 cm^2 V^{-1} s^{-1} (*21*). The VAGS possessed good field emission properties, with a turn-on field of 1.81 V μm^{-1} at 10 μA cm^{-2}, a field enhancement factor up to

17,140, and cyclic stability of over 120 h (*22*). The anisotropic quantum transport and other properties of VAGS were also investigated (*23*).

Perspectives

Though IOP has achieved significant progress in the study of SiC over the past 20 years, several challenges remain. Research and commercialization of SiC-based devices is burgeoning worldwide. The cost of substrates, however, remains the major block to its mass application. High-quality, low-cost SiC substrates with larger sizes are highly desired. While increasing the growth rate using the PVT method is an effective way to reach this goal, other competitive growth methods need to be invented. Moreover, investigations of the physical properties of SiC are far scarcer than those of silicon (Si) and gallium arsenide (GaAs). We believe that deeper understanding of the doping, defects, and interactions of SiC with strong electric fields will definitely augment and widen its application in many fields.

References

1. J. A. Lely, *Ber. Deutsch. Keram. Ges.* **32**, 229–236 (1955).
2. Y. M. Tairov, V. F. Tsvetkov, *J. Cryst. Growth* **43**, 209–212 (1978).
3. R. C. Glass, D. Henshall, V. F. Tsvetkov, C. H. Carter, Jr., *Phys. Stat. Sol. (b)* **202**, 149–162 (1997).
4. H. Q. Li, X. L Chen, D. Q Ni, X Wu, *Diam. Relat. Mater.* **13**, 151–156 (2004).
5. L. N. Zhu, H. Q. Li, B. Q. Hu, X. Wu, X. L. Chen, *J. Phys. Condens. Matter* **17**, L85–L91 (2005).
6. T. H. Peng *et al.*, *Cryst. Res. Technol.* **44**, 357–362 (2009).
7. G. Wang, X. L. Chen, *Phys. Stat. Sol.(a)* **207**, 2757–2768 (2010).
8. C. J. Liu *et al.*, *J. Cryst. Growth* **394**, 126–131 (2014).
9. W. Sun *et al.*, *Mater. Express* **5**, 63–67 (2015).
10. T. Dietl, H. Ohno, F. Matsukura, J. Cibert, D. Ferrand, *Science* **287**, 1019–1022 (2000).
11. B. Song *et al.*, *Appl. Phys. Lett.* **94**, 102508 (2009).
12. B. Song *et al.*, *J. Am. Chem. Soc.* **131**, 1376–1377 (2009).
13. Y. Liu *et al.*, *Phys. Rev. Lett.* **106**, 087205 (2011).
14. Y. T. Wang *et al.*, *Sci. Rep.* **5**, 8999 (2015).
15. S. C. Wang *et al.*, *Laser Photonics Rev.* **7**, 831–838 (2013).
16. C. H. Xu *et al.*, *J. Appl. Phys.* **115**, 113501 (2014).
17. H.-T. Fan *et al.*, *Opt. Lett.* **39**, 6249–6252 (2014).
18. W. W. Zhong *et al.*, *Phys. Chem. Chem. Phys.* **18**, 28033–28039 (2016).
19. K. X. Zhu *et al.*, *Appl. Phys. Lett.* **100**, 023113 (2012).
20. W. Lu *et al.*, *Adv. Mater.* **27**, 7986–7991 (2015).
21. Y. P. Jia, L. W. Guo, J. J. Lin, L. L. Chen, X. L. Chen, *Chin. Sci. Bull.*, **57**, 3022–3025 (2012).
22. Q. S. Huang *et al.*, *Small* **7**, 450–454 (2011).
23. J. Huang *et al.*, *J. Phys. Condens. Matter* **26**, 345301 (2014).

Acknowledgments

We are grateful to all our current and former graduate students, postdocs, and collaborators who have contributed to the work presented here. This work was partially supported by the National Natural Science Foundation of China, the Ministry of Science and Technology of the People's Republic of China, the Chinese Academy of Sciences, the Xinjiang Production and Construction Corps, and the Beijing Municipal Science and Technology Commission.

Synergetic Extreme Condition User Facility (SECUF)

Jinguang Cheng*

Introduction

States of matter usually vary in response to changes in external parameters, such as temperature, pressure, magnetic field, or even time. Currently, we rely on extreme conditions that can be realized in our laboratories to better understand matter. It has become an important paradigm to discover new states of matter or novel phenomena by pushing our available laboratory conditions to all types of extremes.

The Institute of Physics, Chinese Academy of Sciences, is leading a key national project to establish the world-class Synergetic Extreme Condition User Facility (SECUF), with a total investment of RMB 1.576 billion (USD 250 million). This project aims to bring together physical sciences–related experimental techniques and to push them to the limits of ultralow temperatures (T), ultrahigh pressures (P), ultrahigh magnetic fields (B), and ultrafast time resolution. The SECUF project was launched on September 28, 2017, and is expected to be completed in five years. Upon completion, SECUF will achieve technical targets such as the lowest temperature of $T \leq 1$ millikelvin (mK); the highest pressure of $P \geq 300$ gigapascal (GPa); the strongest magnetic field of $B \geq 26$ Tesla (T) via hybrid superconducting magnets; and an ultrafast laser pulse of ≤100 attoseconds (as) as the extreme conditions; and $B/T \geq 10{,}000$ T/K; $B \bullet P/T \geq 2{,}800$ T•GPa/K; and $P \bullet T = 60{,}000$ GPa•K as the synergetic extreme conditions.

FIGURE 1. Overview of Synergetic Extreme Condition User Facility (SECUF, Beijing branch) located in Huairou Science City.

*Corresponding author: jgcheng@iphy.ac.cn

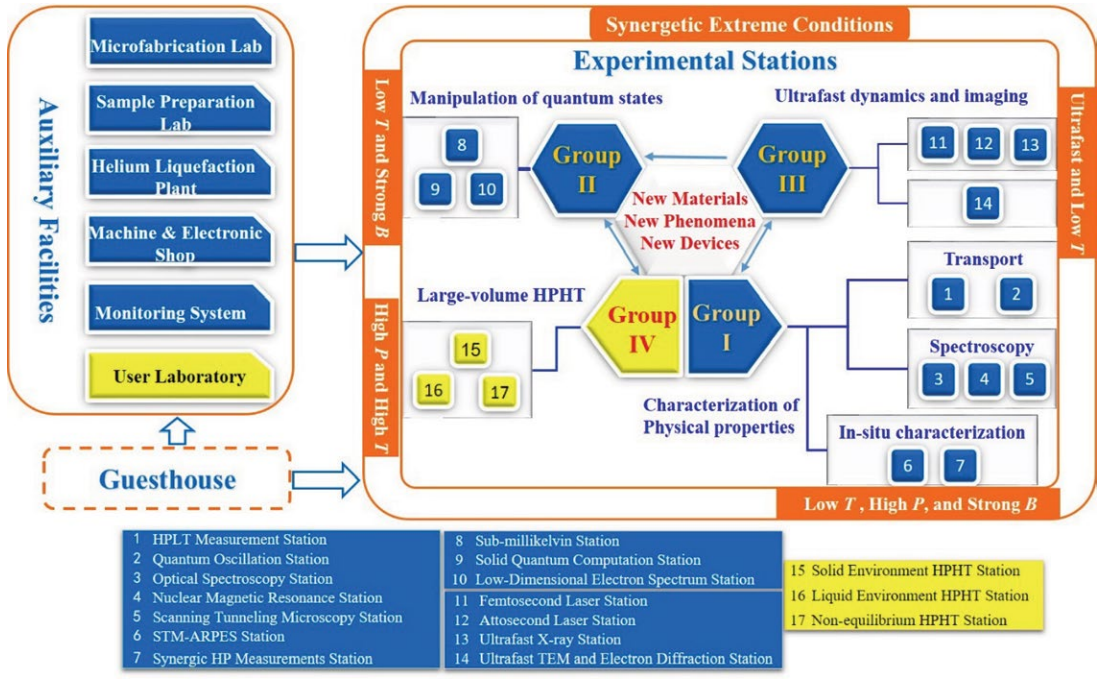

FIGURE 2. Organization scheme of Synergetic Extreme Condition User Facility (SECUF). ARPES, angle-resolved photoemission spectroscope; HPLT, high-pressure, low-temperature; HPHT, high-pressure, high-temperature; STM, scanning tunneling microscope; TEM, transmission electron microscope

Objective

The scientific objective of the SECUF project is to expand our current research capability with the use of synergetic extreme conditions to promote the discoveries of new states of matter, phenomena, and devices. Based on the research field and methodology, the 17 experimental stations in SECUF are divided into four groups: Group I for characterizing various physical properties of matter under extreme conditions; Group II for manipulating quantum states under extreme conditions; Group III for studying the dynamics of molecules, atoms, and electrons under ultrafast time resolution; and Group IV for materials research under high-pressure, high-temperature (HPHT) conditions. The construction site for Groups I, II, and III is in the Huairou Science City (Beijing branch, ~ 21.5 acres; see Figure 1), and that for Group IV is in the Jilin University campus (Jilin branch, ~8 acres). The three groups at the Beijing branch are close to each other and will be interconnected with a fourth-generation synchrotron radiation facility, which will be constructed nearby. The group at the Jilin branch will take advantage of the well-developed high-pressure research facilities at Jilin University.

Organization

Figure 2 shows the organizational scheme of the SECUF project. Group I comprises seven experimental stations (1–7) dedicated to characterizing the physical properties of condensed matter under multiple extreme conditions. Station 1 will be used to study electronic transport and magnetic properties under pressure via advanced high-pressure techniques including diamond anvil cells ($P \geq 100$ GPa) and cubic anvil cells ($P \geq 15$ GPa) integrated with helium-3 (^{3}He) or dilution refrigerators and superconducting magnets for providing extreme temperature conditions ($T_{min} \leq 500$ mK) and a magnetic field ($B_{max} = 14$ T), respectively. Station 2 will feature an all-superconducting 26-T magnet equipped with a dilution refrigerator; helium-4 (^{4}He) fridge; and high-precision rotation probes, focusing on quantum oscillation measurements, which can probe the Fermi surface and electronic structures of metals down to 30 mK with a voltage resolution better than 10 nV. Station 3 will comprise a terahertz/infrared spectroscope (including a 14-T splitting magnet and a 20-T superconducting magnet; $T_{min} = 4$ K, and $\Delta f = 0.2$–3 THz) and a Raman scattering spectroscope [$P_{max} = 100$ GPa, $B_{max} = 14$ T, $T_{min} = 4$ K, and $\Delta t = 50$ femtoseconds (fs)], both of which feature ultrahigh temporal/spatial resolution and will provide useful information about charge/lattice excitations and dynamics under multiple extreme conditions. Station 4 will integrate a solid-state nuclear magnetic resonance spectrometer with a domestic-made 26-T superconducting magnet with high homogeneity (10 ppm/cm^3 and 10 ppm/h) and a dilution refrigerator. It can be used to probe microscopic properties of matter down to 20 mK. Station 5 will take advantage of the excellent key techniques developed by our team members to achieve high spatial resolution (0.1/0.001 Å for horizontal/longitudinal direction) and energy resolution (0.5 meV) for scanning tunneling microscopy (STM) under ultralow temperatures ($T_{min} = 20$ mK) and a strong magnetic field ($B_{max} = 18$ T). Station 6 will combine the angle-resolved photoemission spectroscope (ARPES) ($T_{min} = 4$ K and

ΔE = 3 meV), STM (T_{min} = 0.5 K, B_{max} = 16 T, ΔE = 0.1 meV), molecular beam epitaxy, and pulsed laser deposition to construct an in situ high-precision measurement system to probe low-energy excitations in both real and momentum space for various quantum materials. Station 7 will bring together multiple in situ high-pressure probes for synergetic measurements of various physical properties under multiple extreme conditions ($P \geq$ 300 GPa, T_{max} > 3,000 K, T_{min} = 4 K, and B_{max} = 9 T).

Group II is divided into three experimental stations (8–10) according to the requirements in different research fields to achieve the optimal conditions for manipulating quantum states. Station 8 aims to achieve a sub-millikelvin temperature range using an adiabatic demagnetization technique and to perform electron quantum transport measurements at $T \leq$ 1 mK and B up to 16 T, with $B/T \geq$ 10,000 T/K. Station 9 will be dedicated to solid-state quantum computation based on superconducting, topological, and electronic spin systems by constructing a platform with extremely low noise under extreme conditions (T_{min} = 30 mK, B_{max} = 12 T, and residual field <20 nT). Station 10 will be used for performing spectroscopy and manipulating the quantum state of low-dimensional electron systems (T_{min} = 350 mK, B_{max} = 20 T, and resolution = 0.1 cm^{-1}).

Group III consists of four experimental stations (11–14) that will use different ultrashort pulse sources ranging from infrared, visible, soft, and hard X-ray photons, to irradiate electrons to either initiate or probe the dynamic processes in matter under transient states in multiple disciplines such as physics, chemistry, materials science, biology, and medical sciences. Station 11 will perform ultrafast experiments with carrier-envelope phase–stabilized femtosecond lasers with a temporal resolution better than 7 fs. This station will be optimized for fields including atomic/molecular physics and chemical reaction dynamics. Station 12 will construct the attosecond source with a pulse width below 100 as. In combination with the cold-target recoil-ion momentum spectrometer [momentum resolution 0.05 atomic units (a.u.)–0.1 a.u.], photoemission electron microscopy (spatial resolution ≤20 nm), and ARPES (energy resolution <50 meV), this station will allow studies of atomic/molecular physics, nanoscale plasmon physics, and surface ultrafast physics as well as ultrafast processes in condensed matter, such as high-T_c superconductors. The ultrafast X-rays generated via radiating solid targets with intense ultrashort lasers can be used for diffraction and imaging with high spatial resolution. In addition to femtosecond laser ultrafast detection, Station 13 will construct a four-dimensional (4D) super-high spatial/temporal resolution ultrafast X-ray apparatus to probe both the transient structure and ultrafast dynamics of matter. Station 14 will build an ultrafast transmission electron microscope and electron diffractometer to simultaneously achieve the best temporal and spatial resolutions globally, i.e., a temperature range of 10 K–1,200 K, a temporal resolution of ≤300 fs, a spatial resolution of ≤3 Å, an energy resolution of ≤2 eV for the former, and an electron pulse energy range of 20 keV–100 keV, a time resolution of ≤500 fs at 100 keV, and a spatial sensitivity of ≤0.01 Å for the latter.

Group IV consists of three experimental stations (15–17) specializing in material syntheses and characterization using large-volume HPHT apparatuses. The three stations are distinguished by their different sample environments. With the sample in a solid environment, Station 15 will construct several apparatuses for HPHT synthesis up to 28 GPa and 2,500 K, with in situ electron transport and ultrasonic measurement capabilities. Station 16 will feature a liquid high-pressure environment (P_{max} = 1.8 GPa, and T_{max} = 1,000 K) specially designed for research pertaining to biology and supercritical reactions. Station 17 is intentionally designed for achieving nonequilibrium high-pressure conditions, such as fast compression to 10 GPa within 20 ms.

In addition to these major experimental stations, there are several auxiliary facilities: a helium liquefaction plant, a lab for fabricating micro- and nanoscale devices, a machine and electronic shop for precision machining, instrument maintenance, and development as well as a sample preparation laboratory. A guesthouse will also be built to accommodate users and visitors to SECUF.

Future

In line with its ideal of being an "open, sharing, mobile, cooperative" institution, SECUF will be open to both domestic and overseas users. In addition, some financial support will also be provided to attract talented and distinguished teams to participate in collaborative research at the facility. SECUF is expected to provide a firm foundation for China to march toward world-class levels in various scientific research fields and to join the international scientific effort to benefit society.

Accelerated materials discovery at the Institute of Physics

Yanhui Liu* and Weihua Wang*

Materials are the foundation and driving force of science, technology, and culture. They play central roles in almost all areas of human life and activities, from high-end technologies such as manufacturing, infrastructure, national security, and medical care, to all facets of our daily life, from vehicles to kitchenware. In the long history of humanity, materials have always been a part of our existence. We shape new materials and they in turn shape us into who we are (*1*). Many revolutionary technologies that have changed our world are often associated with the emergence and use of new materials (*2*).

The development and discovery of a technologically useful material is never a trivial task. The relationship between composition, processing, structure, and properties is not linear, but complex and multifaceted. Currently, there are no theories that can comprehensively and accurately predict such a relationship. In most cases, new materials have been developed by time-consuming, labor-intensive, sequential trial-and-error approaches, and some successes have depended on chance. To speed up materials discovery, new strategies are required.

Center for Materials Genome Initiative

In 2011, the United States announced the Materials Genome Initiative (MGI). The primary goal of the initiative is to double the pace of materials discovery and deployment at half the cost (*3*). At the same time, the European Union launched the Accelerated Metallurgy Project, with a focus on advanced materials such as high-temperature superconductors, phase-changing materials, and high-performance alloy materials (*4*). Japan plans to build a comprehensive materials database that includes glass, ceramic, alloy steel, and other materials. The MGI approaches, integrating high-throughput computation, high-throughput experimentation, and database management and data mining, have been recognized as an efficient strategy for materials discovery (*5*).

Although China has made remarkable achievements in advanced materials, there is still a big gap compared with domestic demands. According to a survey, China can only produce 14% of the 130 key materials needed for industry. The lack of key materials has long been a weakness of China's national defense, energy, information, environment, transportation, and medical care sectors, among other areas. This scarcity poses a threat to national security and limits social and economic development. For example, China's capability to manufacture high-performance aircraft engines has been seriously impeded by the scarcity of superalloys and related materials. In the new energy and electronics field, access to key materials is also restricted. The annual cost of importing semiconductor chips is USD 200 billion (RMB 1.2 trillion), which is nearly twice that of imported oil. The situation calls for a change in the materials development and innovation system in China.

Around the time the United States announced the MGI, members of the Chinese Academy of Sciences (CAS) and Chinese Academy of Engineering organized the Xiangshan Science Conference, which was held in December 2011. The attending experts reached a consensus that China should take immediate action to accelerate the development of new materials. In numerous seminars from 2012 to 2014, materials scientists and funding agencies in China agreed that materials genome approaches can help China leapfrog development in materials science and engineering.

In this context, CAS and the Beijing municipal government quickly reached an agreement that a center focusing on materials genome research should be built in Beijing. The center will be one of the core parts of the Beijing National Science and Innovation Center in Huairou Science City, and is expected to be the first, largest, and most advanced facility for materials genome research in China. Owing to a strong research team and exceptional achievements in materials science and condensed matter physics, the CAS Institute of Physics is assigned the task of planning, constructing, and operating the center. The construction of the center started in May 2017, and is scheduled for completion by the end of 2020. The total budget is RMB 540 million (USD 86 million).

Architecture of the center

As planned, the center should cover all the three key components of materials genome approaches, including high-throughput computation, high-throughput experimentation, and data management. In addition, a strong technique support team should also be included so that new techniques for high-throughput experimentation can be developed more efficiently. Under such consideration, the center will be designed to comprise three main divisions (Figure 1, next page): materials computation and data processing, high-throughput syntheses and fast characterizations, and high-throughput techniques and development. Materials computation and data processing not only provide theoretical prediction for new materials, but also develop new methods for data management and data mining. High-throughput syntheses and fast characterizations enable experiments on combinatorial materials fabrication and rapid screening of new materials, with emphasis on single-crystal thin films, alloys, and bulk

Institute of Physics, Chinese Academy of Sciences, Beijing, China
*Corresponding authors: yanhui.liu@iphy.ac.cn (Y.L), whw@iphy.ac.cn (W.W.)

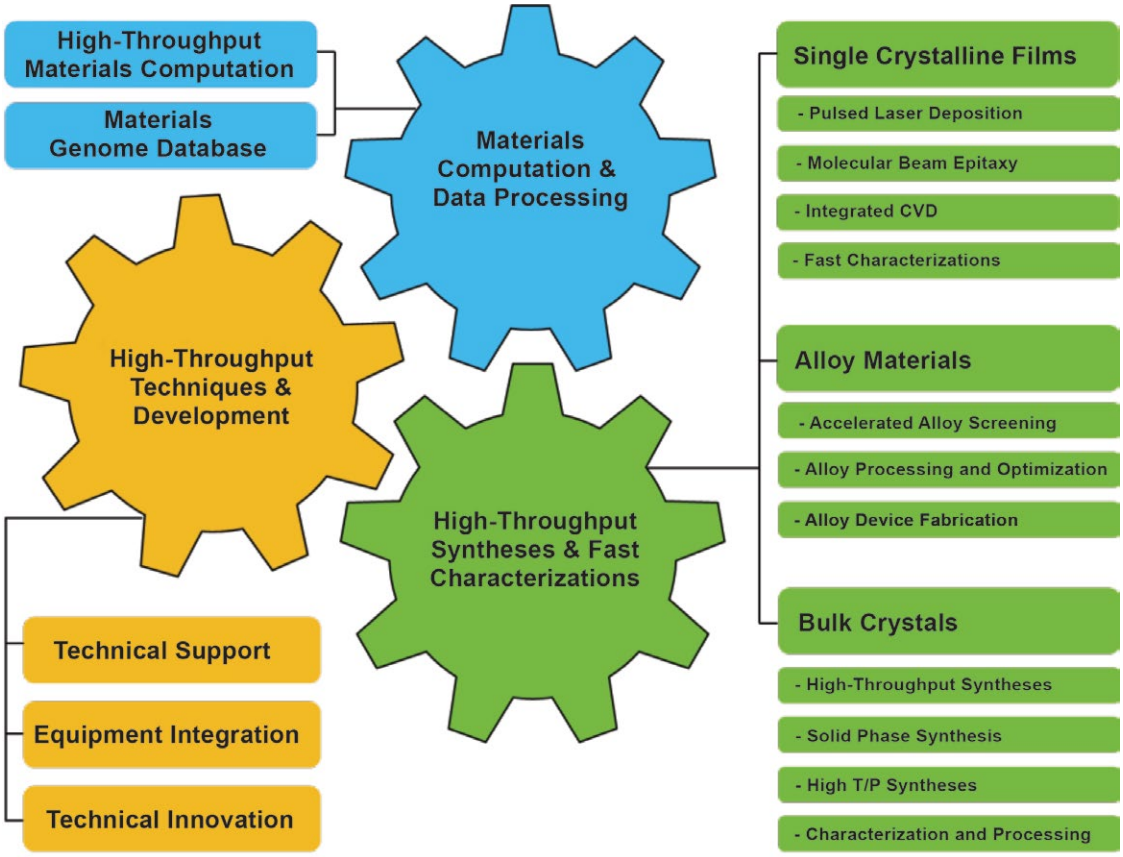

FIGURE 1. Key components of the Center for Materials Genome Initiative at the Institute of Physics.

crystals. High-throughput techniques and development play an important role in technique support and development of new equipment for high-throughput experimentation.

After completion, a center integrating materials computation, experimentation, and technique innovation will greatly improve China's strength in new materials R&D and in basic and applied research in condensed matter science, such as high-temperature superconductors, quantum materials, advanced alloys, and magnetic materials. Furthermore, the center will be open to the global research community so that exciting ideas can be generated and exchanged, and so more attractive materials can be discovered.

Along with the center, the Synergetic Extreme Condition User Facility will be established—its construction started in September 2017. An advanced synchrotron light source is also scheduled to be built nearby. On the one hand, such large facilities enable high-quality materials characterization and sophisticated measurement of materials properties that will lead to a deeper understanding of materials science. On the other hand, the Center for Materials Genome Initiative will provide various materials for research based on the work of these other facilities—so all of these resources will thus benefit from each other.

Conclusion

In the past decades, the world has witnessed China's rapid economic development and infrastructure construction. However, we still rely heavily on imported materials in many areas. With the opening of the Center for Materials Genome Initiative, we are hoping to design, develop, and deploy new materials at an unprecedented pace, materials that are essential for the Chinese economy and sustainable development. We believe the world will again witness China's rapid growth in materials discovery.

References

1. M. Miodownik, *Stuff Matters: Exploring the Marvelous Materials That Shape Our Man-Made World* (Penguin Books, London, UK, 2013).
2. *The Coming of Materials Science,* Pergamon Materials Series, vol. 5, R. W. Cahn, Ed., (Elsevier Science, London, UK, 2001).
3. Materials Genome Initiative, website, www.mgi.gov.
4. European Commission, Community Research and Development Information Service (CORDIS), "Final Report Summary—ACCMET (Accelerated Metallurgy—the Accelerated Discovery of Alloy Formulations Using Combinatorial Principles," http://cordis.europa.eu.
5. C. L. Phillips, P. Littlewood, *APL Mater.* **4**, 053001 (2016), doi: https://doi.org/10.1063/1.4952608.

FIGURE: YANHUI LIU, WEIHUA WANG

Technical Support Services at the Institute of Physics

Junjie Li*, Xiunian Jing, and Changzhi Gu

The Division of Technical Support (DTS), a public platform, provides technical services related to condensed matter physics for Institute of Physics (IOP) research groups. The DTS consists of five departments—the Laboratory of Microfabrication (LMF), Electronics Service and Scientific Instruments (ESSI), Materials Analysis and Characterization Center (MACC), Cryogenic Service (CS), and Mechanical Engineering Facility (MEF)—associated with the following respective service fields: micro-/nanofabrication for novel structures and devices; R&D of signal detection technology and advanced integrated experimental facilities; materials analytical testing and characterization through Raman spectroscopy, X-ray diffraction, and inductively coupled plasma–atomic emission spectrometry/mass spectrometry; production and supply of liquid nitrogen and liquid helium; and equipment-unit precision machining.

As a typical DTS department, the LMF is introduced here. The LMF opened in 2002 and occupied over 1,000 m^2 in the cleanroom area, as a new IOP-based multidisciplinary research center to facilitate cutting-edge research in nanoscience and nanotechnology. LMF's primary focus is the fabrication and characterization of artificial micro-/nanostructures from

Laboratory of Microfabrication, Division of Technical Support
*Corresponding author: jjli@iphy.ac.cn

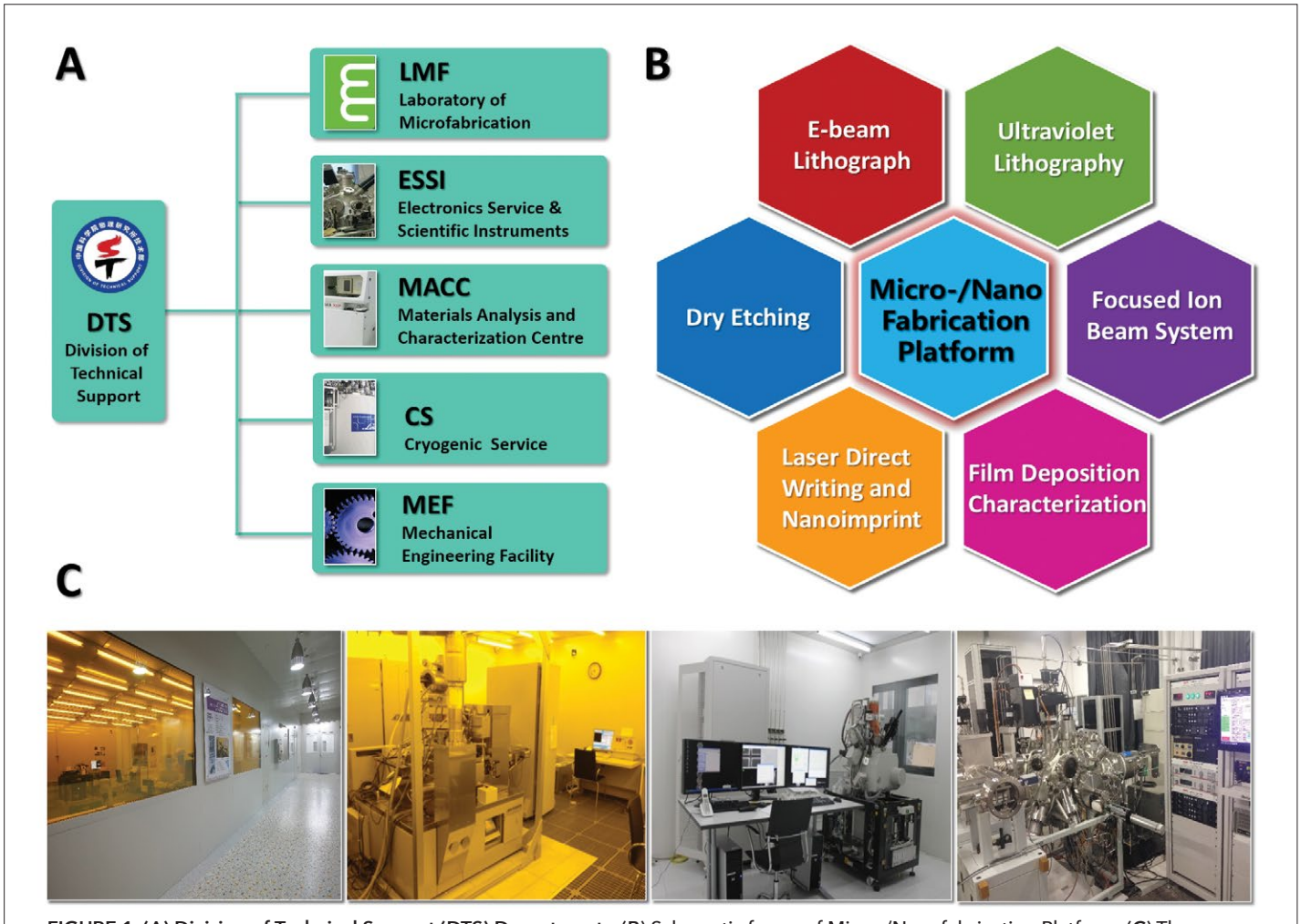

FIGURE 1. (A) Division of Technical Support (DTS) Departments. (B) Schematic frame of Micro-/Nanofabrication Platform. (C) The cleanroom and primary nanofabrication techniques in LMF: electron-beam lithography, focused ion beam direct writing, and thin-film deposition.

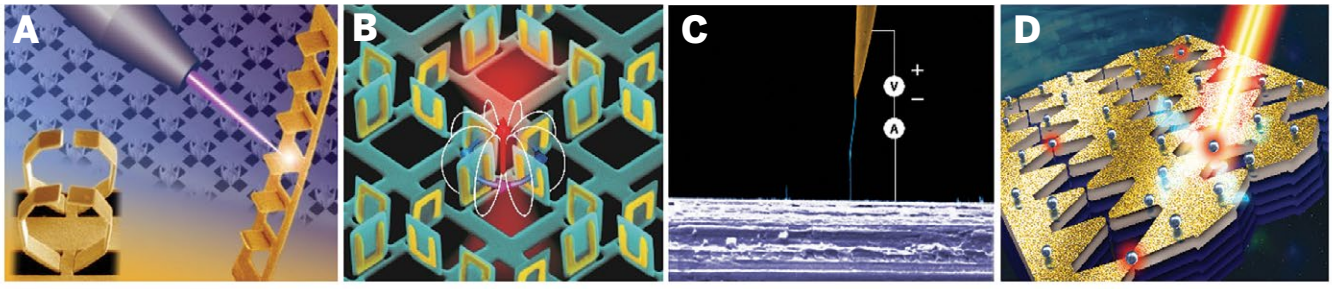

FIGURE 2. Nanofabrication for functional devices. (**A**) and (**B**) 3D folding micro-/nanostructures of metamaterials. (**C**) In situ measurement for electronic transport in a single carbon nanotube. (**D**) Nanocrack-defined metal nanogap arrays for sensoring systems.

low to three dimensions (3D), with devices and technology for integration. It provides technical services and advice to IOP and international researchers. User training is given, and summer schools are hosted regularly, providing a bridge toward research careers for young researchers with strong capabilities in the underlying disciplines of engineering, physical sciences, and biomedicine. LMF's goal is the provision of world-class technical support while satisfying major requirements in the fields of information processing, microelectronics, clean energy, environment, and bioscience.

LMF was founded considering several academic and scientific requirements, including development of novel nanofabrication technology to provide strong support for construction of new artificial nanostructures and nanodevices, thereby facilitating exploration of underlying quantum phenomena and novel physical effects. It ranks among the leading micro-/nanofabrication facilities worldwide. Additionally, a wide range of facilities, operations, and management functions are carried out at LMF to maintain critical infrastructure functionality, and to fully support the research needs of the IOP and other organizations in China.

LMF provides access to a full range of cutting-edge instruments for fabrication and characterization on the nanoscale, offering services in the Zhongguancun area and internationally. These instruments include ultraviolet (UV) lithography and electron-beam lithography (EBL) equipment, focused ion beam (FIB) and laser direct writing systems, and dry etching and thin-film deposition equipment. Cleanrooms and equipment within LMF are accessible to external academic or industrial users. Processing is available for structures ranging from a few nanometers to a few hundred micrometers, and in formats from quantum dots to 3D, based on various materials [including silicon (Si), III-V semiconductors, carbon-based materials, dielectrics, metals, metal oxides, polymers, and biological materials]. We also explore and provide technology for the construction of various devices, such as field effect transistors; for quantum computing, superconducting, and magnetic information storage; for nano-optical, single-photon, single-electron, plasmonic, and other new energy devices; and for biodevices, sensors, and detectors. To date, LMF has reported important technical achievements in fabrication, characterization, and device development, especially regarding the formation of sub-5-nm metal gap arrays, folding of 2D film into 3D nanostructures, in situ measurement of local properties, and 3D metamaterials. LMF has also achieved important research outcomes, including multichannel ballistic transport in multiwall carbon nanotubes (*1*), an all-metallic logic gate based on current-driven domain wall motion (*2*), optical control by 3D folding metamaterials and applications (*3, 4*), and sub-5-nm metal nanogap arrays for sensoring and memory (*5–8*), greatly advancing the development and status of LMF.

References

1. H. J. Li, W. G. Lu, J. J. Li, X. D. Bai, and C. Z. Gu., *Phys. Rev. Lett*. **19**, 086601 (2005).
2. P. Xu *et al*., *Nat. Nanotechnol.* **3**, 97–100 (2008).
3. A. J. Cui *et al*., *Light Sci. Appl.* **4**, e308 (2015).
4. Z. Liu *et al*., *Adv. Mater.* **29**, 1606298 (2017).
5. Z. S. Hu *et al*., *Small* **18**, 3933(2014).
6. A. J. Cui *et al*., *Adv. Mater.* **27**, 3002 (2015).
7. A. J. Cui *et al*., *Adv. Mater.* **28**, 8227 (2016).
8. S.H. Pan *et al*., *Nanoscale* **10**, 3171 (2018).

Acknowledgements

Figure 2D is reproduced by permission of the authors and the Royal Society of Chemistry from S. H. Pan *et al*., *Nanoscale*, **10**, 3171 (2018).

IOP
Invites Talented Applicants

The Institute of Physics (IOP) of the Chinese Academy of Sciences (CAS) is currently recruiting personnel for the following positions:

Preferred fields of research

- Materials science
- Condensed matter theory and computational physics
- Experimental condensed matter physics
- Optics
- Surface sciences
- Energy materials
- Magnetism
- Nanoscience
- Biophysics
- Ultracold atoms
- Quantum information
- Research using large scientific facilities (Synergetic Extreme Condition User Facility, Beijing Synchrotron Light Source, China Spallation Neutron Source, etc.)

Vacancies

Overseas High-level Talents

- Professor or equivalent position from a well-known overseas university or research institute.
- Principal Investigator or key contributor to research projects with significant achievements.
- To be recommended for the national "Thousand Talents Program"/ Chinese Academy of Sciences "Hundred Talents Program"- Class A.

Hundred Talents Program -Class A

- PhD degree with research experience from a well-known overseas university or research institute.
- Assistant Professor or equivalent level.
- Significant scientific achievements, extensive international influence, leadership ability.
- Preferably under 40 years old.
- To be recommended for the national "Thousand Talents Program" for Distinguished Young Scholars / Chinese Academy of Sciences "Hundred Talents Program" - Class C.

Hundred Talents Program -Class B

- PhD degree with research experience from a well-known overseas or domestic university or research institute.
- Significant scientific achievements.
- Preferably under 35 years old.
- To be considered for the national "Thousand Talents Program" for Distinguished Young Scholars / Chinese Academy of Sciences "Hundred Talents Program" - Class C.

Key Technologists

- PhD degree with research experience from a well-known overseas or domestic university or research institute.
- Significant technological achievements.
- Preferably under 40 years old.
- To be considered for the Chinese Academy of Sciences "Hundred Talents Program" - Class B.

Benefits

- Competitive salary;
- Sufficient start-up funding;
- Well-furnished apartments to rent;
- Children to be enrolled into good schools.

Contact: Ms. Qi Fu, Email: fuqi@iphy.ac.cn, Tel: 86-10-82649469, Fax: 86-10-82649218
Address: Institute of Physics, Chinese Academy of Sciences, P.O. Box 603, Beijing 100190, China

IOP

Invites Talented Applicants

Beijing National Science and Innovation Center
Huairou, Beijing

With a planned area of 100.9 sq. km., Beijing National Science and Innovation Center will see the construction of a series of large scientific facilities, interdisciplinary frontier research centers, and national labs, to form a world-renowned comprehensive national science center.

A new, world-class, state-of-the-art national science center.

A vibrant and unique location to study, work, and live.

One Facility, Two Centers: The CORE of Huairou Science City.

1 Synergetic Extreme Condition User Facility

The world's first user facility that integrates extreme conditions including ultralow temperature, ultrahigh pressure, ultrahigh magnetic fields, and ultrafast light fields.

2 Center for Clean Energy

China's first professional platform for comprehensive analysis and tests of clean energy materials and devices, from atomic to macro dimensions, and from materials to systems.

3 Center for Materials Genome Initiative

China's first materials genome research center and also the world's largest, with the most complete methods.

Vacancies

- Overseas High-level Talents (Full Professors and Chair Professors)
- Hundred Talents Program-Class A (Tenure-Track Associate Professors)
- Hundred Talents Program-Class B (Tenure-Track Associate Professors)
- Key Technologists

Contact: Ms. Qi Fu, Email: fuqi@iphy.ac.cn, Tel: 86-10-82649469, Fax: 86-10-82649218
Address: Institute of Physics, Chinese Academy of Sciences, P.O. Box 603, Beijing 100190, China